Using VSP to improve interpretation of ocean bottom seismic

Christine Thorgersen

Master thesis

in

Geosciences, Petroleum

Department of Earth Science

University of Bergen

February 2011

ABSTRACT

Operating companies work continuously on increasing their knowledge about the reservoir. In mature areas of the North Sea many wells have been drilled, which can be used to obtain improved images of the subsurface in the area. 3D- and time-lapse (4D) techniques have evolved making it possible to monitor the production to a large degree. Likewise, seismic data processing methodologies and processing flows have been designed utilizing the seismic data to a high degree. However, yet much knowledge is to desire, and traditional methods only partially succeed. Therefore, additional methods must come in place.

One such method is the use of converted (S) energy in seismic exploration. Anticipating the same source and similar attenuation mechanism for both P- and S-waves, the resolution of S-wave images should be superior to that of P-waves. Therefore, complementary information about the subsurface formations may be obtained by the careful analysis of S-waves. Due to multi-component seabed acquisition it is now possible to record and process converted (S) waves also in marine environments. One major drawback however is the poor quality of the converted energy of such data. It is often difficult to correlate the S-events to the P-events. This study is an attempt to increase the confidence of correlation between an S-event and the corresponding P-event on the multi-component data. To accomplish this task we make use of information from VSP.

VSP (Vertical Seismic Profiling) is a seismic survey method whereby the receivers are positioned downhole in the wellbore, while the source is located on the surface. VSP has several advantages. By placing receivers in wells, closer to the structures we aim to map, we can improve the imaging of formations where the surface seismic fails to achieve interpretable results. It is also possible to construct seismic image of reflectors which extend laterally away from the borehole.

In VSP we record both P- and converted (S)-waves. Beneficial to our purpose, the interpretation of the VSP will give information about mode-conversion taking place in the subsurface. We are able to tell whether the conversion has taken place as a reflected or a transmitted conversion (up or down), we may identify the formation tops acting as converting interfaces, and we may compute the formation interval S-wave velocity with confidence.

A depth-velocity model incorporating VSP survey geometry, performed over the Snorre field, was built for both P- and S-waves. The models show the basic geometry of the VSP survey, and the raypaths, and the S-wave model also shows the mode conversion. The VSP data is compared to a 3D multi-component seabed seismic survey in the same area. The interpreted horizons in the 3D volume correlate well with the interpreted horizons of the VSP seismic profile. It is therefore shown that the use of both P- and S-waves from the VSP data can be used to correlate the interpretation of the converted (S) 3D volume to the regular P-wave 3D volume, and in addition provide new constraints on lithology (sand/shale ratio).

PREFACE

I want to thank my supervisors Harald Knoop and Rolf Mjelde for guidance, technical help and correction reading throughout this thesis. Then I want to thank Statoil for the data received from them. Also great thanks to Lars Zuehlsdorff from NORSAR, Bent Ole Ruud and Morten Vetaas for help with the NORSAR, Geovecteur and Petrel software. And my fellow geophysical student Kseniya Hladka for correction reading and support.

Finally, I would also like to thank all my fellow students for five wonderful years at UiB, and my family and friends for great support during this thesis.

Christine Thorgersen

February 2011

Table of Contents

1 Introduction

Operating companies work continuously on increasing their knowledge about the reservoir. In mature areas, where much exploration has been done and production from known reservoirs has commenced, it is important to maintain the production at a constant high rate, an important fact which has also been clearly stated by the NPD. Even though 3D- and time-lapse (4D) techniques have evolved making it possible to monitor the production to a large degree, and seismic data processing methodologies and processing flows have been designed utilizing the seismic data to a high degree, more information is desired. In the mature areas of the North Sea a lot of wells have been drilled, which can be used to obtain improved images of the subsurface in the area.

VSP (Vertical Seismic Profiling) is a seismic survey method whereby the receivers are positioned downhole in the wellbore, while the source is located on the surface. VSP has several advantages. By placing receivers in wells, closer to the structures we aim to map, we can improve the imaging of formations where the surface seismic fails to achieve interpretable results. It is also possible to construct seismic image of reflectors which extend laterally away from the borehole. This technique is efficient for locating faults, determine dipping reflectors and in general make more secure interpretations of structures which can be difficult to map with surface seismic.

The most important part of VSP surveys is the recording of converted (S-) waves. Anticipating the same source and similar attenuation mechanism for both P- and S-waves, the resolution of S-wave images should be superior to that of P-waves. Therefore, complementary information about the subsurface formations may be obtained by the careful analysis of S-waves.

VSP provides information about whether the wave conversion has taken place as a reflected or a transmitted conversion (up or down), and we may identify the formation tops acting as converting interfaces, and compute the formation interval S-wave velocity with confidence. In ocean bottom seismic, S-waves are also recorded, but in these surveys it is often difficult to correlate the S-events to the P-events. This study is an attempt to increase the confidence of correlation between an S-event and the corresponding P-event on the multi-component data.

The goal of this thesis is to construct ray-tracing models of VSP survey geometry, and improve these models by correlating with observed VSP seismic from the area. And correlate these models, and the observed VSP seismic with the ocean bottom seismic 3D-cubes. Two VSP survey types are included in this thesis; Normal (also called Vertical) Incidence, and Rig Source. These models can give insight to the wave conversion interface, and the depth of these interfaces.

2 The Snorre Field

2.1 Introduction

The Snorre field is located in the Tampen area in the northern part of the North Sea (see Figure 2-1). The field was discovered in 1979 by the exploration well 34/4-1. The platform Snorre A is located in the south part of the field and Snorre B in the north. Snorre A was set in production in 1992 and Snorre B in 2001. After being operated by Saga Petroleum ASA and Norsk Hydro ASA, Statoil became the operator in 2002 (NPD 2011, Seldal *et al* 2008).

The Tampen area is bounded by the East Shetland Basin to the west, the Marulk Basin to the northwest, the Marflo Ridge to the east, and the Viking Graben to the southeast. The Snorre fault block is a large westerly rotated fault block situated in the south-southeast part of the Tampen area. The Snorre Fault Block is a very pronounced structural high, due to uplifting in Late Jurassic combined with Jurassic/Cretaceous subsidence. The Snorre Fault Block covers a large part of the Blocks 34/4 and 34/7. The main structural elements in the area are NNE-SSW- to NE-SW-striking faults, which give the rotated fault blocks. The major faults related to the Snorre Fault Block are the Murchison Fault, the Outer Snorre Fault, the Southern Snorre Fault, and the inner Snorre Fault (see Figure 2-2 and Figure 2-3). The field consists of several large fault blocks, which means complex geology, and is therefore difficult to map with surface seismic. The water depth ranges between 300 and 350 m in the area (Glennie 1998, Dahl *et al* 1993).

The producible part of the Snorre reservoir consists of the Lunde Formation and the Statfjord Formation, consisting of more than 1000 m of fluvial sandstones. Volume estimates indicate that there are 513 MSm^3 Stock Tank Oil Original In Place (STOOIP) and associate Gas Initial In Place (GIIP) of 52 GSm^3. The reservoirs at the Snorre Field contain light under saturated oil, and the main reservoir drainage strategy is through water injection, gas injection, and water-alternating-gas (WAG) injection. Currently 123 wells have been drilled in the area, where 13 are exploration wells, and 110 are development wells. The field is containing the largest remaining reserves of the fields operated by Statoil on the Norwegian Continental Shelf, so the area has a significant potential for increasing oil recovery (Seldal *et al* 2008, NPD 2011).

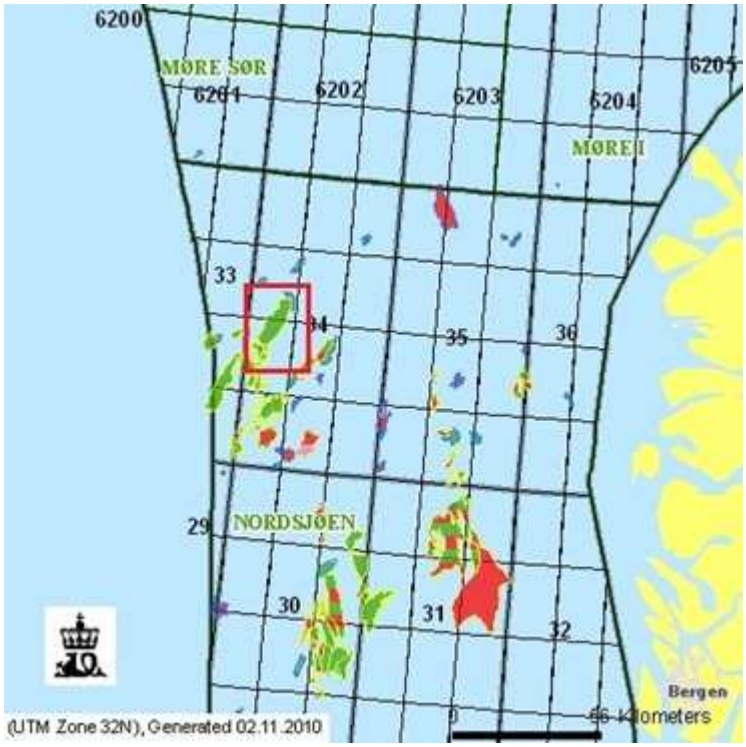

Figure 2-1: Location of the Snorre Field (NPD)

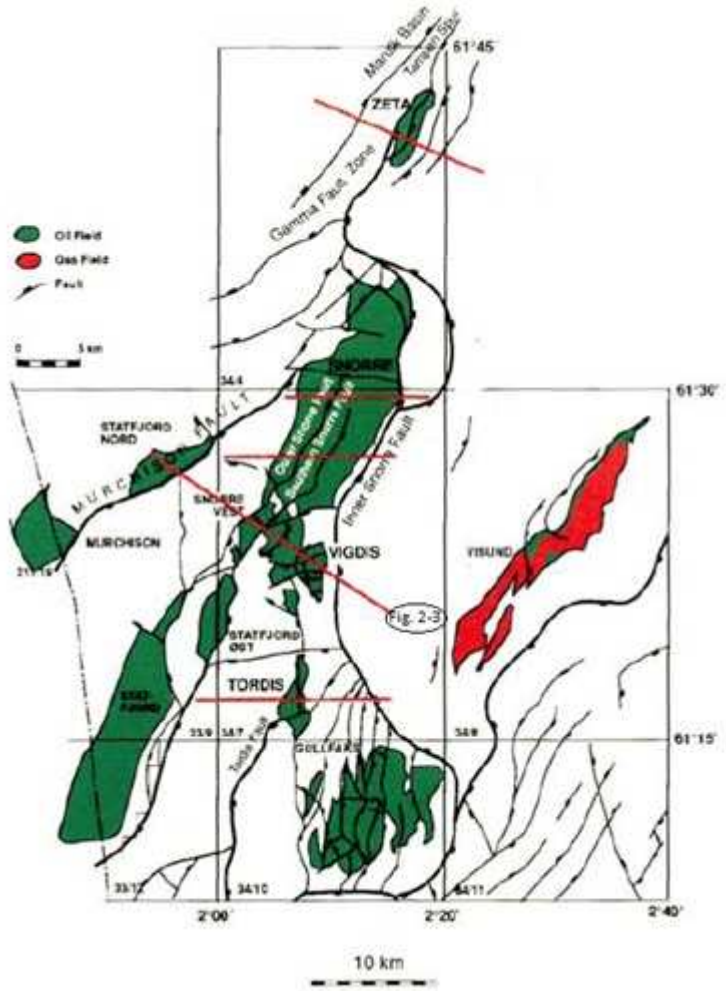

Figure 2-2: The Snorre Field and surrounding areas (Dahl *et al* 1993).

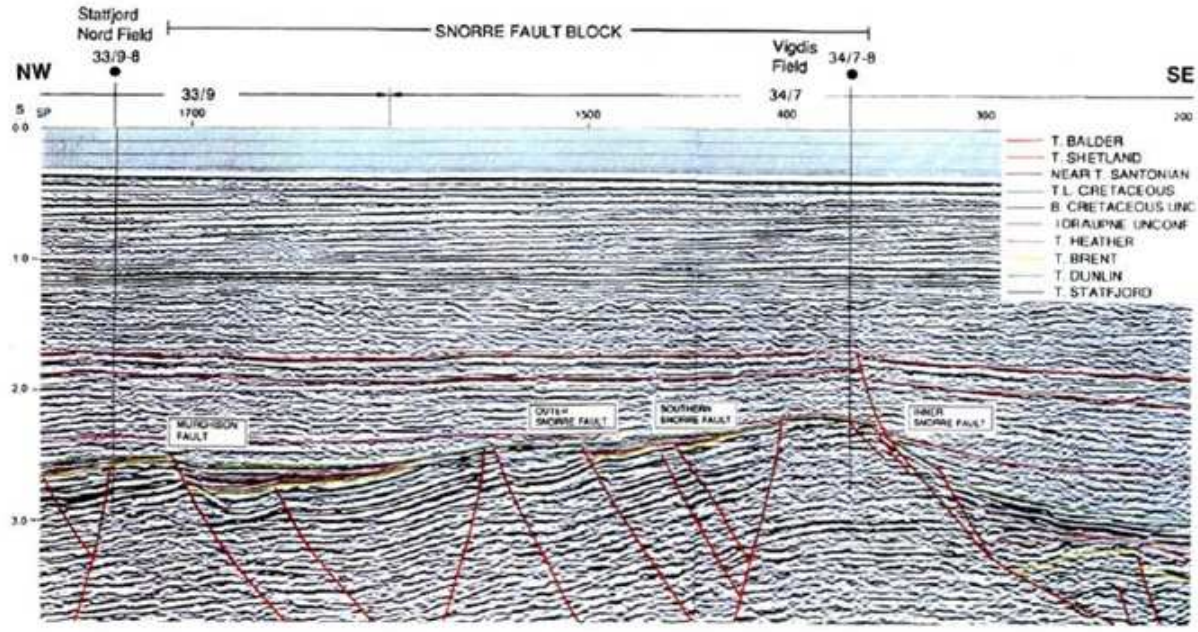

Figure 2-3: A seismic section from the Statfjord Nord Field across the Snorre Fault Block to the Vigdis Field in the east (Dahl *et al* 1993)

2.2 Structural setting and geological history

The Tampen Spur is a late Jurassic to Cretaceous structure within the continental Permian-Triassic Rift Basin of the Northern North Sea. The North Sea is an intracratonic basin with a complex history. It begins with the formation of the Pangean mega-continent, and the corresponding Caledonian orogeny. Following was the Hercynian phase, where the North Sea area was in the foreland of an orogenic belt which extended from Germany to South Wales. In present day, evidence of progressive phases of shear, rift and passive sag supports this. Then the early Pangean break-up commenced in early Permian, leading to a period of rifting and associated igneous activity (Ziegler *et al* 1986).

2.2.1 Triassic

Following the Permian rifting a regional subsidence took place during most of the Triassic and to the early Jurassic. Fluvial material was deposited within wide alluvial plains by rivers flowing towards a seaway located to the north. Large amounts of sediments were accumulated in the subsiding continental basin during the Triassic, and these sediments belong to the Hegre Group. The Hegre Group consists of intervals of interbedded sandstones, shales, claystones, and mudstones associated with sequences of dominantly sandstone or shale. The Hegre Group is divided into three formations; the Teist Formation, the Lomvi Formation, and the Lunde Formation (Dahl *et al* 1993, Lervik 2006).

The Teist Formation has an early Triassic age, and is characterized by a generally continuous interchange of red sandstones and mudstones. The Lomvi Formation has an early to middle Triassic age, and is described as more than a hundred meters thick, blocky, massive kaolinitic sandstone, with thin, minor layers of red marl and claystone. These sediments have been interpreted to have a fluvial origin. The Lunde formation is late Triassic, and is subdivided into three Members; Lower, Middle and Upper. The Lunde Formation is a succession of very fine to very coarse-grained sandstones, claystones, marls and shales. The Lunde Formation is also considered to be of fluvial origin, and the formation represents a major depositional fluvial system. In the Snorre field the Lunde Formation is an important reservoir (Dahl *et al* 1993, Lervik 2006).

2.2.2 Jurassic

The regional subsidence which took place in the Triassic continued into the Early Jurassic with a decreasing rate of subsidence. The oldest Jurassic sediments are the sands of the Statfjord Formation, which accumulated as braided stream deposits on an alluvial plain (Nystuen *et al*. 1989). During the following marine transgression the Statfjord Formation were overlain by the Dunlin Group, consisting of shallow marine siltstone and shales.

In the Middle Jurassic the cooling of the crust, after the Permian-Triassic faulting, approached a state of thermal equilibrium, and the Brent delta developed and propagated northwards into the marine basin. The Brent Group is divided into four lithostratigraphic units in the Snorre Fault Block; Rannoch, Etive, Ness and Tarbert Formations. The deposition pattern of the Rannoch and Etive is the same as the earlier formations, but the deposition of the Tarbert Formation was affected by renewed fault activity towards the end of the Middle Jurassic (Dahl *et al* 1993).

A second major rifting episode began in the end of the Middle Jurassic. The thinning of the crust by rifting was followed by syn-rift initial subsidence, resulting in the formation of the Viking Graben. During the increase in relative sea-level the syn-tectonic marine shales of the Heather Formation were deposited. The crustal extension focused mainly on easterly dipping faults of NNE-SSW to NE-SW orientation, but also N-S striking faults were reactivated. The Snorre Fault Block was rotated in a southwesterly direction, and the crest of the block was uplifted above the erosive base. In the northern part of the Snorre Field pre-rift sediments are eroded and Triassic sediments of the Lomvi Formation are directly overlain by Cretaceous sediments. The Viking Group is dominated by the marine mudstones of the Heather and Draupne Formation. The pelagic sediments of the Viking Group cover the uplifted Snorre Fault Block in a direction from SW to NE. The Intra Draupne Unconformity, which is a truncational sequence boundary, divides the Draupne Formation into an upper and lower part. Two pulses of crustal extension by rifting are recognized in the syn-rift Viking Group, and have affected the deposition of the Heather and lower Draupne Formation. The upper Draupne 'hot shales' cover and drape the rifted basin topography (Dahl *et al* 1993).

2.2.3 Cretaceous

In early Cretaceous uplift and relative sea-level drop exposed newly deposited sediments to erosion. During the following marine transgression, carbonate sediments of the Lower Cromer Knoll Group covered the Snorre Fault Block. Then following a hiatus, sediments of the shalier Upper Cromer Knoll Group were deposited. In the early Cretaceous, only the faulting and differential subsidence along the major faults continued. The movements were not associated with any significant fault-block rotation and may be a consequence of differential compaction in the rapidly subsiding Cretaceous basin.

In late Cretaceous shales of the Lower Shetland Group were deposited followed by a hiatus of Santonian age. The deposition of the Upper Shetland Group followed. Towards the end of Cretaceous the topography of the Snorre Fault Block was filled in with sediment (Dahl *et al* 1993).

2.2.4 Tertiary

In Tertiary fault activity continued along the Inner Snorre Fault, in addition to faults of dominantly NW-SE direction. The basin subsidence continued into Tertiary, only interrupted by a short episode of uplift and erosion, and the Rogaland and Hordaland Group were deposited. Fault activity decreased through Tertiary, and from Oligocene there were no seismically observable faults in the area. A major episode of relative uplift and erosion in the Miocene was followed by deposition of sands of the Utsira Formation of the Nordland Group (Dahl *et al* 1993).

2.3 Reservoir description

The reservoir of the Snorre Field is found in the Lower Jurassic and Triassic sandstones of the Statfjord and Lunde formation. The Middle and Lower Lunde Formation do not contain hydrocarbons on the Snorre Field. Both the Upper Member of the Lunde Fm. and the Statfjord Fm. are present in the western, southern and central part of the Snorre Field. In the north and eastern parts the Base Cretaceous unconformity (BCU) truncates the Upper Member of the Lunde Formation and the Statfjord Formation (Seldal *et al* 2008).

2.3.1 The Upper Member of the Lunde Fm. (SN1-SN10.3)

The Upper Member of the Lunde Formation is divided into 10 main reservoir zones, which are also divided into smaller subzones. The formation is built up of interbedded, medium grained, white, pink or grey channel belt sandstones. The sandstones are interbedded with

red brown to green caliche-rich siltstones and mudstones of continental origin (Seldal *et al* 2008).

Braided Channel Systems on Upper Alluvial Plain (SN1-SN7): The zones SN-SN7 consists of channel sandstone most likely deposited in braided shallow channels. The sandstones have varying size vertically, but most of them are in the fine to medium range. Fining upwards units, vertically stacked sandstone bodies and coarse grained channels are found in these zones (Seldal *et al* 2008).

Meandering Channel and Distributary Channels on Lower Alluvial Plain: The channel sandstones in the zones SN8-SN10 are interpreted to have been deposited in an environment dominated by meandering and distributary channels. The meandering channels have high sinuosity and deposit much of the bed load at the inside of meander loops, where point bars are formed. Point bars form the most important sandstone depositional element on an alluvial plane where meandering rivers are flowing. Lateral migration of the channel will result in a characteristic fining upward section typical for point bars. In the upper zones distributary channel sandstones, characterized by low sinuosity, occur frequently. This is because the main channel on the lower alluvial plain tends to split into several distributary channels when it's approaching the upper delta plain (Seldal *et al* 2008).

2.3.2 The Statfjord Formation (SN10.3-SN11)

This formation is only divided into one main reservoir zone (SN10.3-SN11). The formation consists of more carbonaceous silt and mudstones, which implies a more coastal plain depositional setting, and the sandstones have in general coarser grains than observed than observed in the Upper Lunde Member (Seldal *et al* 2008).

Coastal Plain (SN11): The Statfjord Formation consists of high permeable lateral extensive sandstones, expected to be deposited on the coastal plain, with a depositional environment including embayment deposits, coastal plain channels, crevasse splays and paleosoils. It is assumed that both fluvial and tidal processes deposited and reworked the sediments. The sediments have a dominating grain size ranging from medium to coarse grained. The upper parts contains the coarsest grains, while the lower parts have finer grained paleosoil sediments (Seldal *et al* 2008).

Figure 2-4 show the depositional setting explained above, and the approximate thickness of the different zones.

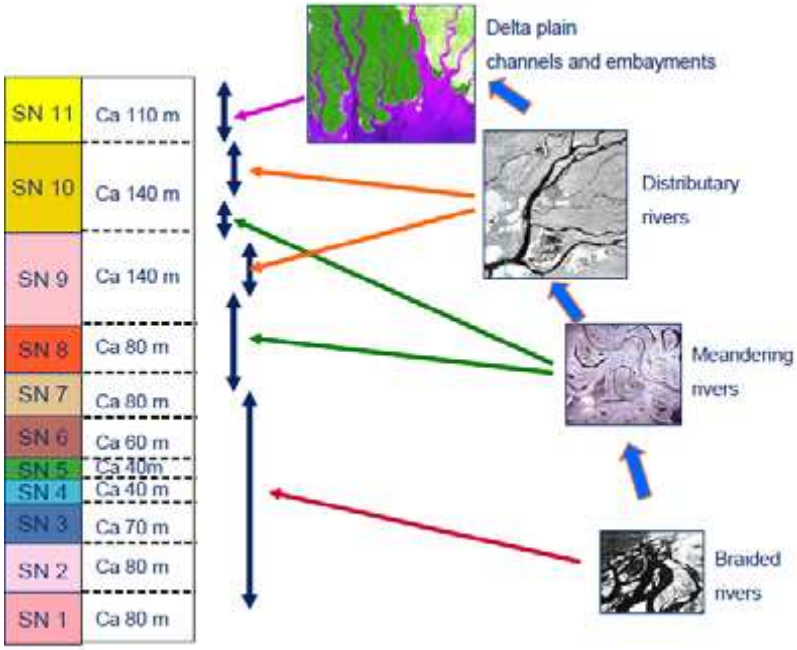

Figure 2-4: Depositional settings in the different Snorre zones (modified from Seldal *et al* 2008).

3 Method

This chapter explains the theory behind, and the methods used to find the results of this thesis. Basic theory about Ocean Bottom Cable (OBC) (also called ocean bottom seismic in industry), and Vertical Seismic Profiling (VSP) will be explained, as well as acquisition and processing of these kind of surveys. Then the principles of the geological interpretation of the dataset and the ray-trace modeling of a VSP-survey will be discussed. In this thesis only marine seismic surveys will be discussed.

3.1 Seismic acquisition

3.1.1 Basic seismic theory

Seismic is the most used exploration method in the oil industry. Figure 3-1 shows the basic principle of reflection seismic method. An acoustic pulse generates a spherical expanding wave front. At each point we have a ray trajectory perpendicular on the wave front (showed with arrows in figure). When the wave front hits a boundary (marked with thick black line in figure) some of the energy will be reflected, and some transmitted. A boundary is the line between two layers of different acoustic impedance. The reflected energy will be registered by seismic receivers, and this is the basis of reflection seismic. The reflection seismic will give information about the two-way travel time, in addition to the amplitude of the reflected energy (Hart 2000).

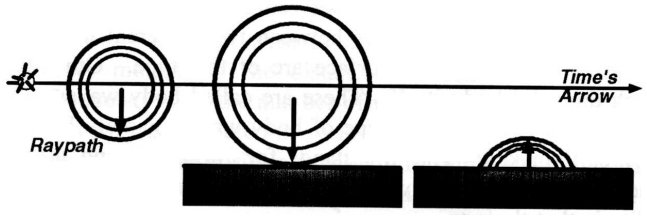

Figure 3-1: Illustrated principle for reflection seismic (Hart 2000).

In seismic surveys the two most important waves to be used and interpreted are the compressional (P-) wave and shear (S-) wave. These waves are called body waves because they propagate through the interior of an elastic body. The velocities of the body waves are given by the formulas

$$\alpha = \left(\frac{K + \frac{4}{3}\mu}{\rho} \right)^{1/2},$$

$$\beta = \left(\frac{\mu}{\rho} \right)^{1/2}$$

where α is the P-wave velocity, β the S-wave velocity, and ρ is the density, μ the shear modulus and K the bulk modulus of the medium the wave propagates through.

When an incident compressional plane wave hits a layer boundary the wave is not just partitioned into reflected and transmitted compressional wave components, but also reflected and transmitted shear wave components. Hence, a fraction of the incident P-wave is converted into a reflected S-wave (see Figure 3-2). In marine seismic acquisition the source will only generate P-waves (S-waves are not transmitted in the water column because the shear modulus is zero), so the S-wave information obtained will be converted waves created at the boundaries (Yilmaz 2001).

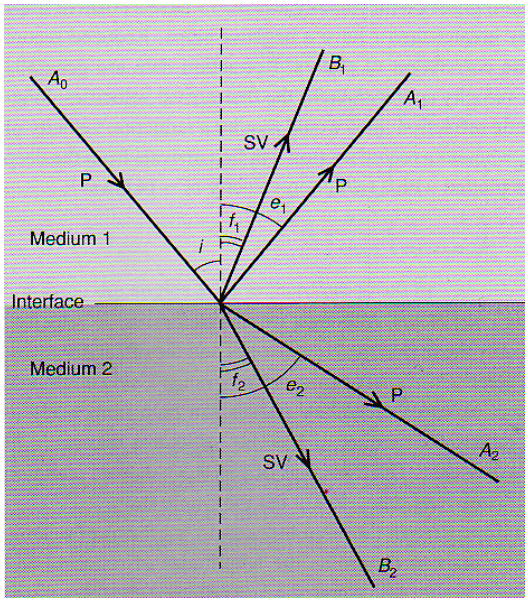

Figure 3-2: Waves generated at an interface between two elastic media by an incident P-wave. The incident P-wave has amplitude A_0 and angle of incidence *i*. The reflected P- and SV-waves have angles of reflection e_1 and f_1 and amplitudes A_1 and B_1, respectively. The transmitted P- and SV-wave have angles of refraction e_2 and f_2 and amplitudes A_2 and B_2, respectively (Fowler 2005).

3.1.2 Marine survey sources

Different kinds of sources can be used in marine survey, and the choice of source depends on the resolution and scale of the image. For imaging of the top kilometers of the subsurface the most used source is several air guns of different volumes in a “tuned array”.

An air gun is a device that discharges air under very high pressure into the water. Pressures up to 10 000 psi are used, but 2000 psi is most common. The two chambers are filled with high pressure air that enters at the top left of the upper chamber, and is passed into the second chamber through an axial opening in the “shuttle”. The latter is held in closed position by the air pressure. To fire the gun, the solenoid at the top triggers a valve that opens the ports and the high pressured air from the lower chamber is released into the water (see Figure 3-3a) (Sheriff & Geldart 1995).

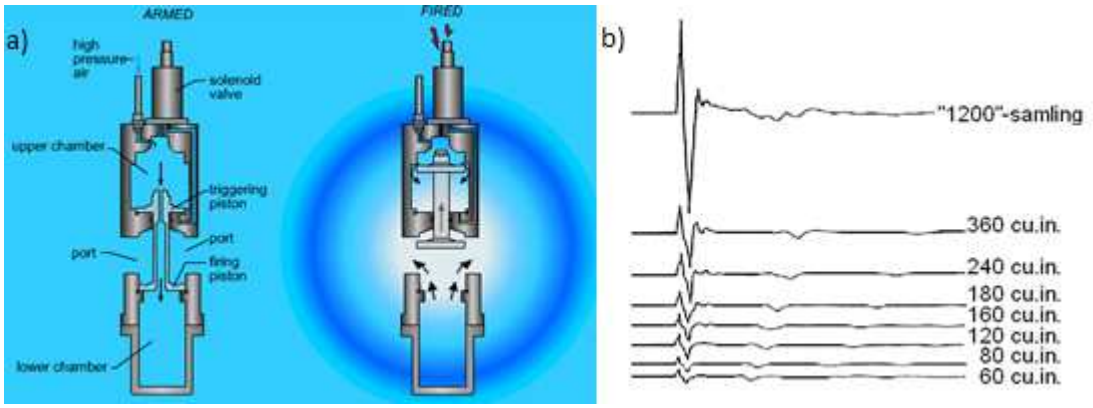

Figure 3-3: a) Armed and fired configuration of an air gun (Mjelde 2010). b) Air gun signature of 7 guns with volume ranging from 60 cu.in. to 360 cu.in. and with a total of 1200 cu.in. The source signal interferes constructively, while the bubble pulse interferes destructively. Therefore the source/bubble pulse ratio improves (Mjelde 2003).

The waveform emitted by a single air gun oscillates because of the bubble effect. The bubble effect applies to all sources that injects high pressure air or gasses into water. The bubble pulse is the oscillating pulse that forms when hydrostatic pressure makes the air bubble expand and collapse alternatingly. By increasing the number of air guns of different volumes, the bubble pulse will interfere destructively and the source signal will interfere constructively, giving a better source/bubble pulse ratio (see Figure 3-3b), also the directivity is increased. The directivity is described as how much energy which is propagated in a given direction. By different placement of the sources the energy can be focused in a fixed direction. Directivity applies to both the sources and the receivers, and is given by various factors like the number of air guns and geophones/hydrophones, the distance between them, volume and sensitivity. Up-going energy from the source which is reflected by the sea surface is called a ghost multiple, and can represent a problem in marine seismic. We get a better source signal if we achieve constructively interference between the direct down-going wave and the ghost multiple, on the source and receiver side, by adjusting the depth. The receiver has to be placed a bit deeper than the source, since attenuation makes the up-going signal more low-frequent (Sheriff & Geldart 1995).

3.1.3 Marine survey receivers

In conventional marine seismic surveys, hydrophones are used in streamers to record the seismic signals. A hydrophone consists of two circular piezoelectric plates with opposite polarities, placed above one another in a bronze cylinder. Pressure variations from seismic waves will be summed and converted to an electric signal, while acceleration related movements will be cancelled (see Figure 3-4) (Sheriff & Geldart 1995).

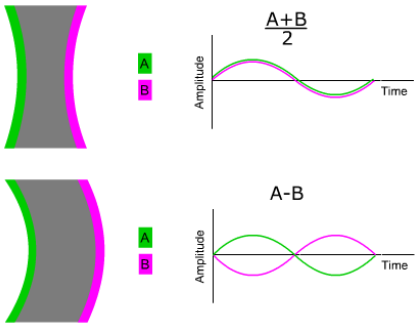

Figure 3-4: Hydrophone (Mjelde 2010).

In the seismic surveys described in this thesis, geophones are also used as receivers. The most common geophone is the "moving coil" system (see Figure 3-5). It consists of a cylinder-shaped magnet with a circular opening. Inside this opening there is a coil. When a seismic wave disturbs the ground the magnet will move with the ground but the coil will remain still, and a current in the coil, proportional with the relative velocity between the coil and the magnet, will be induced (Mjelde 2010).

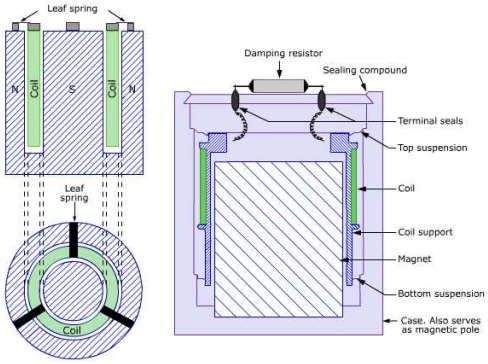

Figure 3-5: Geophone (Mjelde 2010)

3.1.4 OBC acquisition

In Ocean Bottom Seismic, or marine 4-C, the receivers are placed in ocean bottom cables positioned at the seafloor. A vessel tows the sources (air guns), and shoots in a grid depending on the volume to be mapped (see Figure 3-6a). The receiver components are 4C-receivers, receivers with 4 components; three orthogonally mounted geophones with gimbal-suspension and one hydrophone (see Figure 3-6b). These kinds of receivers measure both P- and S-waves when placed on the sea bottom. Two of the geophones will be deployed in the horizontal direction perpendicular to one another; this is because even though the wave direction is vertical the particle motion of the shear waves is horizontal. The vertical geophone measures the vertical particle motion of the compressional waves to complement the recording of the pressure wave by the hydrophone. The final product of a four-component (4-C) seismic survey is a pair of P-wave and S-wave volumes. The P-wave data are associated with P-to-P reflections (PP/PZ), and S-wave data with P-to-S converted waves (PS) (Yilmaz 2001).

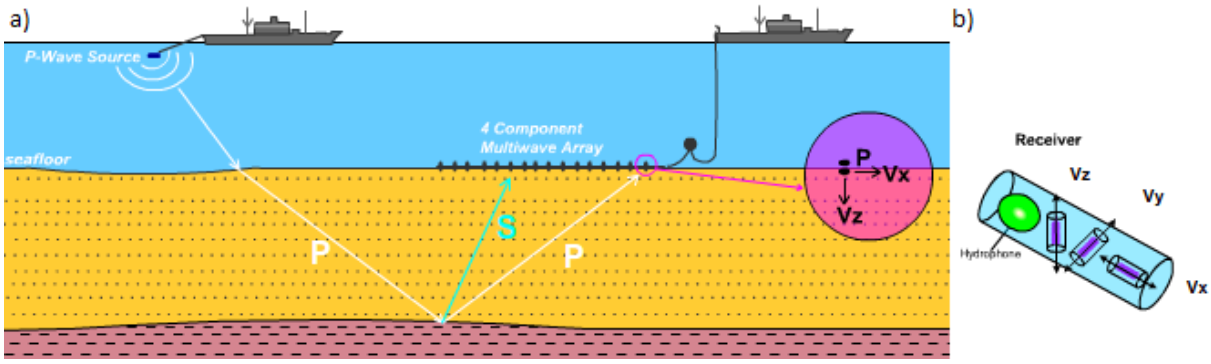

Figure 3-6: a) Geometry of a OBC/4-C seismic survey, and rays associated. b) A 4-C receiver (Mjelde 2008).

Although 4-C is a much more expensive and challenging seismic survey to perform than regular marine seismic, the S-wave data collected has potential to increase knowledge about the subsurface and hydrocarbon reservoir. The known potential applications of converted-wave data are:

- Imaging beneath gas plumes,
- Imaging beneath salt domes,
- Imaging beneath basalts,
- Delineating reservoir boundaries with a higher S-wave impedance contrast than P-wave impedance contrast,
- Differentiating sand from shale,
- Detection of fluid phase change from oil-bearing to water-bearing sands,
- Detection of vertical fracture orientation,
- Mapping hydrocarbon saturation,
- Mapping oil-water contact.

Especially important is the fact that while P-wave data often clearly show oil-water contact, the S-wave data will show the top- and base- reservoir unit instead. However, the S-wave data is not a replacement for the P-wave data, but is instead complimentary (Yilmaz 2001).

When recording an ocean bottom cable or 4-C survey, the receivers used are of gimbaled type; as such, the vertical geophone is guaranteed to measure the vertical component of the particle motion. The two horizontal components measure the particle motions in two orthogonal directions, and are intended to be oriented in such a way that one of them is aligned in the direction of the receiver cable (See lower right corner of Figure 3-7). However, the horizontal receivers are not guaranteed to be in the inline and crossline positions in a real survey. As a result of this the horizontal geophones associated with a common-shot record measure particle motion in arbitrary directions instead of the desired common inline and crossline directions. This is caused by seabed conditions such as currents, unconsolidated sediments and the roughness of the seabed surface. For the recording geometry for a 4-C OBC survey two or more cables are laid down on the seabed parallel to each other and the data are recorded using a conventional seismic vessel with source

locations aligned in the direction perpendicular to the receiver lines (see Figure 3-7) (Yilmaz 2001).

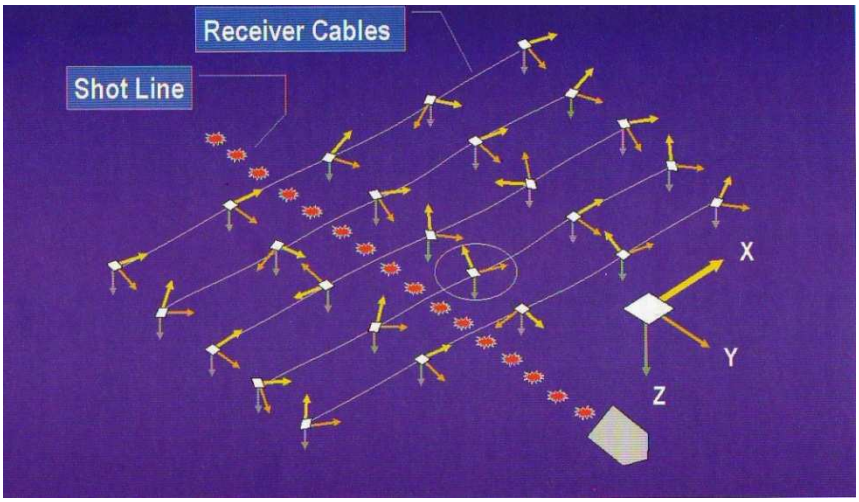

Figure 3-7: An ocean bottom cable layout of a three-component geophone system

3.1.5 VSP acquisition

Vertical Seismic Profiling is a measurement procedure where a seismic signal is generated at the surface, and then recorded by geophones placed at various depths in a drilled well. The geophones record both up-going and down-going waves. There are three types of VSP-surveys; 0-offset, where the source is placed close to the borehole, single offset, where the source is placed at a significant distance from the borehole, and multi offset (or walk-away), where the source is moved away from the borehole while firing. In deviated boreholes, walk-away VSP (see Figure 3-8) is used (Hardage 2000).

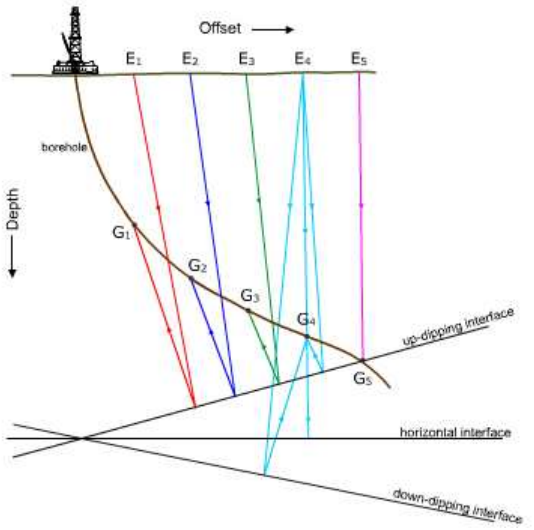

Figure 3-8: Simple illustration of a walk-away, vertical incidence VSP survey in a deviated well (Mjelde 2009).

Zero-offset VSP is used to match seismic events to specific interfaces. Because the depth of the well is known accurately, time-depth relationships are established precisely, and thus reliable reflection identification and subsurface seismic velocities are obtained. Zero-offset VSP is also used to identify multiples and other events, and to study the reflections from below the bottom of the borehole. Offset and walk-away VSP is used to look for changes laterally away from the borehole, such as faults, reefs, salt domes and dipping reflectors. The greater resolution of the VSP may help discover small faults, stratigraphic changes, and thin

reservoir sands. Detection of reservoir just missed by the borehole is especially useful where hydrocarbons indicators are observed from previous surveys. The use of three-component geophones also gives information of the direction from which the energy approaches the geophone and also helps distinguish converted wave energy. VSP can also be used for calculating absorption and acoustic impedance logs, correlation between logs and surface seismic, lithology prediction, anisotropy measurements, monitoring of the reservoir and so on (Sheriff & Geldart 1995, Hardage 2000).

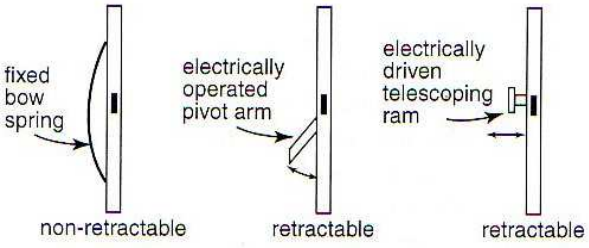

Figure 3-9: Three general types of geophone locking system (Hardage 2000).

The sources used in marine VSP are usually air guns, which are described in chapter 3.1.2. The receivers used in VSP are typically three-component geophones, that measures both P- and S-waves. Because of the high-pressure environment in a deep well, the VSP geophone assembly is usually 25 to 30 times longer and perhaps 500 times heavier than a typical surface geophone. It is also important for the VSP geophone to have some kind of locking tool, to insure that the geophone is rigidly clamped to the borehole wall. There are three general types of geophone locking, one non-retractable and two retractable (see Figure 3-9). The non-retractable were used in early designs, but now only a few of these are still in use. This is due to the fact that these geophones often can get stuck in the borehole, resulting in an expensive fishing job. Therefore the retractable geophone locking systems are preferred. The most popular of these has motor driven pivot arms that moves outward until it meets resistance and then applies a small force against the borehole wall to keep it in place (see Figure 3-10). The lateral force is increase with the slacking of the cable, so that the tool's weight causes and additional force about the fulcrum point of the extended arm. This principle is called "locking by vertical wedging".

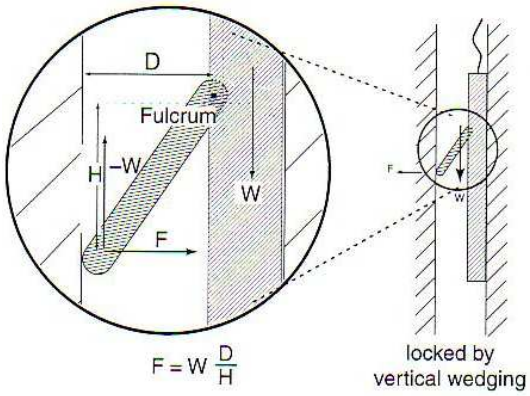

Figure 3-10: Concept of coupling VSP geophone to a formation by vertical wedging (Hardage 2000).

Figure 3-11 shows an ideal VSP borehole geophone for oil and gas exploration, and the desired characteristics. When conducting a VSP survey tube waves, interface waves propagating along the borehole wall, are generated. To reduce the tube waves reflected the geophone should have pointed ends. The diameter of the geophone package also determines how much of the tube wave's amplitude is reflected, and the geophone should therefore have a small diameter. As mentioned above, a retractable arm increases the geophone to borehole coupling and makes it easier to place at the exact position desired. To avoid retraneous coupling resonances the geophone should have minimum mass and maximum contact area with the borehole wall. This means that an ideal geophone should have a small length and low weight. As mentioned in chapter 3.1.4, receivers with three-component geophones that are placed in an XYZ-orientation measures both the P- and S-waves. In a VSP survey, where we wish to measure both P- and S-wave this is therefore an important criteria of the geophone tool. We also need a vertical geophone for callibration, to make sure that the three-componend geophones are placed in the right orthogonal positions. For the same reasons we also need an orientation measuring system. In addition to the above characteristics we need a mechanism to determine the geophone-to-formation coupling, a downhole digitizing of all data sent uphole, and a connection to the other VSP geophone systems.

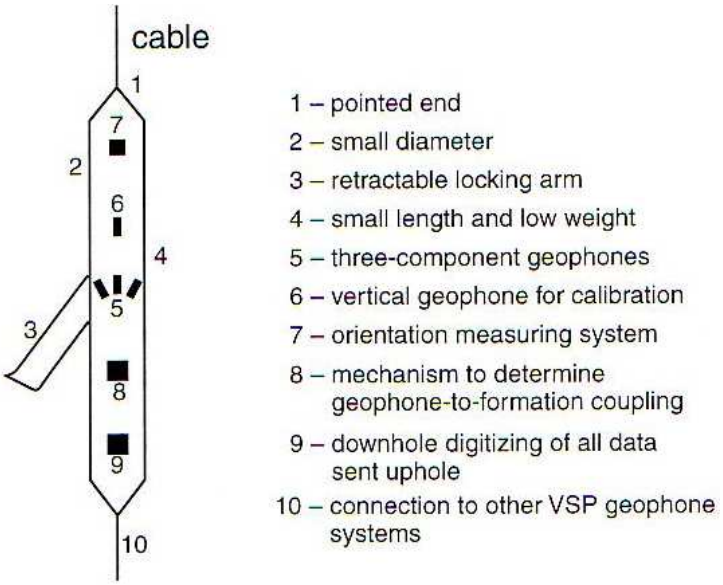

Figure 3-11: Desired characteristics of a VSP borehole geophone (Hardage 2000).

The condition of the borehole is also important in VSP surveys. The collection of VSP data in vertical wells are both easier and less expensive than that of deviated wells. This is mostly due to uncertainties about the position of downhole geophone relative to the energy source, and because the source will have to be moved to several different locations during the course of data recording. Casing and cementing conditions of the borehole is also important. In order to get a good geophone to borehole wall coupling, the locking system described above as well as the condition of the borehole wall is important. Figure 3-12 shows the preferences of the borehole wall. Cased wells are desirable because the borehole is then protected against sloughing and differential pressure sticking problems. In cased wells, VSP can be performed several times due to the secure and protected environment. However, a cased well needs some kind of medium between the casing and the borehole wall to ensure good coupling. The best medium is cement, but sometimes uncemented casing will also suffice. The only casing situation that gives poor VSP data is when multiple

casings are present and the casing strings are not rigidly cemented together, and to the borehole wall (Hardage 2000).

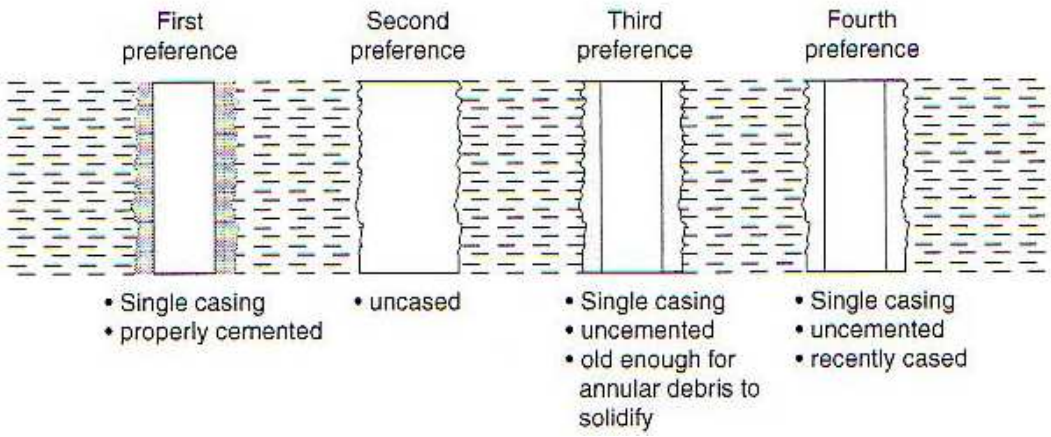

Figure 3-12: Common borehole conditions shown in the order of their preference for VSP data recording (Hardage 2000).

3.2 Seismic processing

In order to read and interpret seismic data, the data must first be corrected for the different source-receiver distances involved, noise must be reduced etc. This treatment or analysis of the data is called processing. Good processing requires understanding in the concepts of both data acquisition and interpretation.

3.2.1 MCS processing

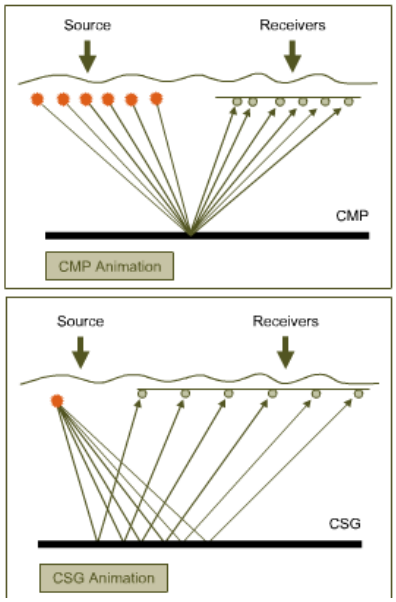

Figure 3-13: CMP and CSG gather of a seismic survey. (Mjelde 2003)

Editing: Editing involves removal of traces that are either dead or contains a lot of noise, for example due to technical problems in the receivers. This will affect the signal/noise relationship negatively by stacking of the data. Bad traces are removed early in the processing sequence, and replaced with interpolated traces, or set equal to zero. Editing also involves reversing the polarities if required.

Sorting from common shot gather (CSG) to common midpoint (CMP): Traces in raw dataset are usually sorted after common shot number. For each shot several recordings will be made on different receivers, and as the shooting vessel moves, shooting at regular intervals, the same reflection points will be recorded by different

receivers (see Figure 3-13). Before stacking of the data we therefore sort the data in to traces with the same common midpoint (Sheriff & Geldart 1995).

Gain recovery: When a shot is fired a pressure wave is generated. At the shot-time the energy is collected in one point, which expands spherically with time in a homogeneous medium like water. With increasing distance the energy will decrease due to geometrical spreading. This loss of energy needs to be corrected in the processing of the data. Energy loss can also be a result of the subsurface not being a perfect elastic medium, so part of the energy will be absorbed. In addition energy loss will happen when the wave hits a boundary, because the wave is split into reflected and transmitted waves. By adjusting the amplification factor the difference in amplitude with increasing time diminishes, and the different arrivals in depth or travel-time will be easier to compare.

Frequency and velocity filtering: The receivers measure both reflections and all kinds of noise. The latter can for instance be high frequent noise, like machine noise, or low frequent noise from the sea surface (waves). By applying a frequency filter this noise can be removed. The different kinds of frequency filters used are low-pass (removes low frequent noise), high-pass (removes high frequent noise), band-pass filters (removes both low and high frequent noise), and notch filters (removes a specific frequency) (see Figure 3-14). To apply a frequency filter the data must be converted from the time domain to the frequency domain through a Fourier transformation. After filtering the data is then converted back to the time domain trough an inverse Fourier transformation. The same principle can be used to convert the data into the frequency-wavenumber (f-k) domain. In this domain different velocities will have different dips, and we can therefore remove certain velocities by using a dip filter. This is especially effective when it comes to removing the seabottom multiple in regular marine seismic, which has a lower velocity than the deeper reflections. Also by converting to the τ-p domain we can use a hyperbolic or linear (”slant stack”) radon transformation to discriminate between real arrivals and multiples.

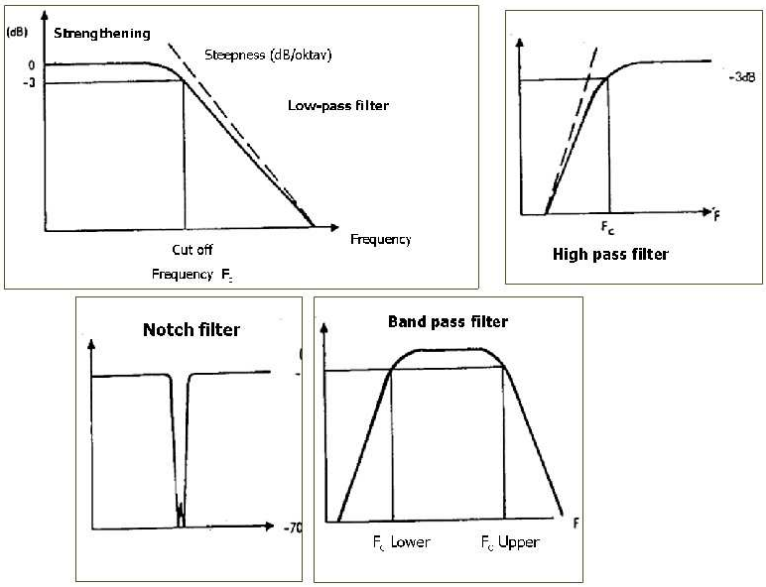

Figure 3-14: Frequency filters. (Mjelde 2003)

Deconvolution: Convolution using an inverse filter is a mathematical operation that separates different signals. Deconvolution is used to remove unwanted arrivals in our data, and to compress the signal. Spiking deconvolution compresses the signal and reduces the

bubble pulse. Predictive (gapped) deconvolution is applied to reduce the multiple effects, assuming that these are periodical, while the primary reflections will arrive arbitrarily. Deconvolution is often applied both before and after stacking (Sheriff & Geldart 1995, Mjelde 2003).

Velocity analysis: One of the reason we perform seismic survey is to determine the velocities of the subsurface. We operate with different kinds of velocities. The average velocity is given by the distance the wave has propagated divided by the travel-time,

$$\overline{V} = \frac{Z_n}{T_n}.$$

Basing the ray path on the Fermat's principle (the ray follows the shortest path in time), the rms-velocity (root-mean-square) is given by

$$V_{rms,n} = \left[\frac{\sum_{i=1}^{n} v_i^{\,2} t_i}{T_{0,n}} \right],$$

where t is the two-way travel-time for layer i, $T_{0,n}$ is the travel time for zero offset and v_i is the constant interval velocity for layer i. The difference between (assumed) vertical two-way travel-time and observed travel-time is called the normal move-out (Mjelde 2003).

Reflections are shown in the seismogram as hyperbolas. Velocity analysis is choosing the velocities that flatten the hyperbolas, and gives a straight line in the NMO-correction. These velocities are called the stacking velocities. By using a simplified velocity model with constant velocities between the surface and the reflecting layers, we get useful results that can be used to determine a simplified geological model. The relation between arrival time and offset for a plane reflector with constant velocity is a hyperbola, and the distance to the reflector can then be calculated with the help of the arrival time, if the velocity is known. The normal move-out hyperbola gives us the difference between observed and calculated travel-time, which increases with increasing offset. The curvature of the hyperbola gives the seismic velocity in the chosen layer. The stacking velocity can be found for each point on the zero offset travel-time curve, and increases normally with depth. By velocity analysis we estimate the velocity that best fits the observed move-out.

NMO-correction: The distance between source and receivers results in variations of the travel-times of the reflection, and this is shown as a hyperbolic curve on the seismogram, as explained above. This difference is called the normal move-out (NMO). NMO-correction consists of applying the velocities found in the velocity analysis to correct the CMP for NMO. The primary reflectors will now be horizontal and the amplitude pulse from the same reflectors will have the same two-way-travel time, and can be stacked together (Mjelde

2003, Yilmaz 2001). The difference in travel time ΔT between reflected arrivals at offset distance x and at zero offset is given by

$$\Delta T = t_x - t_0 \approx \frac{x^2}{2V^2 t_0},$$

where V is the velocity of the layer (Keary *et al* 2002).

Muting: NMO-correction implies differential stretching of the traces. The stretching is very large for the shallow far-offset arrivals. This distorted part of the seismogram is removed through muting (the part is set to zero).

Stacking: During stacking all traces with the same common midpoint will be gathered to one trace. The primary events will then be summed in phase (constructively), and other coherent noise will be summed destructively. The signal to noise ratio will be improved, while coherent noise like multiples will be reduced considerably.

Migration: When the data contain dipping or diffracted events, migration must be applied to get a correct picture of the subsurface. Migration is either done in time or depth. Time migration is used to place events at their correct position in time below the surface, while depth migration must be used to place events at the correct depth (from CMP to common depth point, CDP). Migration can be applied pre-stack and post-stack. Pre-stack migration is very time consuming, and is therefore often replaced by dip move-out (DMO) corrections.

3.2.2 OBC processing

When processing OBC/4-C data we have to include the fact that we have two 3D-cubes to process; the PP/PZ-cube and the PS-cube (see Figure 3-15). For the PP-cube we first calibrate the vertical geophone component Z(t) and sum it with the hydrophone component P(t), to obtain the total PP data. Then a vertical time shift equal to the water depth divided by water velocity must be done to bring the receivers from the seabed to the same datum as the shots. If the water depth is greater than 100 m, the vertical shift may not be valid, and the datuming may have to be done by wave-equation datuming. Except for this the PP-data can be processed like regular 3-D land seismic. The pre-stack processing includes geometric spreading correction, deconvolution, refraction and residual statics corrections to account for the variations in the seabed geometry, velocity analysis, NMO and DMO corrections. Then the post-stack processing includes deconvolution, the previously mentioned time-variant filtering, and migration (Yilmaz 2001).

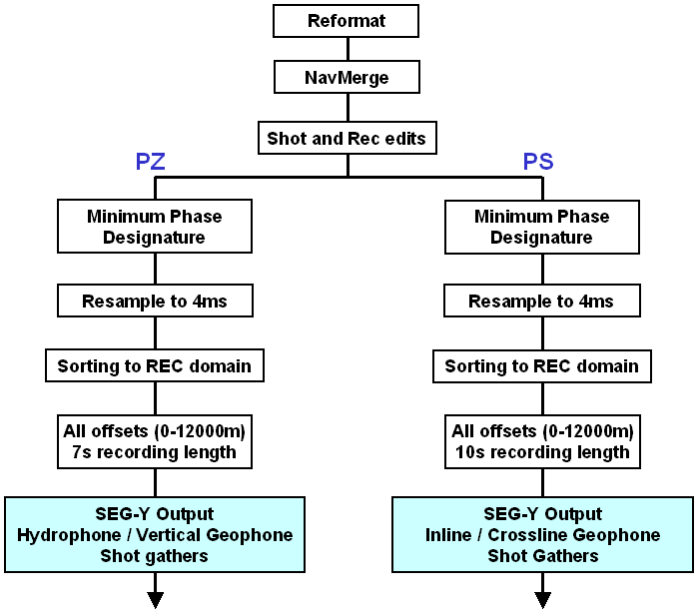

Figure 3-15: Block diagram of the initial processing flow for both PZ and PS components (PGS Geophysical report 2005).

The two horizontal geophones containing the converted wave data are desired to be in a constant inline and crossline direction. However, in practice this is hard to achieve, and the geophones are therefore oriented in arbitrary orientations. We need to realign the horizontal geophones associated with one common-shot gather to a common orientation. The recorded perpendicular components are rotated from the field coordinates to a radial-transverse coordinate system. Normally, the transverse component does not carry any relevant energy after rotation, except in the case of azimuthal anisotropy. So the transverse component is just used in the process of investigating and compensating for the shear-wave splitting (PGS Geophysical Report 2005).

The PP-data was sorted into CMP gathers, the PS-data however has to be sorted into common conversion point (CCP) gathers, such that the traces in the gather has the same conversion point. Binning the PS-traces into CCP gathers requires knowledge about the conversion point coordinate. This coordinate is depended on the depth to the reflector and the P-/S-wave velocity ratio (α/β). The PS-data has a non-hyperbolic move-out, so regular velocity analysis cannot be used. Instead we use the velocities found from velocity analysis of the PP data, the conversion point coordinate, and choose values for the P-/S-wave velocity ratio, instead of the S-wave velocities. DMO correction has to be performed on PS-data even if we don't have any dipping reflectors, due to the fact that reflection-point dispersal happens even on a flat reflector. The DMO impulse response associated with PS data will be different in shape compared to that of PP data. The symmetric form of the impulse response in PP data, will have an asymmetric form in PS data, and will be shifted laterally to the CCP location.

Migration of the PS data can be conceptualized as a summation along a travel-time trajectory associated with a coincident source-receiver pair at the surface and a point

diffractor at the subsurface. The difference between zero-offset PP and the PS diffraction summation trajectories is in the velocities. Once the velocity field has been established the PS-stack can be migrated using any of the algorithms for regular P-wave migration. In the case of seismic anisotropy, the transverse component must go through an anisotropic velocity analysis, DMO-correction and migration (Yilmaz 2001).

3.2.3 VSP processing

After some trace editing, processing of the VSP starts with the separation of the downgoing waves from the upcoming waves (see Figure 3-16 and Figure 3-17). One separation technique is based on f-k filtering. Since the upcoming and downgoing events have opposite dips, the downgoing waves can be suppressed with an f-k dip filter, thereby leaving only the reflection and associated multiples that constitute the upcoming waves. An alternate approach to extracting upcoming waves is to use median filtering. Median filters do a type of data smoothing. Assuming a sequence of statistical samples having variable magnitudes, and arranging these values so that they increase in magnitude, the median value of the statistical data samples is the sample in the (N+1)/2 position of the sequence. Median filtering rejects noise bursts and any event that is not flat. To get the downgoing waves we apply the median filter to the VSP data set with flattened downgoing waves. This result can then be subtracted from the input to obtain the upcoming events. The last step is then unflattening of the data.

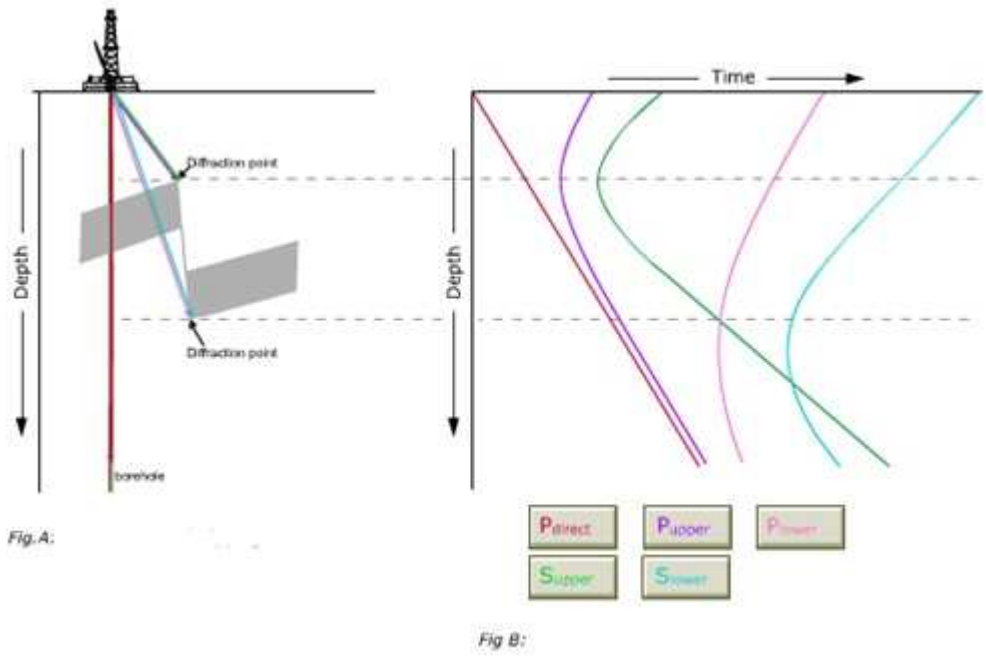

Figure 3-16: A: 0-offset VSP with dipping interfaces. B: Travel-time curves for the model in A (Mjelde 2009).

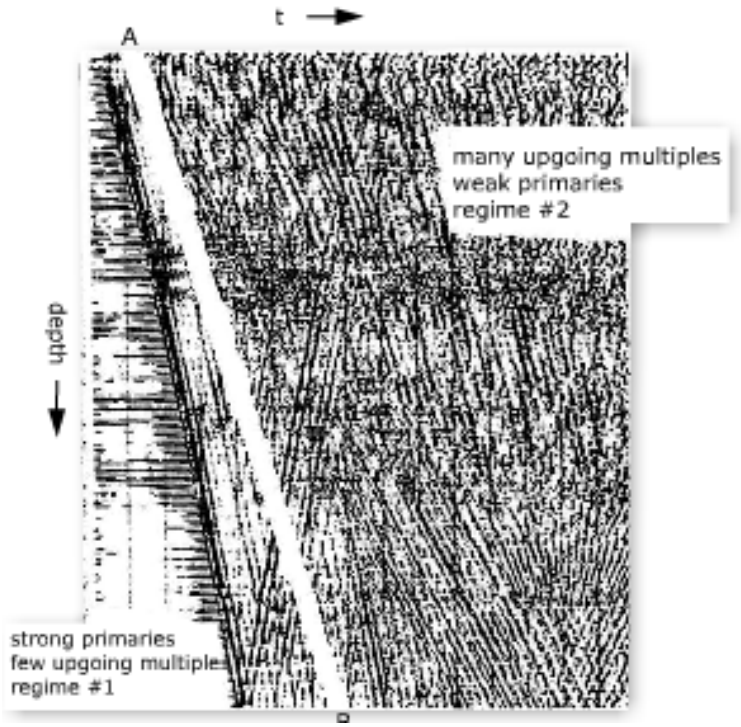

Figure 3-17: A VSP data set can be divided into two regimes by the line AB. Regime 1 contains strong primary reflections and a few multiple reflections. Regime 2 contains weak primary reflections and numerous multiple reflections. The position of AB is arbitrary and varies from one VSP data set to another (Hardage 2000)

The next step in VSP processing involves datuming all receivers to the well head. The static correction is the same as correcting each trace by an amount equal to the one-way travel-time down to the corresponding receiver location. The static correction is followed by deconvolution and filtering. The deconvolution operator is designed from either the upcoming or the downgoing waves. Usually the downgoing waves are used to design the deconvolution operator, due to the fact that downgoing waves are stronger than upcoming waves. The deconvolution operator is then applied to the upcoming wave profile. The last step involves stacking the traces. Stacking normally includes a narrow corridor along the region which upcoming and downgoing waves coincide. To a large degree, corridor stacking prevents the multiples that do not merge with the downgoing wave path from being stacked in. For nonzero-offset data we must also correct for move-out resulting from the offset separation between the well top and the shot location.

When there are dipping interfaces, the upcoming wave profile must be migrated; this includes a VSP-CDP transform of the data. In this transformation, the amplitudes on a single VSP trace are mapped onto several traces on the x-t plane, where x is the lateral distance of reflection points from the borehole. The resulting section (x,t) consists of traces similar to the traces of a migrated zero-offset section. This transformation requires knowledge of the velocity-depth model around the borehole, since we must determine the location of the reflection points in the subsurface to perform the mapping (Hardage 2000, Yilmaz 2001).

3.3 Principles for seismic interpretation and ray-trace modeling

Both seismic interpretation and ray-trace modeling gives a better understanding of the subsurface, in this chapter the basic principles for seismic interpretation and ray-trace modeling will be explained.

3.3.1 Seismic interpretation

Interpretation involves determining the geologic significance of the seismic data, based on basic geophysical principles. In seismic interpretation we assume that the coherent events seen on seismic records or on processed seismic sections are reflections from acoustic impedance contrasts in the earth, that these contrasts are associated with bedding that represents geologic structure, and that seismic detail (wave-shape, amplitude, and so on) is related to geologic detail, that is, to the stratigraphy and the nature of the fluids in the rocks (Sheriff & Geldart 1995).

When interpreting seismic data, geological boundaries, or horizons, are picked using interpretation software, like Petrel. The horizons are picked following consistently either a through or a peak, which represents respectively a decrease or increase in acoustic impedance. It is important to keep in mind the polarity and know whether the signal is in zero phase or minimum phase. Faults are also picked, and drawn onto the seismic data. By picking the horizons and faults on inlines and crosslines of the 3D-cube and then gridding the horizon and fault lines into surfaces, which are then converted from time to depth, a geological model with the right depth coordinates is made. This model can then be used for further interpretation work in the area, or be used to locate hydrocarbons. When interpreting seismic, there is, most of the time, no exact interpretation which is correct. What makes a good model is consistency, rather than correctness. So in order to make a good interpretation, the interpreter must have a good knowledge of geology and the different structures to be found in the seismic data, in order to make a consistent and reasonable interpretation. Having information about the geological history of the area is also important for the interpretation (Sheriff & Geldart 1995).

When interpreting seismic we extract nonstructural information from the seismic data; this is called seismic stratigraphy or seismic facies analysis. Facies refers to the sum of total features that characterizes the depositional environment of the sediments. Facies involves, among other things, the sedimentary structure, the form of bedding, and the shape, thickness and continuity of sedimentary units. Seismic facies concern the distinctive characteristics that make one group of reflections look different from another. For example parallel reflections suggest uniform deposition on a stable or uniformly subsiding surface, whereas divergent reflections suggest variations in the rate of deposition from one area to

another or else gradual tilting (see Figure 3-18). Chaotic reflections suggest either high depositional energy, variability of conditions during deposition, or disruption after deposition. A reflection-free interval suggests uniform lithology, such as massive carbonates or relatively homogeneous marine shale. Reflection terminations such as onlap, downlap and toplap, are also important in seismic facies analysis (see Figure 3-19) (Sheriff & Geldart 1995).

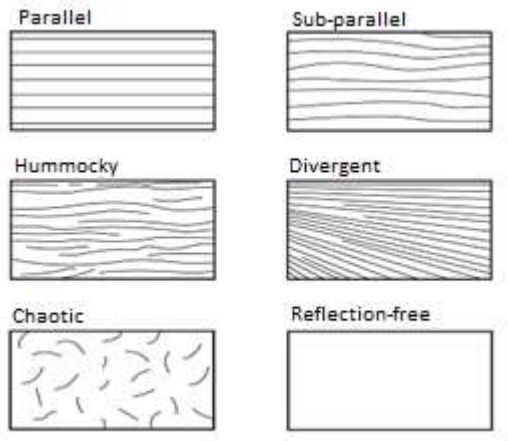

Figure 3-18: Reflection configuration of different seismic facies (Michum et al., 1977).

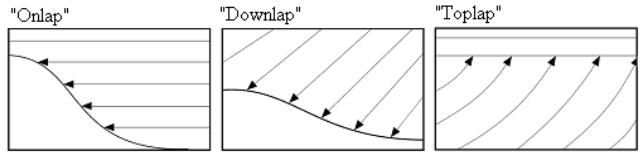

Figure 3-19: Reflection terminations of sedimentary strata against other sequences (Mitchum et al., 1977)

The geology of the North Sea has been subjected to extension and consists of a lot of faulting; we will therefore look closer on the characteristics of faulting. In seismic reflection events, ideally, terminate sharply as the point of reflection reaches the fault plane and then they resume in displaced positions on the other side of the fault. In addition, ideally, the reflection has a sufficiently distinctive character that the two portions on opposite sides of the fault can be recognized and the fault throw determined. In practice however, diffractions usually prolong events, so that the locations of the fault plane are not clearly evident, although often faults do show clearly as a reasonably sharp reflection terminations on migrated lines that are roughly perpendicular to the faults.

Faults are produced when unbalanced stresses exceed the strength of the brittle rocks. The type of fault produced depends on whether the horizontal or vertical stresses are the larger. Normal faults are created when the maximum compressive stress is vertical and the minimum horizontal. When the maximum compressive stress is horizontal, thrust (reverse) faults are created. When both the maximum and minimum compressive stress is horizontal strike-slip faults are created (see Figure 3-20). Normal faults are often created in areas

subjected to extension, while reverse faults are often created in areas of compression (Sheriff & Geldart 1995).

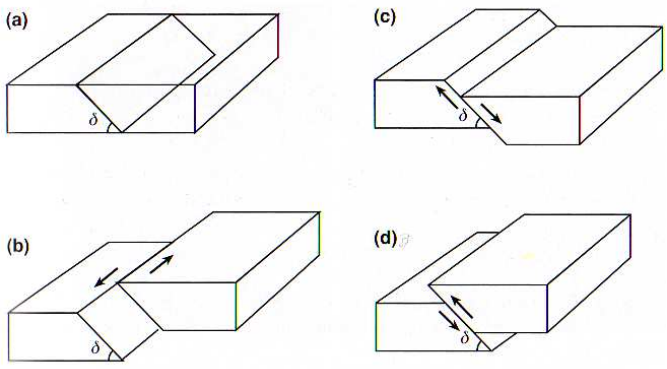

Figure 3-20: Fundamental types of faults and their various names. (a) A block model of a fault before any motion has taken place; δ is the angle of dip. (b) A strike-slip fault; δ is often near 90°. (c) A normal fault; generally 45°<δ<90°. (d) A reverse or thrust fault; often 0°<δ<45°. Arrows show the slip vector, the relative motion between the two sides of the fault. The slip vector always lies in the fault plane. (Fowler 2005)

3.3.2 Ray-trace modeling

When velocities in the subsurface varies laterally, tracing of ray paths through a model obeying Snell's law at each velocity change, is one way of developing an understanding of how a seismic section relates to a portion of the earth where velocity complications exist. By a trial-and-error basis the ray paths can be modeled, and a synthetic seismogram can be formed. This ray tracing can help understand the reflected and transmitted pressure and converted waves (Sheriff & Geldart 1995).

In this thesis a ray-trace model of a VSP-survey will be created and used to help understand the geometry of this kind of survey, as well as the wave conversion taking place in the subsurface. The synthetic seismogram created by the modeling will be compared to the real VSP seismic, to improve the model and to understand the velocity changes in the subsurface better.

3.4 Seismic resolution

Seismic resolution can be defined by the smallest distance in time or depth between two layer boundaries of which they will be displayed as separate reflections (vertical resolution), or by the smallest distance between two events of the same depth of which they will be displayed as separate events (horizontal resolution). ”Resolution” is also often used about the possibility for an object being visible or present (Sheriff & Geldart 1995). Both the vertical and horizontal resolution depends on the signals bandwith (Yilmaz 2001).

4 Data background - acquisition and processing

4.1 OBC acquisition

An Ocean Bottom Seismic survey was performed by Petroleum Geo Services (PGS) in August 2004 to improve the structural imaging of previously acquired surface seismic. The main objectives of this survey were to improve the structural imaging of faults and geophysical boundaries with large degree of accuracy, continuity and focus, and to determine lithology from seismic. The survey was also to be included in a 4D (time-lapse) study of the seismic area.

The 3D survey covers an area of 22 km^2 south of the Snorre A platform and consists of 3 swaths with a total of 8 receiver lines of 8 km length each (see Figure 4-1 and Figure 4-2). The cable separation was 400 meters and the cable length 8 km. The water depth ranges between 280 and 306 m at the receiver stations. Each swath consists of a total of two to three receiver lines spaced 400 m apart. For each swath 28 to 34 source lines with a spacing of 50 m have been acquired (see Figure 4-3). The source line lengths were 15 km (PGS Report 2005). More detailed acquisition parameters are given below in Table 4-1.

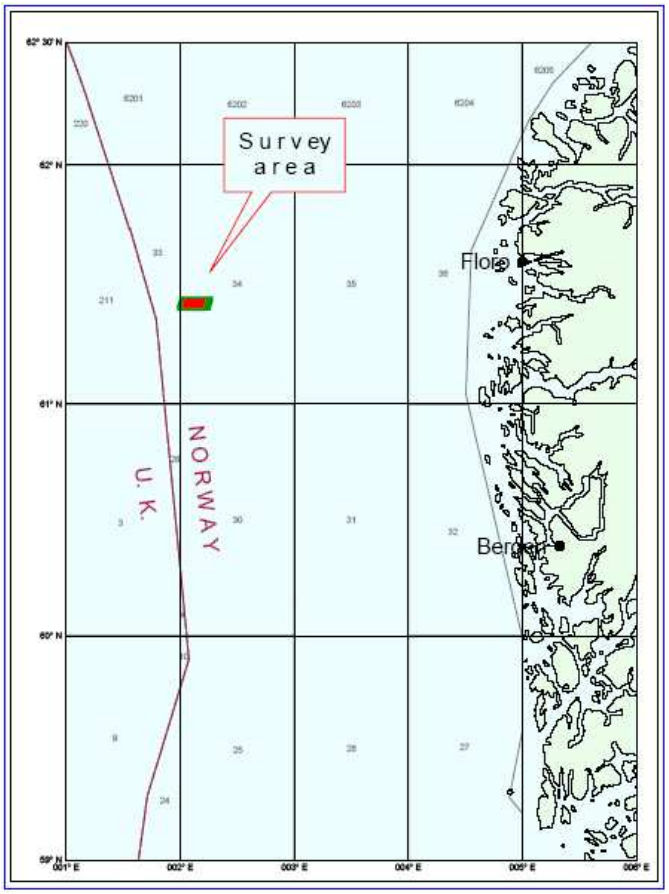

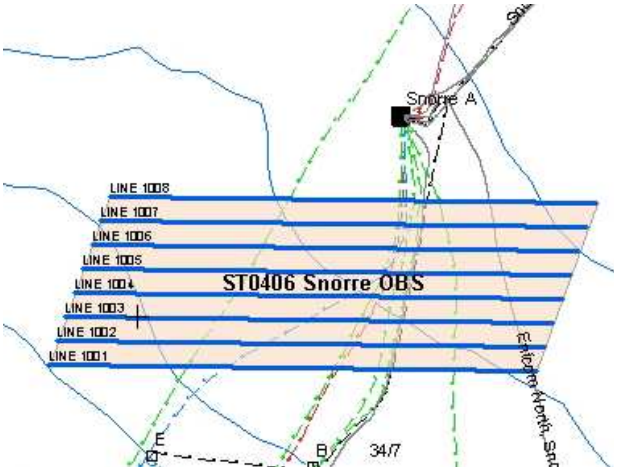

Figure 4-1 (left): Survey area – overview (PGS Report 2005)

Figure 4-2 (above): OBC survey lines (PGS Report 2005).

Table 4-1: Acquisition parameters (Source, Cable, Receivers) (PGS Report 2005).

Source	
Source type	Bolt Guns
Number of sources	2
Source seperation	50 m
Operation pressure	2000 psi
Volume (per source)	3090 cu.inch
No of subarrays (per source)	3
Subarray seperation	8 m
Source depth	6 m
Pop interval	25 m
Shot sequence	Source to the North of the sail line to fire on even SPs
Shot interval	50 m (per source line)
Shot location inline (OBS)	In between receivers
Shot location xline (OBS)	Off receiver lines
Shot line spacing (OBS)	100 m (sailed shot lines)
Cable	
Cable type	FOURcE
Number of cables	4
Cable separation	400 m
Cable length (per cable)	8000 m
Number of nodes (per cable)	320
Node separation	25 m
Cable depth	On seabed
Inline offset (centre source/centre near trace)	3000m to the West/ 4000 m to the East
Xline offset (centre source/centre near)	1175 m (1575 m at outer survey area edges)
Recording	
CMP-line separation	25 m
Bin size acquisition (inline/xline)	12.5 × 25 m
Recording length (after T_0)	10 s
Sample rate	2 ms
Recording filter – Low cut/slope – Hydroph.	5.41/6 Hz/dB per octave
Recording filter – High cut/slope – Hydroph.	215/597 Hz/dB per octave
Recording filter – Low cut/slope – Geoph.	Out
Recording filter – High cut/slope – Geoph.	215/597 Hz/dB per octave
Tape format/media	Seg-D rev 1 8036/IBM 3590

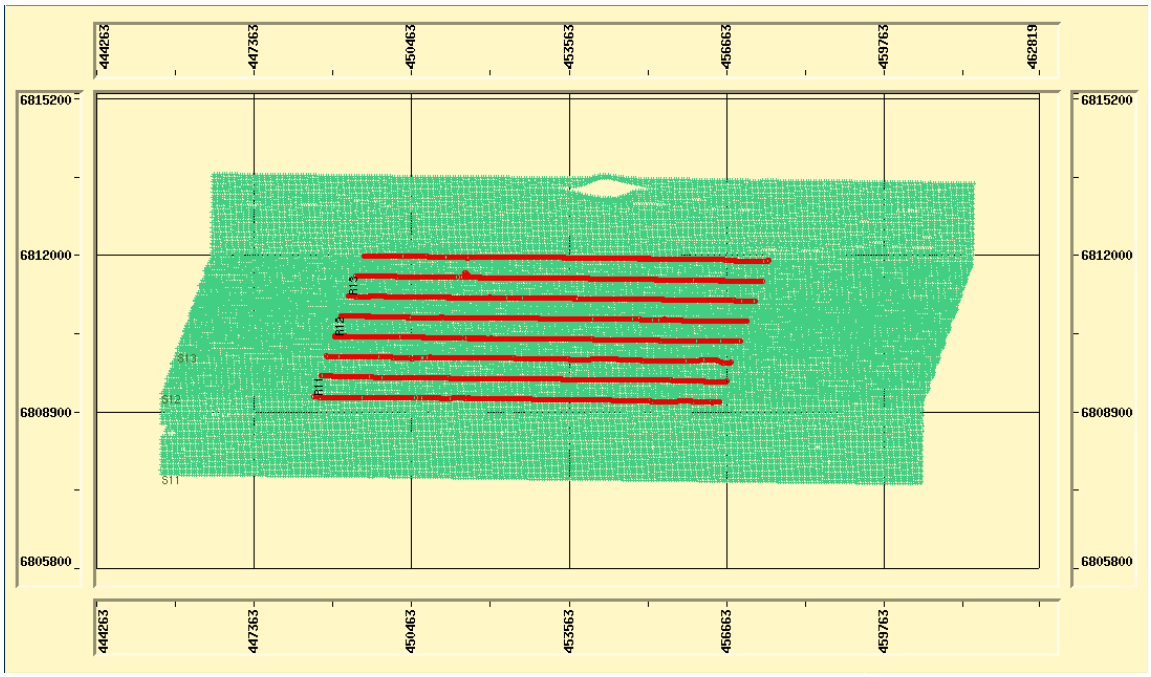

Figure 4-3: Navigation post-plot of the combined swaths 11 to 13 - receiver lines (red) and source lines (green)

4.2 OBC processing

Reformat and preprocessing: Onboard the field data (SEG-D format) was reformatted to PGS Interval Cube Manager format, loaded to disk and then SEG-Y output tapes were created. Before splitting the data into PZ and PS data-sets, receiver and shot edits as indentified by the onboard QZ were applied. These edits were then verified onshore, and some adjustments were made for questionable receiver gathers with noise problems related to coupling effects. Also creation of several new headers and some header manipulation were performed before the processing sequences (PGS Report 2005).

4.2.1 PZ processing:

The flow chart in Figure 4-4 shows the main processing steps for the PZ data-set. In the following sections the basic steps will be explained, and the final result displayed.

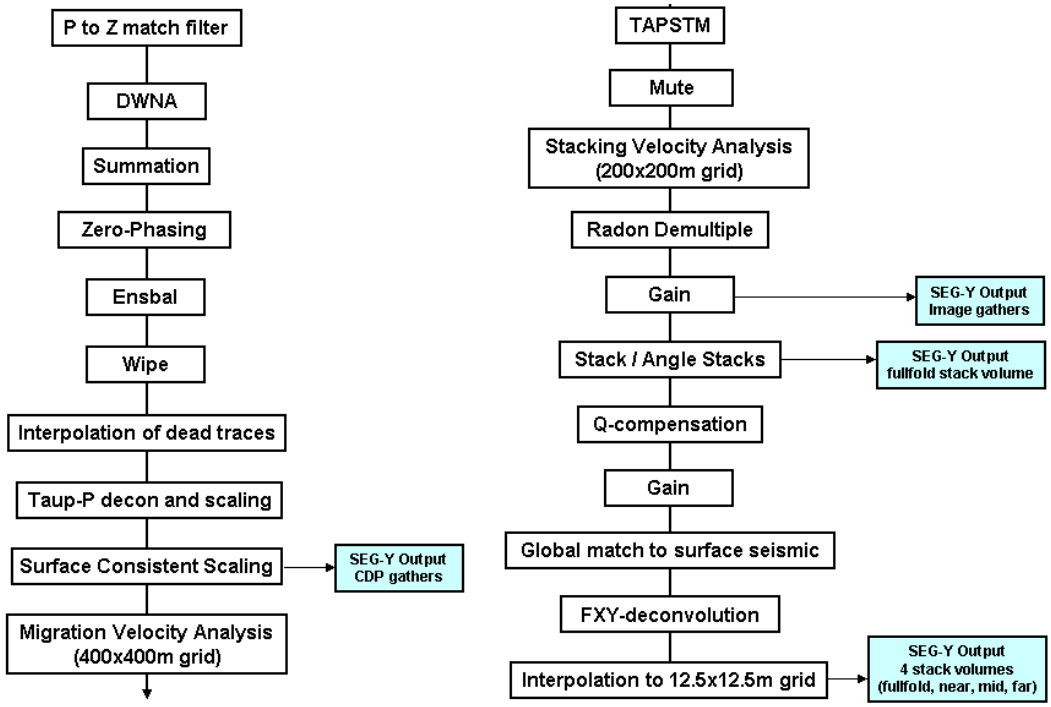

Figure 4-4: Block diagram of the PZ processing sequence (PGS Report 2005).

P-to-Z match filter: Before summation of the vertical geophone data (Z) and the hydrophone data (P) the sets have to be matched. The Z-data is of better quality so it was decided to match the P-data to the Z-data. A receiver-by-receiver match filter is calculated and applied to the P-data. Due to noise bandpass filters were applied to the datasets to improve the quality of the summation. Then a multiplexing procedure calculates the rms amplitudes within a user specified time/offset window for P- and Z-data and estimates receiver-by-receiver scalars to scale the P- to the Z-data. The P-to-Z phase and frequency matching is done by extracting the embedded wavelets for each component and each receiver station.

DWNA (Dual Wavefield Noise Attenuation): The vertical geophone is subjected to different noise pattern than the hydrophone. DWNA takes advantage of the different properties of the upgoing and downgoing wavefield (U=Z+P, D=Z-P), as the signal of the wavefields are different, but the noise is the same. The upgoing wavefield is used as the noise model for the downgoing wavefield, and vice versa, and a least-squares adaptive subtraction in small 2-D windows is utilized to remove the geophone noise from both wavefields. For the first production the noise model was constrained by a confirmed low-pass filter of 12/20 Hz, and afterwards the DWNA production was re-run with a time-variant low-pass filter applied to

the noise model before adaptive subtraction: 12/20 Hz from 0.0-2.0 s, 6/12 Hz from 3.0-7.0 s (PGS Report 2005).

Summation: Dual-sensor summation combines the hydrophone and the vertical geophone component to attenuate the receiver ghost. The chosen technique for this survey was the PGS's patented SCDuWIT (Surface-Consistent Dual-Wavefield Inversion Technique). By summing and subtracting the pressure and vertical phones, we can separate the wave fields into upgoing and downgoing motions. By proper scaling of the downgoing wave field and subsequent recombination of the upgoing and downgoing wavefields, reverberations are attenuated and the primary signals are preserved.

$$\text{Summation} = U + \text{Rho} * D,$$

where Rho is the scaling factor.

Figure 4-5 show the actual SCDuWIT-summation result on stack responses of the target section. These displays with the accompanying QC-FX-displays clearly illustrate a very good multiple attenuation after summation.

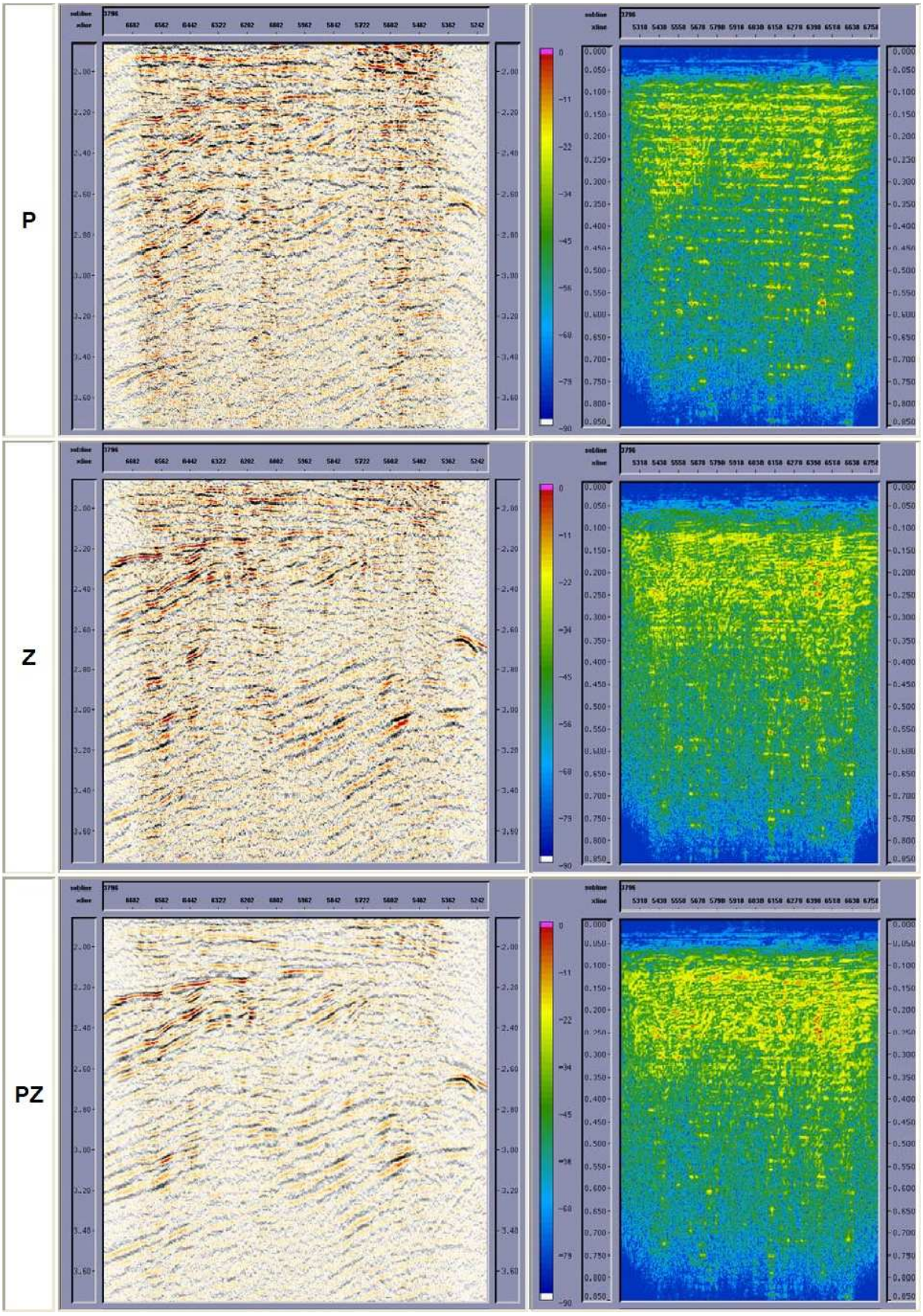

Figure 4-5: P-, Z- and PZ-stack (SCDuWIT) of the target section. The FX-plots to the right illustrate that the frequency notches due to multiple reflections are leveled after summation (PGS Report 2005).

Zero-phasing: A PGS pre-stack wavelet deconvolution procedure PSDECON was used for the zero-phasing. This procedure is based on a realistic convolution model, and assumes that the input wavelet is casual, minimum phase and invariant. The effective wavelet is estimated within a user-specified ensemble and time gate. From this wavelet the inverse filter is calculated and applied to the input ensemble to form the deconvolved, zero-phase output ensemble.

Ensemble Balance, WIPE: Due to random noise spikes and noise bursts in the data, ensemble balancing was applied, which worked effectively in attenuating this random noise while not affecting the primary data. We also spotted strong diffraction events, due to the Snorre A platform, and used the PGS procedure WIPE to attenuate this coherent noise. WIPE determines the affected gathers automatically and flattens the diffractions, and an f-k filter is applied around the position of the diffraction. After that the filtered data is merged back with the original unfiltered gathers, and the time shifts necessary to flatten the diffractions are backed off to restore the data to its original state, minus the surface diffractions.

Tau-P Deconvolution and Mute/Gain: Due to inter-bed ringing and remnant water-bottom multiple energy present in the P-wave data after PZ summation, Tau-P deconvolution was used to attenuate this multiple and ringing energy. In addition a gentle mute function in Tau-P domain was applied to suppress dipping linear noise. A linear Radon transform was employed in the receiver domain, after a few pre-processing steps to avoid aliasing effects. The pre-processing steps include; top-mute of already aliased direct arrival and refracted energy, shot interpolation to 25m-trace spacing, common Cartesian offset binning and reposting of the offset header to the projected inline-offset, spherical divergence corrections, trace length padded from 7000 ms to 10500 ms, 961 P-traces were used to model dips in Tau-P domain, and the minimum and maximum p-values were set to -1/1480 to +1/1480. Figure 4-6 shows the stack result after Tau-P convolution, and Figure 4-7 shows the final mute in Tau-P domain and the effect on Common Receiver Gathers (CRG's) after inverse Radon transformation (PGS Report 2005).

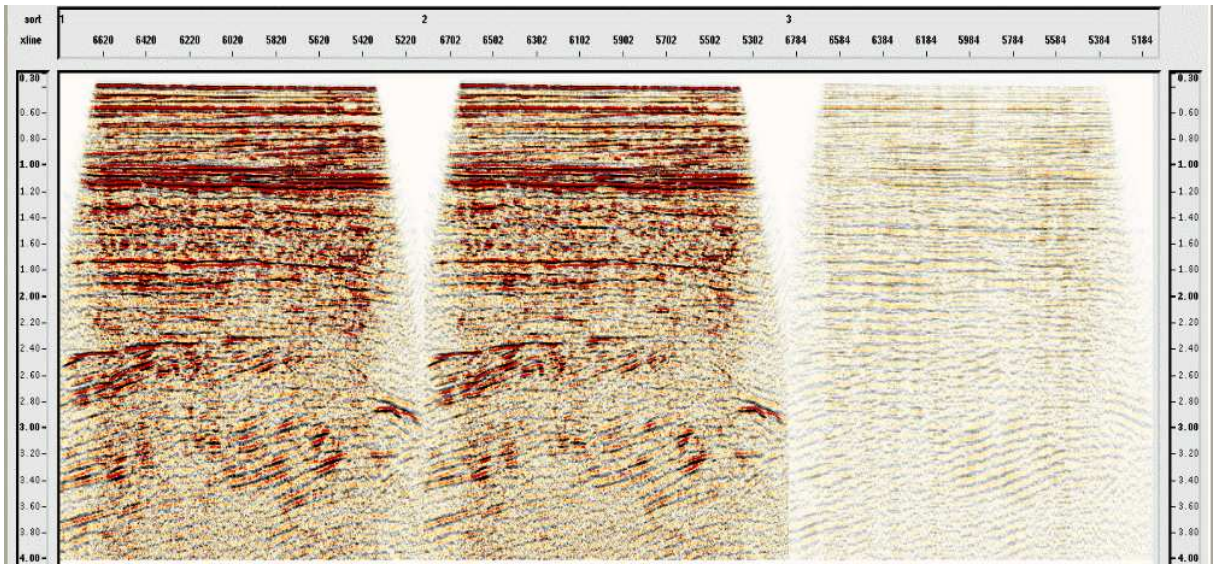

Figure 4-6: Stack response of final Tau-P deconvolution - input (left), after deconvolution (middle) and difference display (PGS Report 2005).

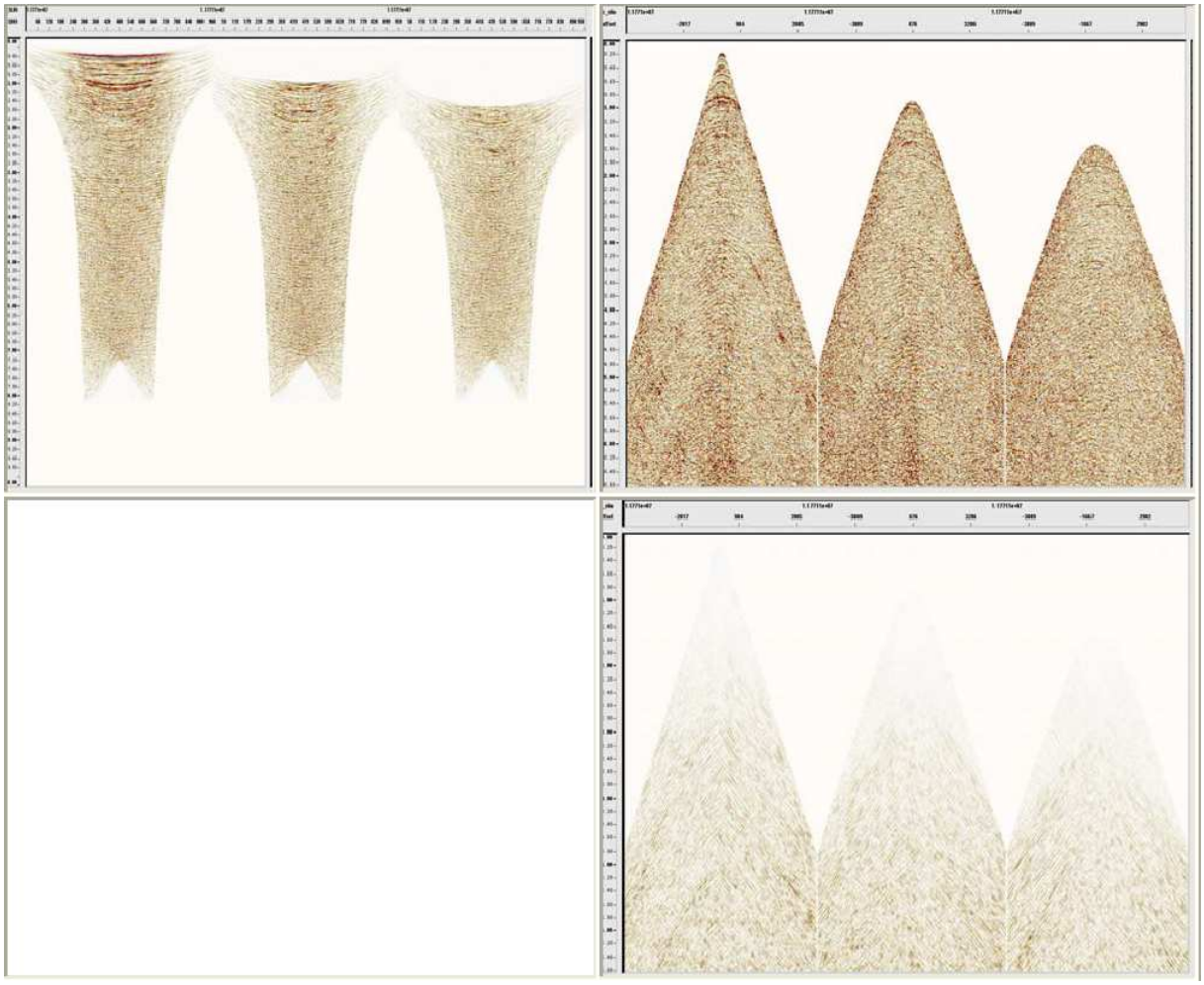

Figure 4-7: Final mute in Tau-P domain (left) and the effect on CRG's after inverse Radon transformation (top right). The difference plot (bottom right) indicates the gentle attenuation of dipping noise (PGS Report 2005).

Surface consistent scaling: Rms-amplitudes are calculated for each trace within a specified offset- and time-window. These amplitudes are then decomposed in a surface consistent way, and scalars are calculated for each receiver and shot in order to remove short wavelength amplitude variations, which occur due to coupling differences.

Migration velocity analysis: After demultiple and surface consistent scaling a migration velocity analysis was done using horizons provided by Statoil as control points (see Figure 4-8).

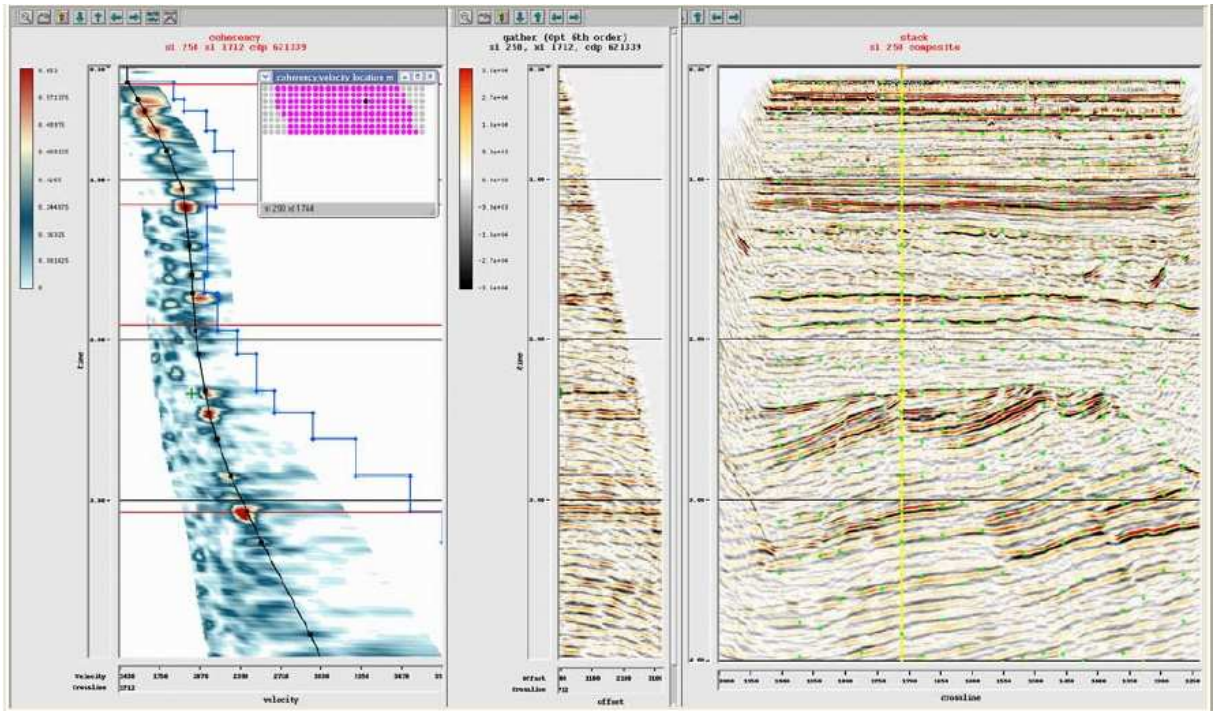

Figure 4-8: PZ-Migration velocity analysis on a 400m × 400m grid – semblance, gather and stack display. The red lines on the semblance display mark some of the provided reference horizons; the blue curve denotes the interval velocity function (PGS Report 2005).

Pre-stack Kirchhoff Time Migration (TAPSTM): TAPSTM performs a 3D pre-stack time-migration using the Kirchhoff migration method, with either straight ray or ray-bending travel time in an isotropic media or a transversely isotropic (VTI) media. The procedure has the ability to migrate the data directly from the acquisition datum. Instead of ray-tracing, a 6^{th} order NMO formula is used to account for ray bending. For the PZ migration production it was decided to utilize the isotropic migration with the bending ray option. Due to large fold variations within each input offset plane, it was decided to run trace interpolation and pre-migration fold scaling.

Final mute: Offset range stacks and gather displays were used to establish the final mute functions. The following top mute was applied to NMO-corrected image gathers (keyed on the water bottom two-way travel time WBT):

Offset (m)	Time (ms)	
	WBT = 380 ms	WBT = 425 ms
50	360	390
350	420	450
850	960	990
2150	2185	2215
5000	4920	4950

In addition the following inner trace mute was approved before Radon demultiple:

Offset (m)	Time (ms)
50	3100
250	3200
350	6000

Stacking velocity analysis: A stacking velocity analysis was performed on the full dataset after migration and radon demultiple (see Figure 4-9).

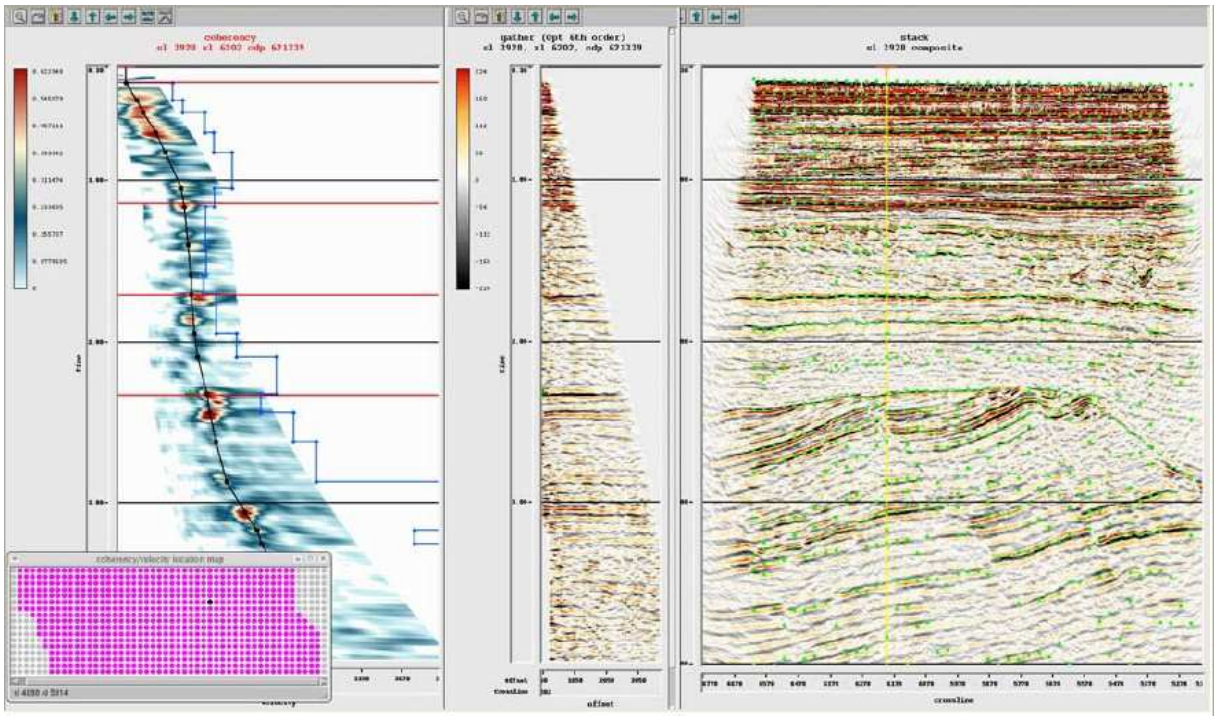

Figure 4-9: PZ - Stacking velocity analysis on a 200m × 200m grid – semblance, gather and stack. The red lines on the semblance display mark some of the provided reference horizons; the blue curve denotes the interval velocity function (PGS Report 2005).

Radon demultiple: Radon demultiple was also applied after the velocity analysis. The radon demultiple parameters applied before the velocity analysis had a slightly harsher parameterization. The final parameters for radon demultiple were:

1. 6th order NMO correction using final stacking velocity field.
2. Removable AGC applied to balance gathers to reduce amplitude artifacts in Tau-p domain
3. The reference offset was set to 4950m
4. Time range for data in Tau-p domain was –100ms – 1600ms.
5. Time range for multiples in Tau-p domain was 1200ms – 1600ms @ 0ms TWT
   600ms – 1600ms @ 1000ms TWT
   200ms – 1600ms @ 1500ms TWT
6. 200 parabolas were used to model data in tau-p domain.
7. An advanced, “dealiased-high-resolution” algorithm was used to reduce transform artifacts in the forward/backward Tau-p transform
8. Adaptive subtraction was used to subtract the modeled multiples from the input data.

Figure 4-10 show the results of the radon demultiple applied to a stack section.

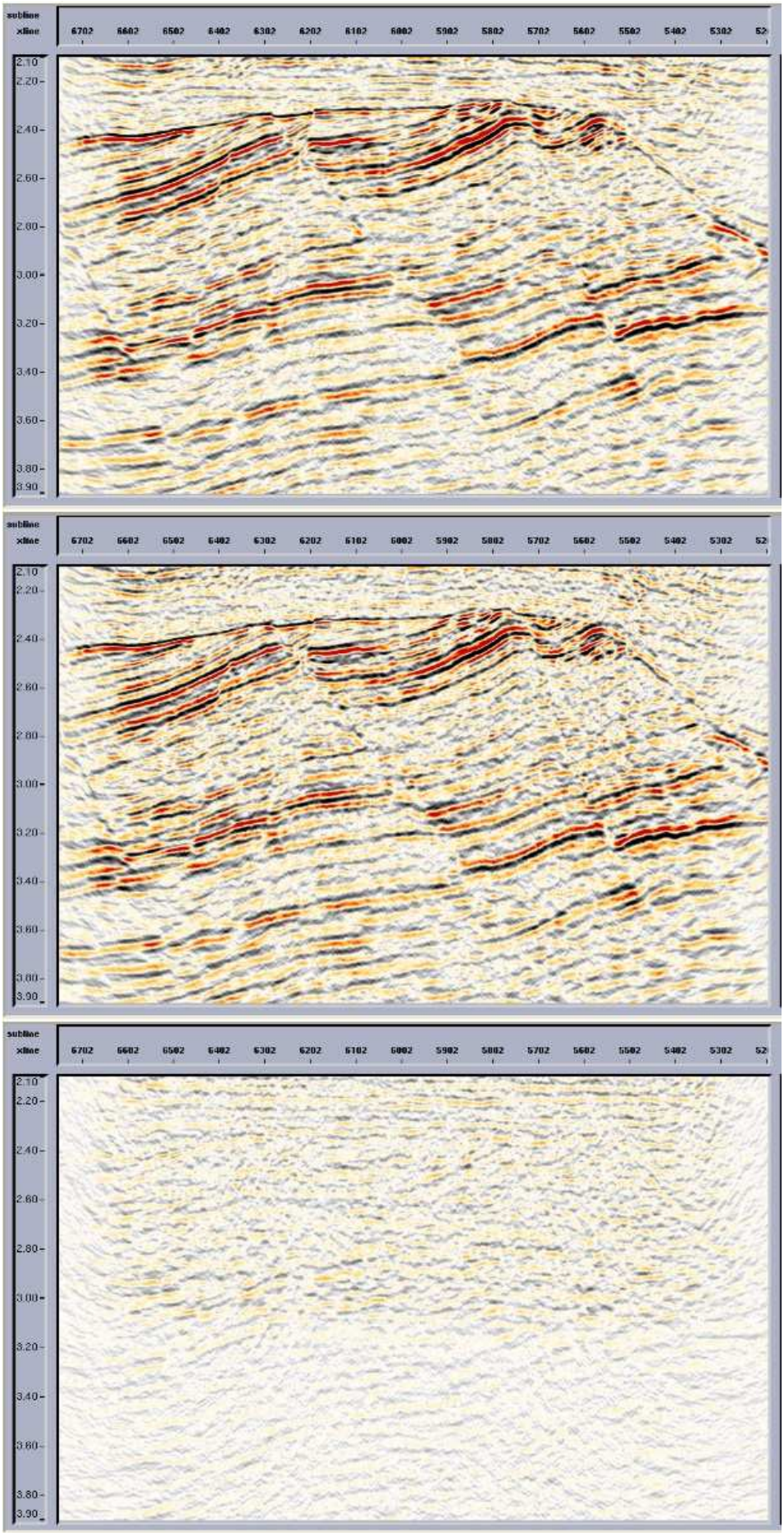

Figure 4-10: Target area of migrated PZ-stack, line 3928, before (top) and after (middle) Radon demultiple. The bottom display shows the difference (PGS Report 2005).

Gain: The following gain function was applied after Radon demultiple:

Time (ms)	Gain (dB)
500	0
2300	25
6000	32

Stack – angle stacks: The image gathers were stacked together and delivered to client as Raw Migration full-fold (full-angle) PZ-volumes, but a split of angles to produce angle stacks were also performed:

Full-angle: 0° - final mute, near-angle: 3°-15°, mid-angle: 12°-25°, and far-angle: 20°- final mute.

Spectral Whitening/Q-compensation: The OBC-volume were to be matched to surface seismic, so the frequency content needed to be brought to a similar level by applying post-stack spectral balancing methods. A post-stack Q-compensation method was chosen. The reference frequency was set to 25 Hz, the Q-value was set to 90, and the amplitude threshold was 20 dB.

Gain: After the application of Q-compensation a final gain function had to be applied to rebalance for amplitude attenuation in the overburden section.

Global match to surface seismic: A global match filter was generated and applied to the OBC dataset. The time shift was set to -1.12 ms, the phase rotation to 36.10°, and the amplitude scalar to 35.23 for the full-angle stack.

FXY-Deconvolution: For further signal enhancement and acquisition footprint removal we applied post-stack fxy-deconvolution. The input 3-D volume is divided into overlapping design cubes of user specified size in x, y, and time directions. Each trace of a design cube is transformed to the frequency domain. Common frequency samples are compared to measure spatial patterns among neighboring traces. Spatial predictive filters are designed for each frequency sample to preserve the observed patterns and are then applied to all traces in the design cube. The filtered frequency samples are then inverse-transformed back to the time domain. For each trace, the final output is built by merging vertically adjacent time gates after the inverse transform. Then the design cube advances in the x direction for the number of traces processed and the prediction exercise is repeated. This is repeated until all traces in the input volume have been filtered.

Interpolation: Before output to final SEG-Y tape the volumes were interpolated from 25m-by-12.5m to 12.5m-to-12.5m trace spacing using FK-interpolator to conform to the clients existing data grid.

Figure 4-11 shows the example inline 3824 as selected from the final PZ-volumes delivered to the client (PGS Report 2005).

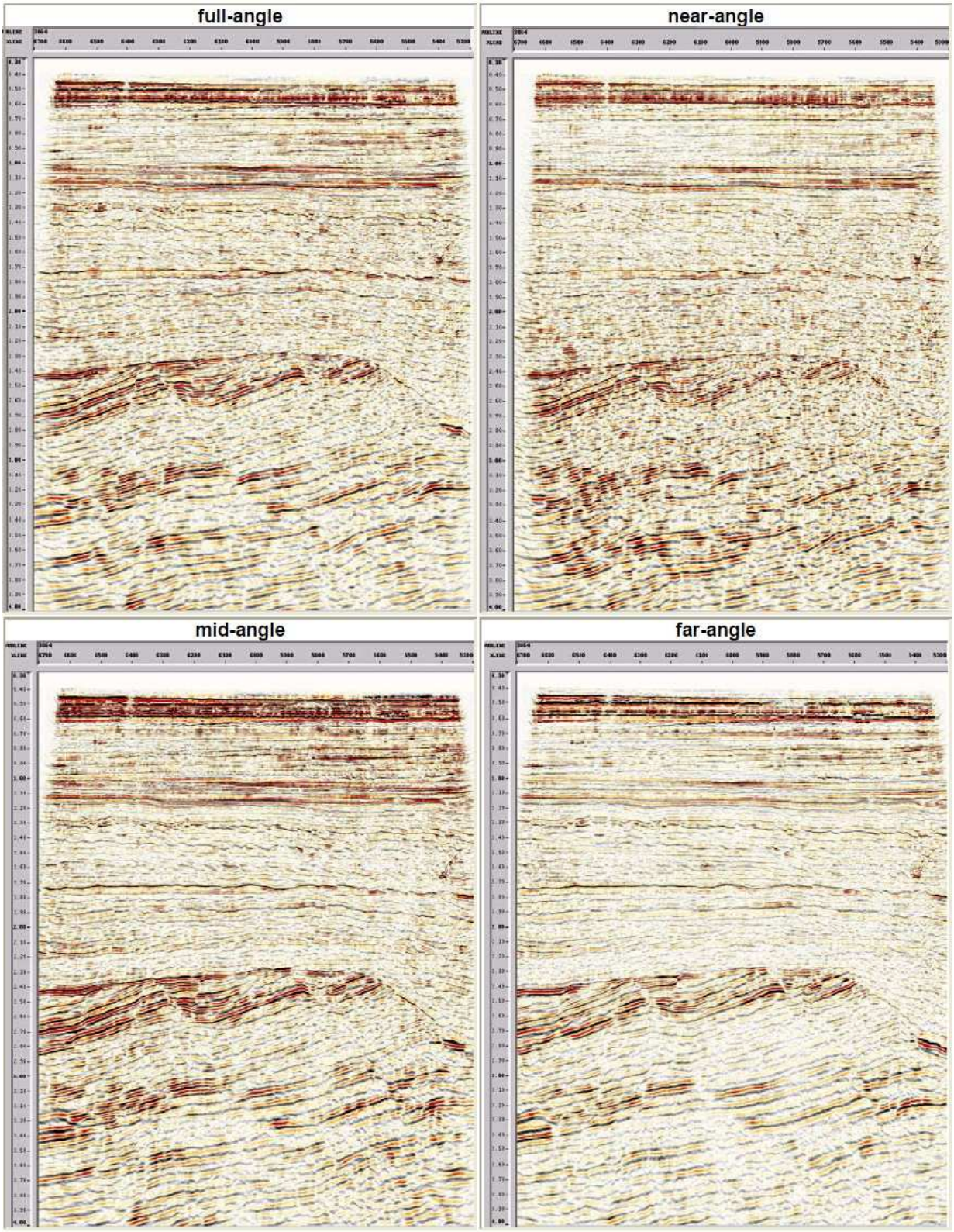

Figure 4-11: Final PZ-volumes; full-, near-, mid-, and far-angle stack of selected inline 3824 (PGS Report 2005).

4.2.2 PS processing

Figure 4-12 shows the main processing steps of the PS processing. Some of the steps are equal to the PZ-processing, and will therefore not be explained.

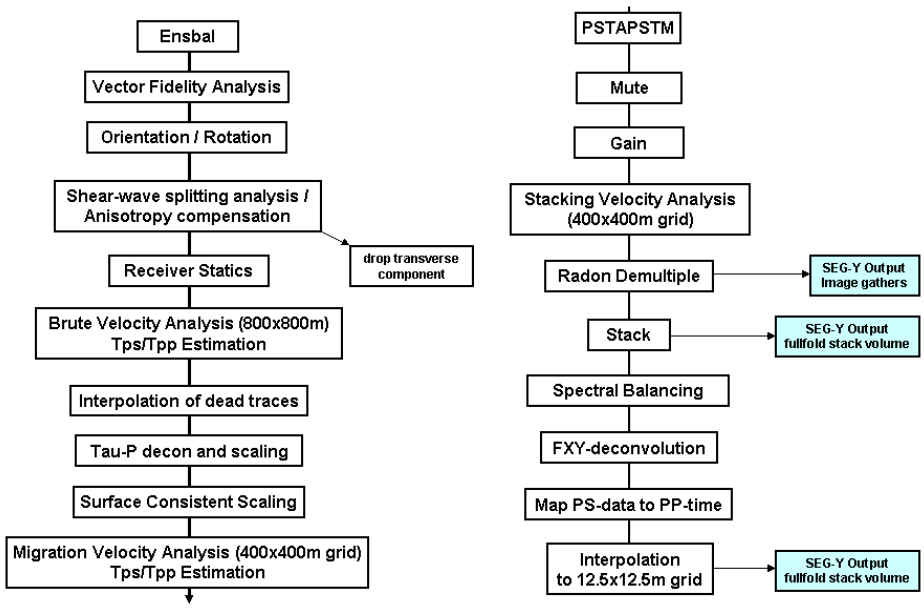

Figure 4-12: Block diagram of the PS processing sequence (PGS Report 2005).

Vector Fidelity Analysis/ Match Filtering: For vector fidelity analysis traces with a shot-receiver azimuth of 45°, 135°, 225° and 315° relative to the nominal line azimuth was selected and the direct arrival signature of the H1 (X) and the H2 (Y) component was investigated. The comparison of RMS values and spectra within the direct arrival time gate revealed good instrument fidelity. With the data selected common receiver stacks of the two components were created covering the shallow part from 0 to 1.5 s TWT. Within this time window the receiver stacks of the H2 component shows slightly lower frequency content, due to coupling differences. To compensate for this, trace-by-trace match filters were calculated based on a direct arrival window and subsequently to match the H2 to the H1 component.

Orientation/Rotation Analysis: Orientation analysis is a critical first step in optimizing converted-wave data quality. In general, there are two ways for rotating the data into radial and transverse components; to use the nominal cable direction as the orientation of the inline (H1) component, or to calculate the orientation of each receiver based on the direct arrival energy. PGS's patented orientation analysis determines the orientation angles of the H1 horizontal receivers relative to North. It is a surface consistent approach that considers source and receiver locations as well as the energy and polarization of the selected waveform. Assumptions of the analysis are that the receivers are horizontal and stationary

throughout the duration of the survey. Both rotation methods were tested, and it was decided to use the actual calculated orientation angles as the H1 direction, because this solution showed a superior result in some areas where the receiver line alignment deviated from the nominal receiver line azimuth like at the front and tail end of a cable or at cable intersections. As a final step the consistency of the polarity along and among receiver lines have been validated (PGS Report 2005).

Shear-Wave splitting Analysis & Compensation for Azimuthal Anisotropy: Remnant, continuous mode-converted energy on the transverse component can be an important indicator for azimuthal anisotropy. Due to fracturing in the bedrock the up-going shear waves are split into a fast S1- and a slow S2- wave mode. The S1 mode is polarized parallel to the fracturing, while the S2 mode is polarized perpendicular to the orientation of the fracturing and travels with a significant time-delay to the S1 mode. The PGS module FRACANA was used to determine the S1 direction (seen as a measure of fracture orientation) and the S2 time delay (seen as a measure of for the fracture density). There are two ways to process from the derived information about anisotropy; radial and transverse components can be rotated into S1 and S2 and processed separately, or the time delay on S2 can be corrected after rotation and then S1 and S2 can be rotated back to radial and transverse component again. If necessary, the latter can be done for several layers in a layer-stripping mode from shallow to deeper sections. In result the radial component reflection events are sharpened and reflection energy is maximized while the energy on the transverse component is minimized and can be dropped for further processing. The last option was used to compensate for anisotropy, and was first done for the entire survey, and then again on a layer from the deeper section (1500 to 2000 ms). Figure 4-13 show the final result of the anisotropy compensation for layer 1 and 2.

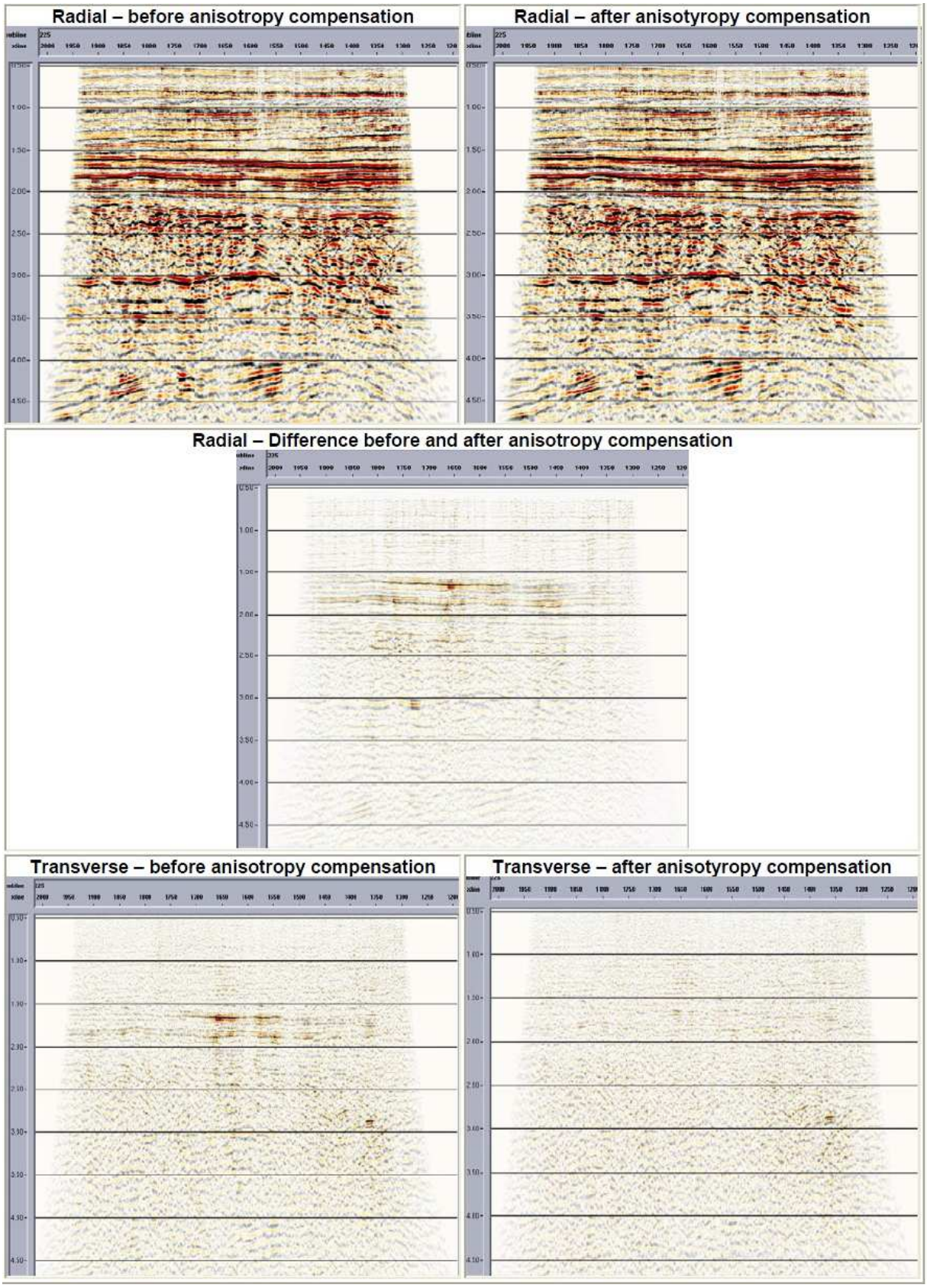

Figure 4-13: CCP stacks of radial (top) and transverse (bottom) component before and after anisotropy compensation for layer 1 and 2 (PGS Report 2005).

Receiver Static Corrections: Receiver static corrections are done by cross-correlation of receiver stacks with an appropriate reference data set within a certain time window. The reference data set is a smoothed version of the input receiver stacks. From the cross-correlation, a static shift is then derived and subsequently applied. Several iterations might be necessary to achieve optimum corrections for long and short wave length static effects. A constant time window of 1600 ms centered along 1200 ms were used, and three iterations were performed. The first iteration corrected for long wavelength trend by use of a low-pass filter. The second removed high-frequent jitter from receiver to receiver, and the last was performed to confirm convergence.

Brute Velocity Analysis – Initial Tps/Tpp ratio estimation: Initial Tps/Tpp time ratio were estimated by event correlation on migrated PS and PZ stack sections (see Figure 4-14) before a brute PS-velocity analysis were performed to establish an initial V_c velocity function for NMO corrections and input to the migration velocity analysis preparation.

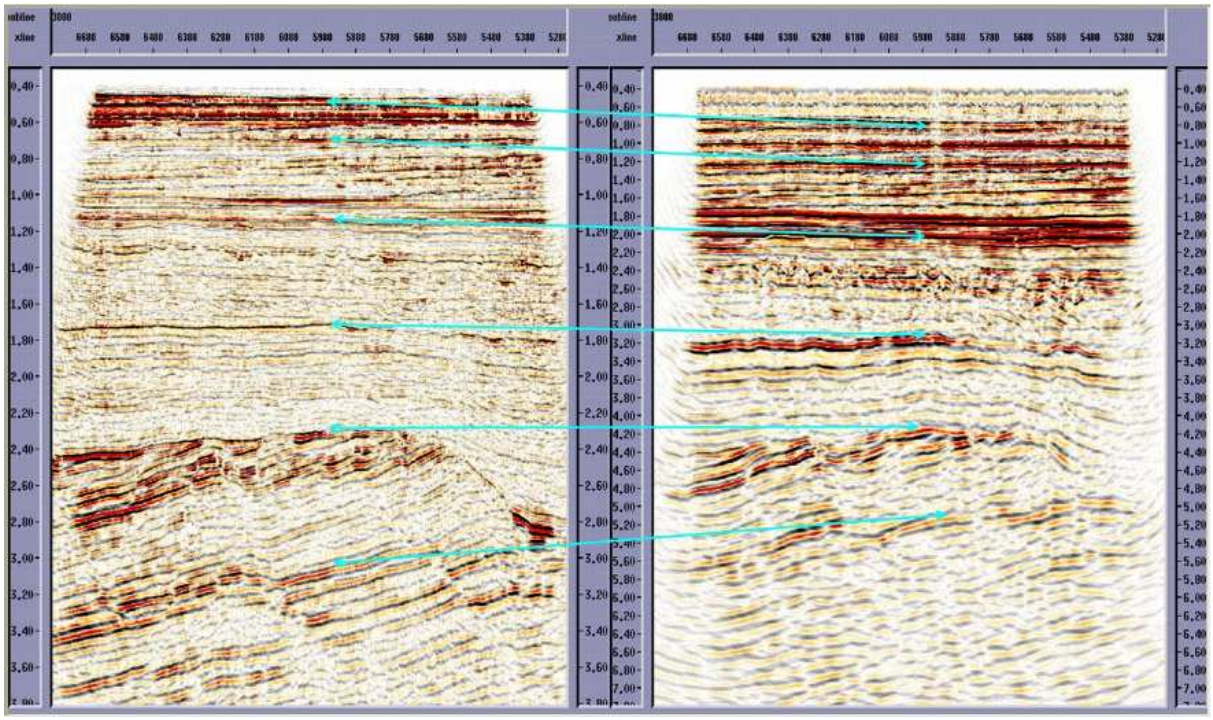

Figure 4-14: Event correlation on PS (left) and PZ (right) stack sections (PGS Report 2005).

Migration Velocity Analysis – Final Tps/Tpp ratio estimation: After Tau-P deconvolution, mute/gain and surface consistent scaling a PS migration velocity analysis were done on the 3D migrated velocity lines. PS horizons as control points were not available. A phase rotation at target reflections at middle to far offsets was discovered and it was therefore decided to limit the offset to 3000 m for velocity analysis and stacking (PGS Report 2005).

PS Pre-stack Kirchhoff Time Migration (PSTAPSTM): This migration is done similarly as the TAPSTM for the PZ volume, except before the migration a time variant filter was applied. The input parameters to the migration were a smoothed version of the migration velocity field (V_c), the lateral varying time-ratio file (T_{ps}, T_{pp}) and the time-aperture pairs. All these parameters are referenced to a constant receiver datum, with the shots time shifted to the sea surface.

Stacking Velocity Analysis: The final PS-stacking velocity analysis was performed on the PSTAPSM gathers after migration and radon demultiple (see Figure 4-15).

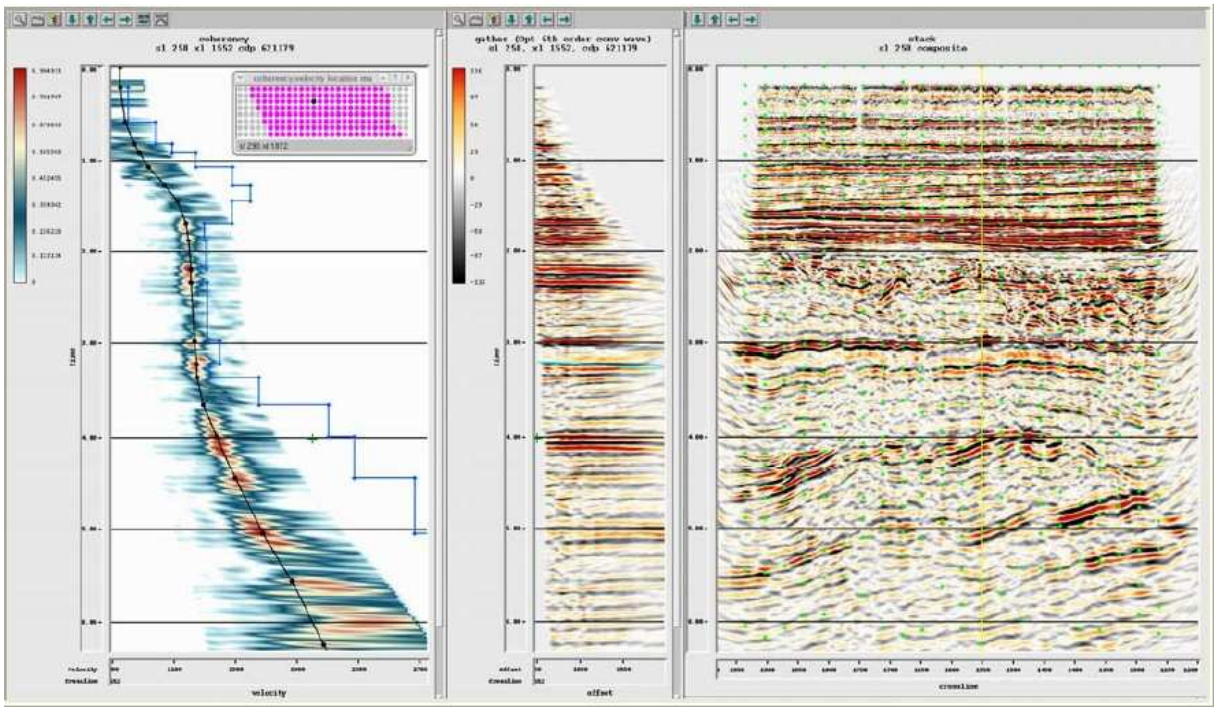

Figure 4-15: PS stacking velocity analysis on a 400m×400m grid – semblance, gather and stack display. The blue curve in the semblance display denotes the interval velocity function (PGS Report 2005).

Spectral Balancing: For post-stack spectral balancing/whitening, SPECBAL, a single-trace, zero-phase algorithm, was used. Each trace's amplitude is balanced while the phase spectrum is left unaltered. Spectral balancing is performed by a) decomposing the traces into series of user-defined band-pass filtered traces, b) scaling the filtered traces to equalize their relative amplitude levels, and c) summing the scaled filtered traces to form the final output series. The top section (0-3sec) was left unaltered and two different frequency decompositions were applied in two different time windows. Merging the three window solutions together using appropriate ramps creates the final traces.

Interpolation: In the last processing step a low-pass filter was applied before interpolating the PS-volume using an FK-interpolator. Then a constant scalar if 1350 was applied to approximately match the amplitude level of the PZ volume. The final migration volumes are shown in Figure 4-16.

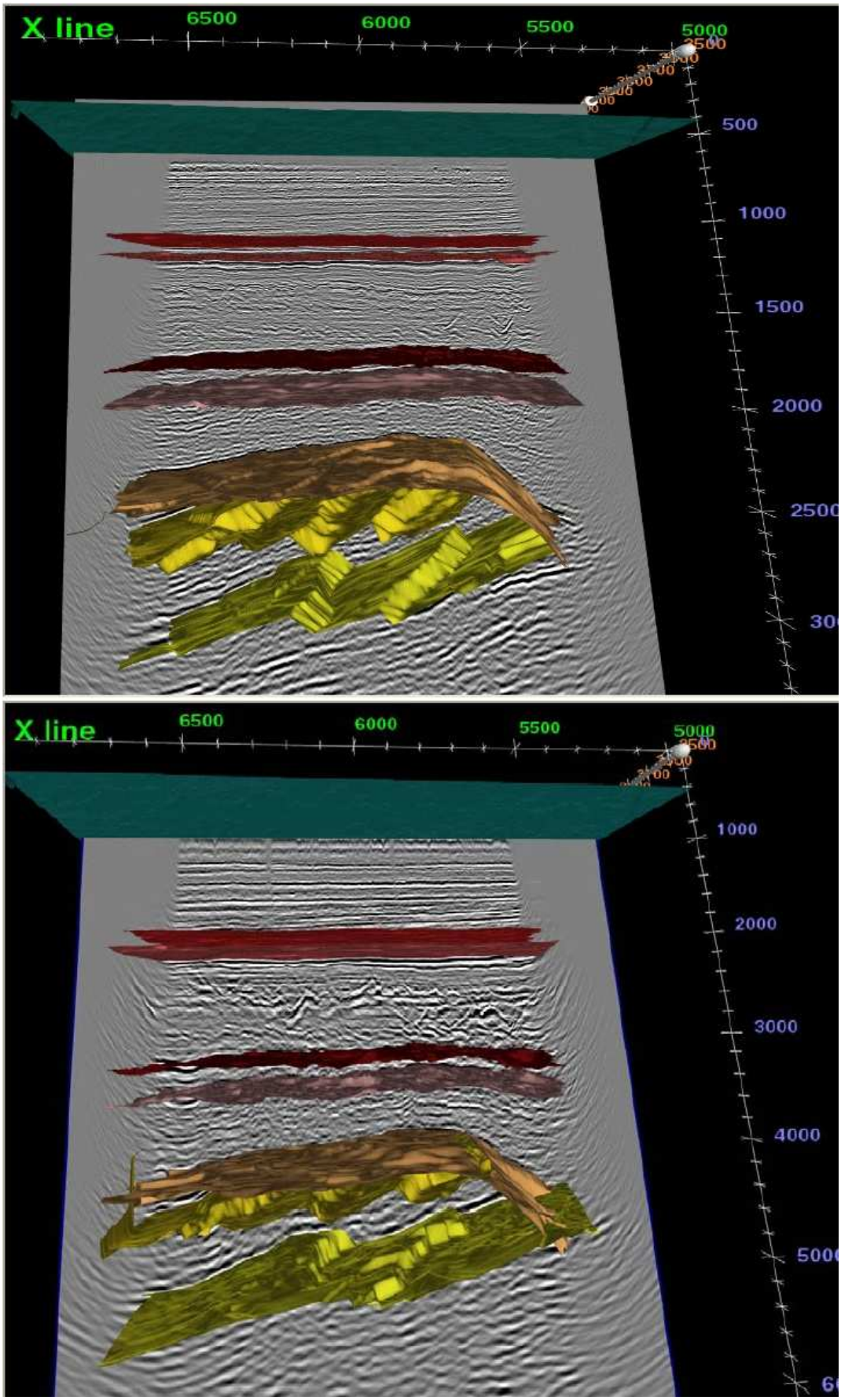

Figure 4-16: Final migration volumes; PZ- (top) and PS- (bot) sections with key horizons. The interpreted horizons have been provided by Statoil (PGS Report 2005).

Mapping PS-data to PP-time: By using interpreted horizons for event matching, the PS-data was converted to PP-time, using two different methods (see Figure 4-17).

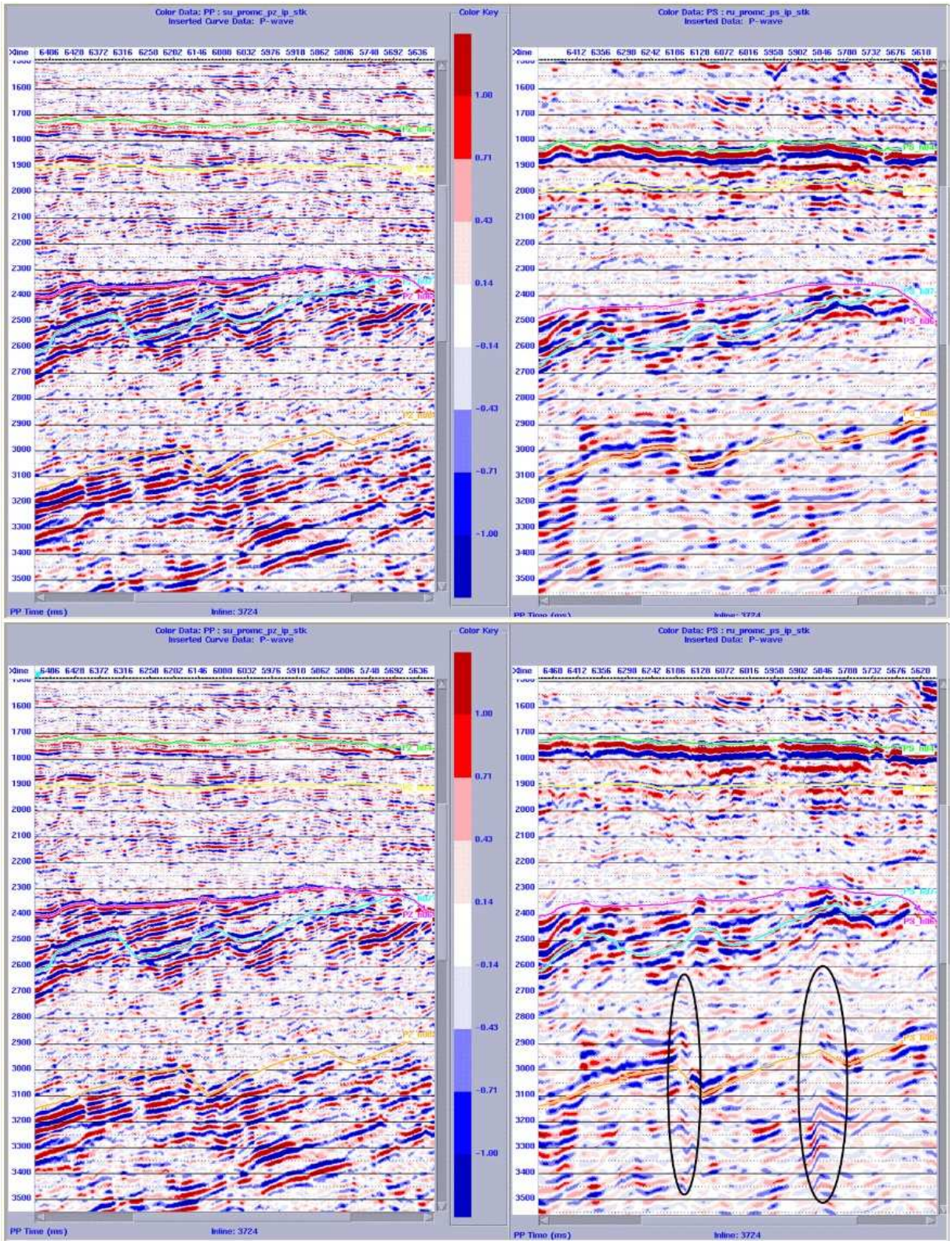

Figure 4-17: ProMC displays of imported PZ- (left) and PS- (right) volumes and horizons. In the top row the PS section has been converted to PP-time assuming a constant Vp/Vs=2.5. In the bottom row the PS-section has been 'squeezed' to PP-time by matching of the client provided PZ- and PS-horizons (except horizon 07, Statfjord, light blue) (PGS Report 2005).

4.3 VSP acquisition

The VSP data was acquired by READ Well Service on the 6th of June 1993 in the deviated well 34/7-P-8, located in the Snorre field (see Figure 4-18). A normal incidence VSP survey and a rig source survey were performed. The seismic source employed for the surveys were two sleeve guns with a total volume of 3000 cu in, depth 3.5 m and air pressure 2000 psi. The near field monitor hydrophone was kept at an offset of 1.0 m. The receiver array consisted of a main tool and 3 satellites, each containing a 3 component geophone cartridge. Thus 4 levels were acquired simultaneously. The normal incidence survey was acquired in one run from 3945 to 1710 m MD RKB, while the rig source was acquired in one run from 3945 to 1550 m MD RKB. For Rig Source VSP one shot point was used for all geophone levels, and for Normal Incidence the shot points were located vertically above the geophones (see Figure 4-19). More detailed acquisition details can be found in Table 4-2 (Saga Petroleum Report 1993)

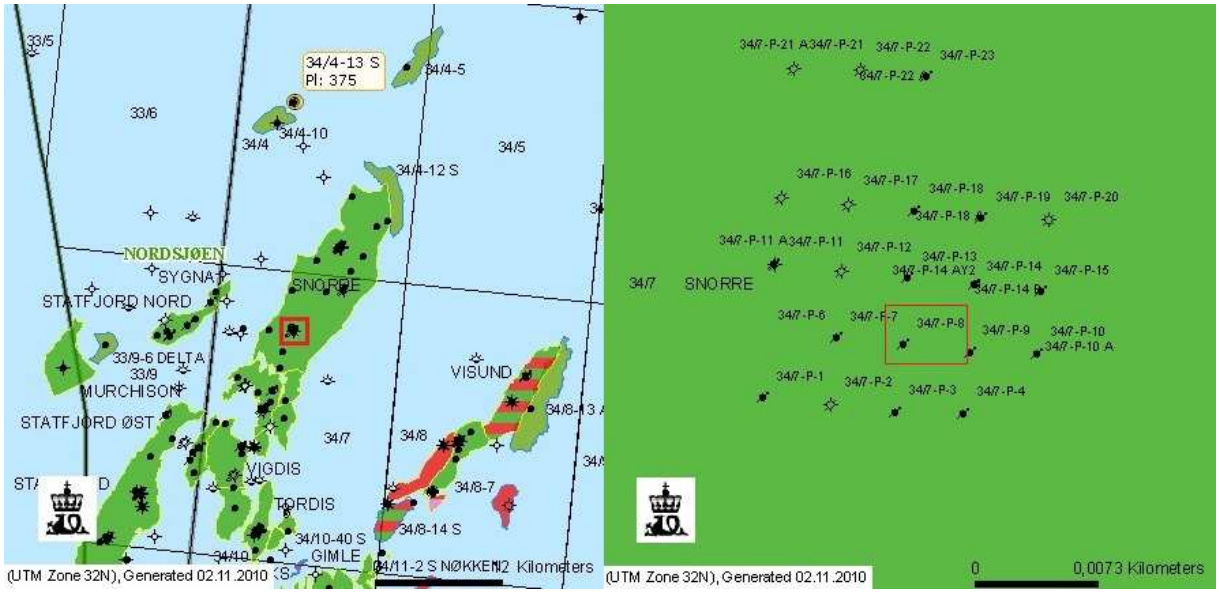

Figure 4-18: VSP survey area (NPD 2011).

Table 4-2: Acquisition parameters for Rig source and Normal Incidence VSP from processing report (Saga Petroleum 1993).

Well		
Well name	34/7-P8	
Well location	6813280 N 454337 E	
Field name	Snorre	
Rig name	Snorre TLP	
Survey type	Zero + VIVSP	
Reference level name	RKB	
Reference level elevation	59.4 m	
Datum name	MSL	
Water depth	309 m	
Rig heading	270°	
Casing programme	30 IN: 539 m	20 IN: 767 m
	17 IN:	13 3/8: 1734 m
	9 5/8: 3210 m	7 IN: 3200 m
Survey		
Record length	5000 ms	
Sample rate	1 ms	
Tape density	6250	
Gun depth	3.5 m	
Gun offset	55 m	
Gun azimuth	200°	
Gun pressure	2000 psi	
Hydro depth	2.5 m	
Hydro offset	55 m	
Hydro azimuth	200°	
No of tapes	1	
Weather wind	Calm	
Direction	SW	
Run No1 From	3940 m	
Run No1 To	1710 m	
No of levels	224	
Depth error	-1.7 m	
Rig Source		
Unit number	005	
Source type	Sleevegun	
Size	2 × 150 cu.inch	
Remote source		
Compressor No.	001	
Source type	Sleevegun	
No. of guns	2	
Total volume	300 cu.inch	
Firing pressure	2000 psi	
Gun depth	3.5 m	
Hydro depth	2.5 m	

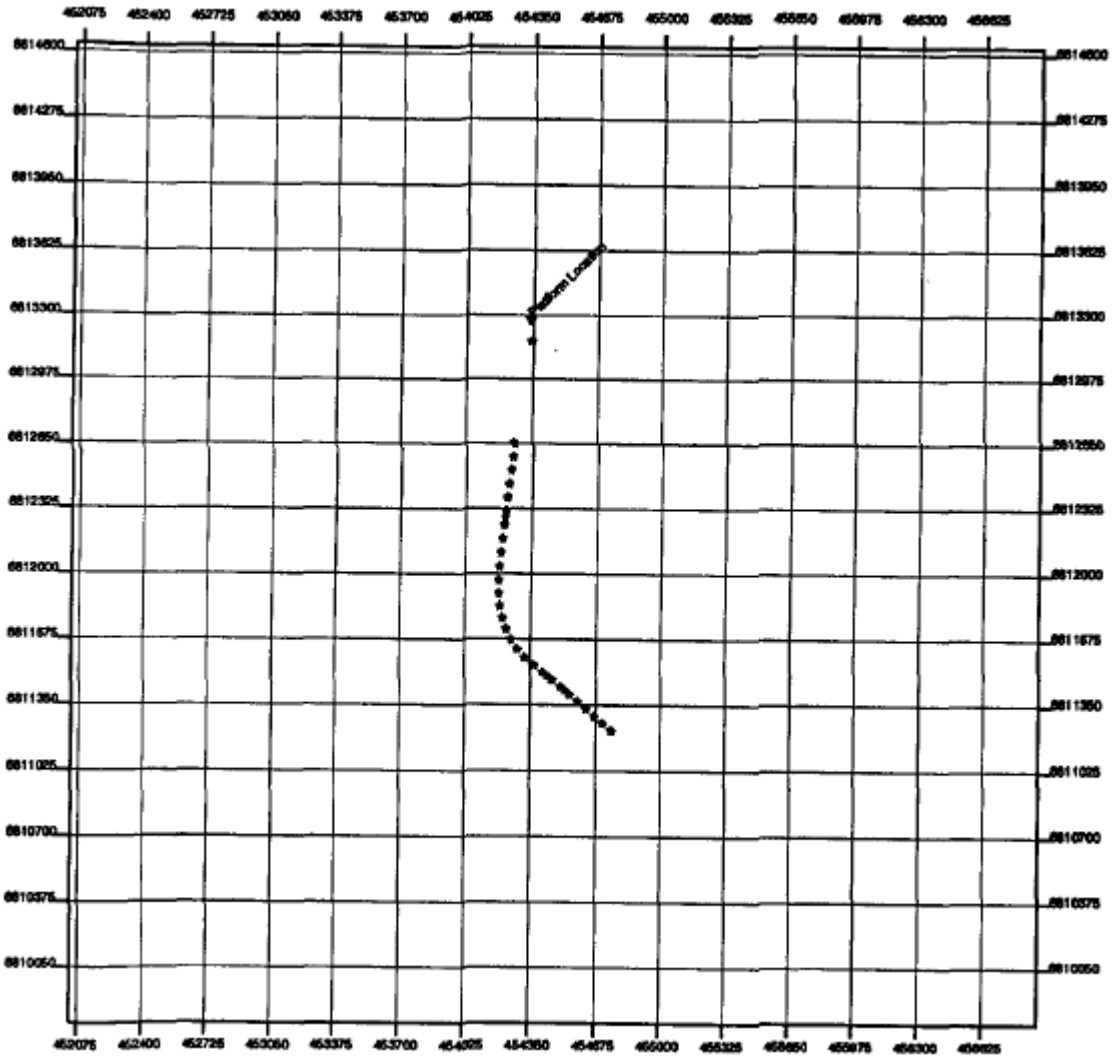

Figure 4-19: Survey overview - shot points (Saga Petroleum Report 1993).

4.4 VSP processing

Two VSP data sets were acquired and needed to be processed, Normal Incidence and Rig Source. Figure 4-20 to 4-23 show the processing sequence performed on the two data sets.

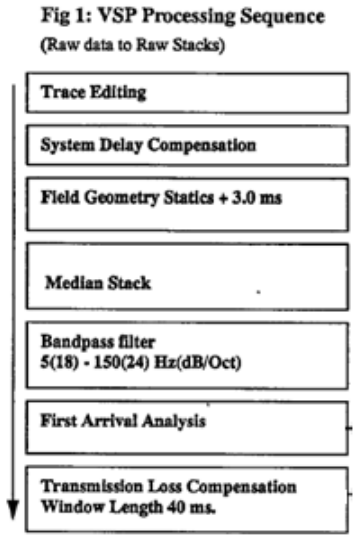

Figure 4-20: Outline of the pre-stack processing sequence for NIVSP (up to Raw Stacks) (Saga Petroleum Report 1993).

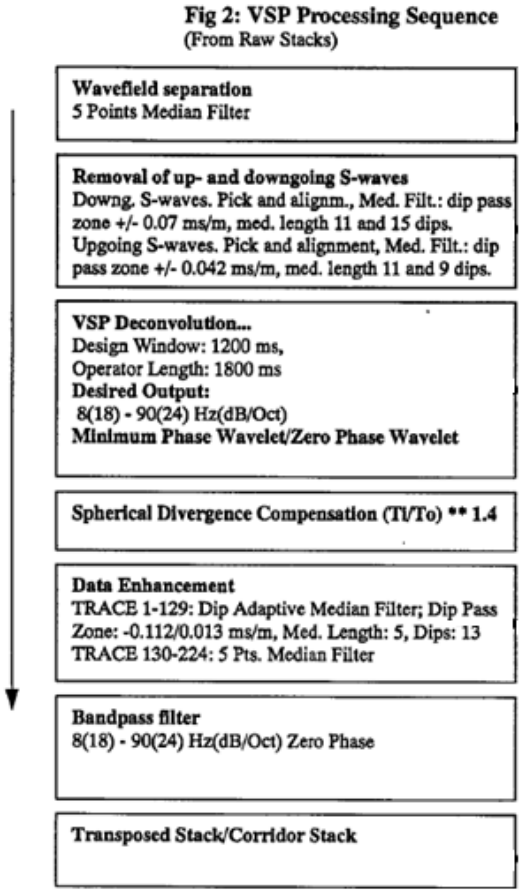

Figure 4-21: Outline of the post-stack processing sequence for NIVSP (Saga Petroleum Report 1993).

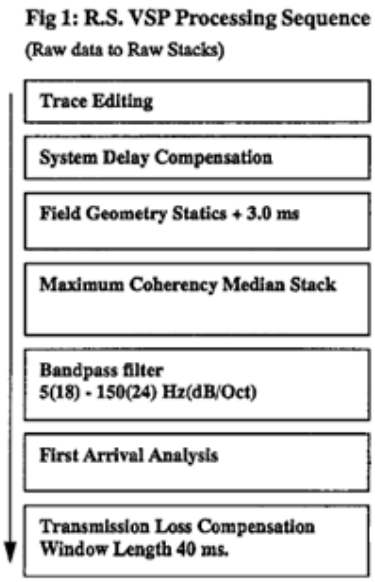

Figure 4-22: Outline of the pre-stack processing sequence for RSVSP (up to Raw Stacks) (Saga Petroleum Report 1993).

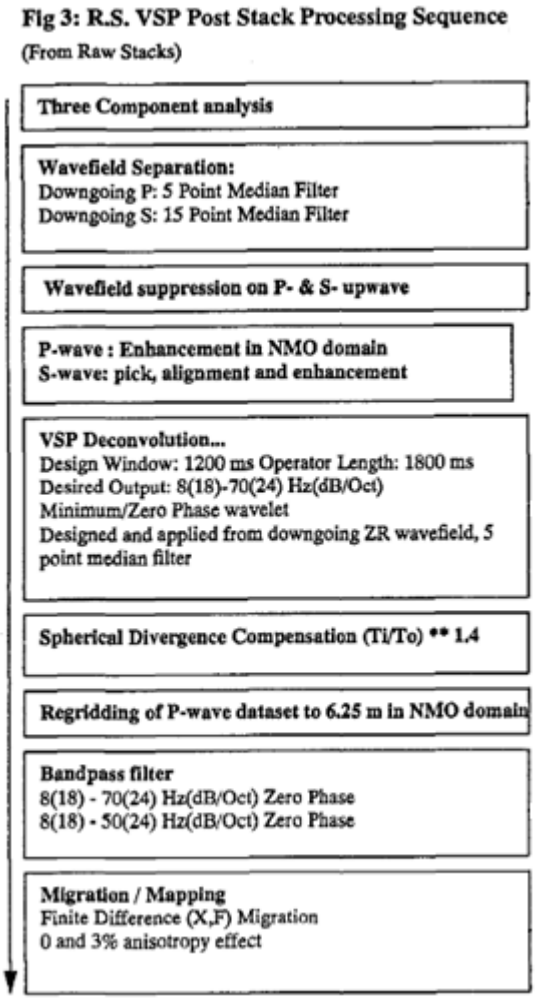

Figure 4-23: Outline of the post-stack processing sequence for RSVSP (Saga Petroleum Report 1993).

Editing, stacking and timing of data: The 3 component geophone data was displayed at large scale and each component edited. The individual near field monitor records were timed to the main peak, and the corresponding geophone traces shifted by this time. It was found that the system delay was stable during the surveys for 17 +/-2ms. For RSVSP the raw traces at each level were aligned by maximizing the cross correlation inside a window (50 ms) after the first arrival, and the data was resampled to ¼ ms for this purpose. Both VSP data sets were then stacked using a median algorithm.

First arrival picking: The two methods commonly used to pick arrival times from VSP data are 'trough-to-trough' and 'break-to-break' measurements. The terms trough and break refer to the part of the waveform on the near field monitor trace and the vertical component geophone trace which are picked. The 'trough-to-trough' method was chosen because it will probably give best 'tie' between the VSP data and the surface seismic. The trough pick can also be made with much greater accuracy due to the timing of a local minimum being virtually indisputable, and in the presence of noise the trough pick is more easily recognizable. The first arrival picking gives us information about the first break times that contributes to producing the check shot report and calibration of the sonic log.

Transmission loss compensation: Energy loss of the direct arrival is compensated for by normalizing the data in a 40 ms window after the first arrival. A single scalar is applied to each trace to force the RMS amplitude in this window to unity.

Three component analysis: For the RSVSP a 3-component analysis was performed in the beginning of the post stack processing. Since the tool orientation downhole is unknown, the same is valid for the h1 and h2 component orientation. Therefore the two horizontal components need to be rotated to a fixed coordinate system before processing. The radial component is defined to point towards the transmitted P-wave, and the transverse component is pointing 90 degrees to the radial component.

Wavefield separation: During wavefield separation the down-going wavefield is subtracted from the total wavefield to give the up-going wavefield. This is done using a Median filter. For the NIVSP a 5 point median filter was used for the down-going P-wave wavefield. For RSVSP both a 5 point median filter for the down-going P-wave and a 15 point median filter for the down-going S-wave wavefield were used.

Removal of down- and up-going waves: In order to enhance the quality of the NIVSP dataset the down-going and up-going S-waves were removed. The procedure started with a pick and alignment of the up- and down-going S-wavefields. The down-going and up-going S-waves were then removed with two Dip Adaptive Median Filters with different parameters.

P- and S-wave enhancement: For RSVSP the P-waves were NMO-corrected and enhanced with a 5 point adaptive Median filter. The NMO-correction was then removed from the dataset. The S-waves were picked and aligned, and then enhanced with a 5 point Median filter.

VSP Deconvolution: Deterministic deconvolution (assumes that measured up-going wavefield is the convolution of the reflection series beneath the geophone with the down-going wavefield measured at the geophone) was applied to the data set, using operators derived from the down-going wavefield directly after the first arrival, and applied to the corresponding trace in the up-going wavefield. For RSVSP the operator was designed and applied from the downgoing ZR (radial component in the vertical plane) wavefield. The desired output was specified as a Butterworth filter designed in the frequency domains 8(18)-90(24) Hz (dB/Oct) for NIVSP and 8(18)-70(24) Hz (dB/Oct) for RSVSP, with both minimum and zero phase wavelets.

Spherical divergence compensation: The loss of energy due to spherical divergence is compensated for by applying a scalar S_i to sample i, where $S_i = (T_i/T_0)^{**}X$, and T_i is the time of sample I, T_0 the first arrival time, and X a data dependant parameter in the range 1.0 to 1.5. Due to experience with VSP's in the Snorre area, a parameter of 1.4 is chosen.

Regridding and filtering of the dataset: The RSVSP data set (P-wave) was regridded to 6.25 m in the NMO-domain and then filtered (P- and S-wave) with a zero phase Bandpass filter.

Finite difference (X, F) migration: The RSVSP P-wave data was migrated with a X, F migration algorithm. The finite difference depth migration algorithm is a Pre-stack Migration (shot record migration) algorithm. By assuming reciprocity, interchanging the source and receivers, the receiver wavefield is back-propagated from the surface. Modeling of the source wavefield is delayed until extrapolation of the receiver field reaches the depth at which the receiver is located. The current algorithms for anisotropy migration assume elliptical anisotropy. The vertical velocities are kept unchanged from the modeling of Normal Incidence VSP, and the estimates for the horizontal velocities are varied. The anisotropy effect compensation used here is 3 %.

The displays for Normal Incidence and Rig Source VSP are shown in Appendix A.

5 Seismic interpretation and ray-modeling

5.1 Introduction

The datasets received from Statoil were opened in GEOPAD and ProMAX for quality control and to get an overview of the data received. The 3D cubes (P and S-wave) were then imported into Petrel. The VSP SEGY-files had missing header information that needed to be fixed before loading into Petrel. The changing of the header information was done in ProMAX. The P- and S-wave cubes were interpreted in Petrel, and the VSP seismic was loaded into Petrel and correlated with the interpreted horizons.

A ray-tracing model for the VSP surveys was made with the NORSAR-3D modeling software. The interpreted horizons from Petrel were loaded into the survey, along with the survey geometry. The velocities used were taken from the NIVSP processing report. A graph of the interval velocities measured was blocked into the different layers, and an average velocity for each layer was calculated. Since the interval velocities measured are approximated for the top layers, the velocities are uncertain and had to be changed during the modeling, for a better fit with the measured direct wave arrivals. The ray-tracing was then run for both Normal Incidence VSP and Rig Source VSP.

5.2 Interpretation and ray-modeling software

5.2.1 GEOPAD and ProMAX 2D/3D/VSP

GEOPAD (also called Geovecteur, GeoUNIX and Geocluster) is an environment for viewing and handling files without too much knowledge of the UNIX commands. The GEOPAD window consists of:
A menu bar: Allows to perform certain actions quickly.
A command line: Allows to enter and execute UNIX commands and to keep a history of the commands for later editing.
User and Project panels: Made of one or several lists displaying files in directories.
Icon bar: Short cut for most frequently used functions.

GEOPAD is a set of utility programs written in script language, fortran, tcl or Java. All utility programs are now organized by categories which are as follows:

- File Management
- Geometry
- Geophysical
- Libraries management
- Production management
- Statics
- Miscellaneous utilities
- Velocities

The GEOPAD environment can be used for instance to process, trough XJOB and viewing SEGY-files, trough Teamview (CCG Veritas 2006).

ProMAX 2D was first introduced in 1989, and has grown into a complete UNIX workstation-based, interactive, and batch environment for the interactive and batch analysis and processing of 2D seismic data. It provides disk-based and tape-to-tape input/output, parallel processing using multiple machines linked via a network, high resolution graphics, bitmapped color displays, tight links to various interpretive software systems, and hard-copy output.

ProMAX 3D is a superset of the ProMAX 2D package. The existing functionality of the ProMAX 2D product is supplemented with 3D-specific modules such as 3D residual autostatics, 3D one-pass migration routines, 3D DMO, and 3D Interactive Velocity Analysis. Absolutely essential to a successful 3D package was the development of tape-to-tape processing, including a tape catalog system, and parallel processing using multiple machines.

ProMAX VSP handles processing of zero-offset and offset vertical seismic profiles. The software also supports well-to-well and surface-to-well tomography (Landmark 1997).

5.2.2 Petrel

Petrel is a seismic-to-simulation software developed from 1996 as a result of a growing trend of specialized geoscientists working in increasing isolation. The result was an integrated workflow tool that allows Exploration and Production companies to think critically and creatively about their reservoir modeling procedures and make it easier for geoscientists to work together seamlessly. With the enhanced geophysical tools and the integration of ECLIPSE reservoir simulation software and streamline simulation, Petrel is a complete seismic-to-simulation application for 2D and 3D visualization, mapping, interpretation and reservoir modeling (Schlumberger 2008).

5.2.3 NORSAR 3D

NORSAR-3D is a 3-dimensional ray-tracing package for seismic modeling. NORSAR-3D combines well-established dynamic ray-tracing techniques with some fairly new concepts: Open Ray Models and Wavefront Construction. The new techniques simplify model building and provide efficient and robust multi-arrival ray-calculations even for large survey simulations. An important QC-tool during modeling is the comprehensive 3d visualization of the various aspects of the process (NORSAR 2008).

NORSAR-3D consists of several modules, each designed for a specific task.

Model Builder: Generates a model of general complexity with P- and S-wave velocities and densities. Anelasticity may be included by means of Q-factors. The model may either be created directly as a depth model, or by depth converting digitized time horizons.

Depth Mapper: The purpose of the depth mapper is to construct a reliable transformation (mapping) between the migrated time and depth, and to map interpreted data between the two domains by means of the transformation.

Ray Tracer: Performs kinematic and dynamic ray tracing. It handles configurations like Common Shot VSP, and Shot Direction. Also applicable for simulating zero offset tracing with Normal Incidence of Image Rays, which represent unmigrated and migrated data, respectively.

Horizon Displayer: Plots horizons. Each horizon may be given specific color and sample markers. Applicable for f.ex., comparing digitized interpretations of time horizons with traveltimes for Ray Tracers.

Seismogram Generator: Creates synthetic seismograms by convolving ray tracing results with a selected pulse. The traces are either the pressure response, or displacement response decomposed along a wanted direction.

Seismogram Displayer: Displays synthetic seismograms. The user may also overlay horizons from ray tracers, and digitize horizons from seismic data (NORSAR 2008).

5.3 Seismic interpretation

The data received were all of zero phase, which means that the pulse is symmetric, and the reflector lies at the top point. The interpretation was done in the 2009-version of Petrel, where normal polarity and the color scale 'seismic' and 'red, black and white' have been used. Positive trace pulse, marking an increase in acoustic impedance, is marked with red color (seismic) and black color (red, black and white), and negative trace pulses with blue color (seismic) and red color (red, black and white). This was double checked using the 'show wiggle trace option' (see Figure 5-1)

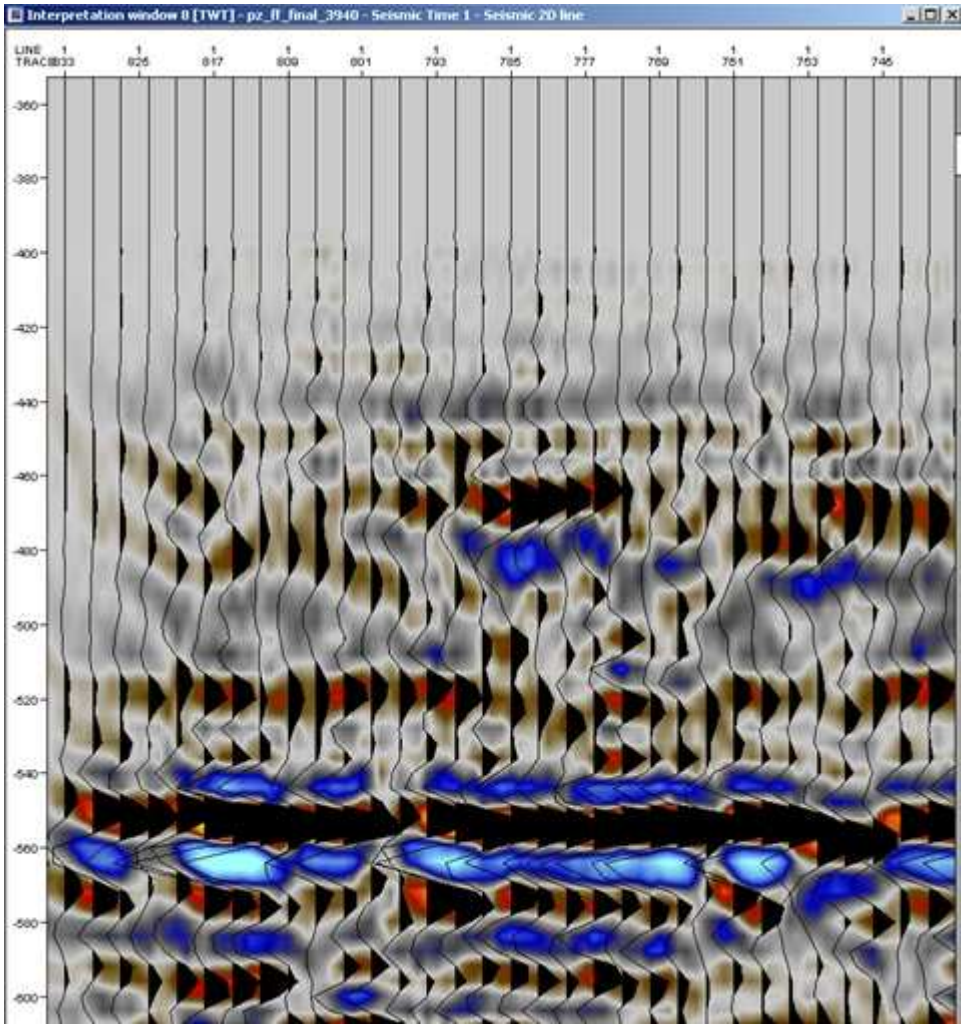

Figure 5-1: Section of the 2-D line 3940, with wiggle trace function turned on.

The data imported into Petrel were three 2D lines (3940, 3986 and 3992), three 3D cubes (PZ, PS PP-time, PS PS-time), and a VSP SEGY-file (see Figure 5-2).

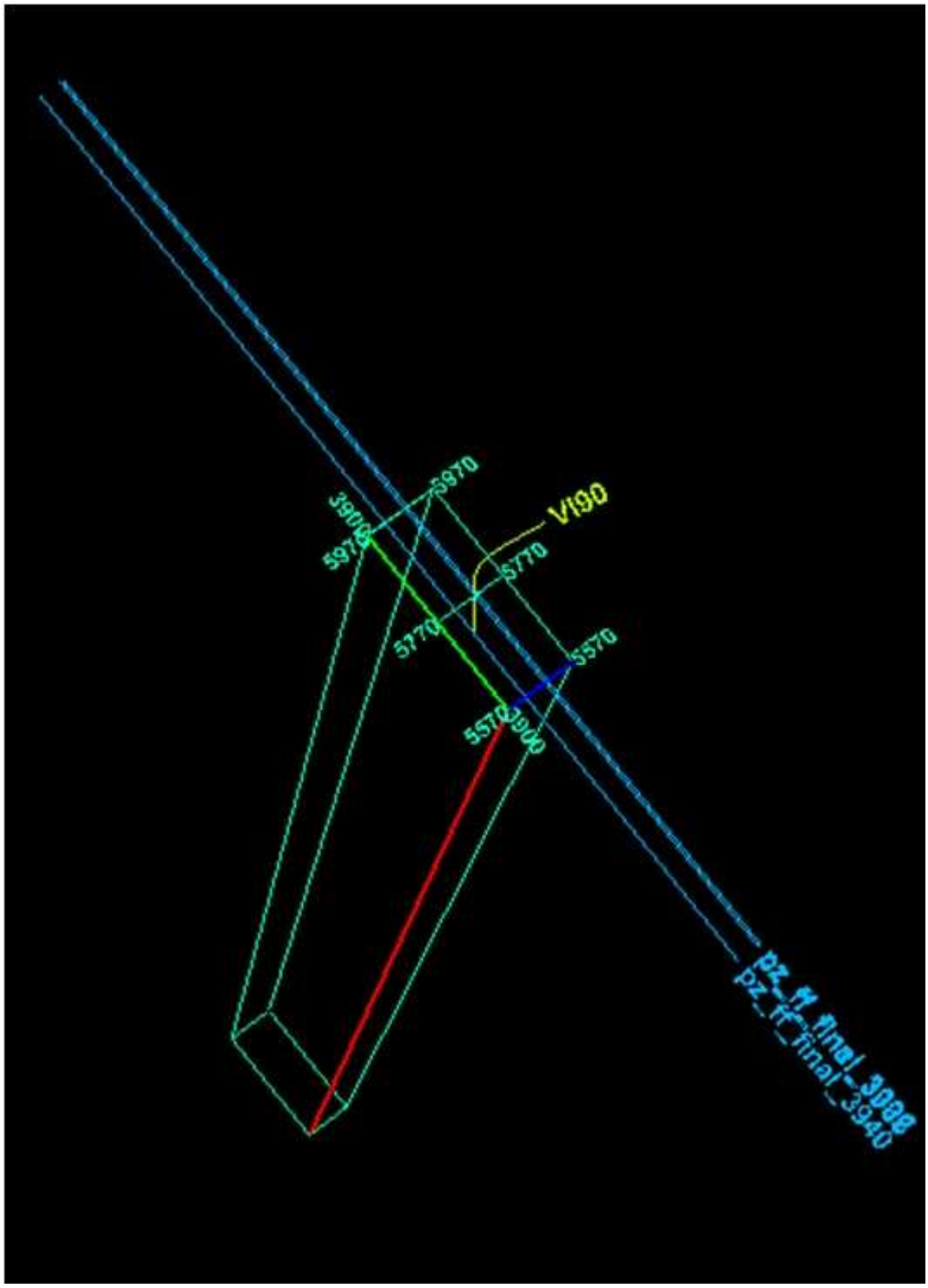

Figure 5-2: 3D window from Petrel displaying the lines and cubes received.

The SEGY-data received were of good quality, with good seismic resolution. In addition to the 3D-cubes and the three 2D-lines for the P-wave interpretation, we also received 6 interpreted horizons; Top Hordaland Group, Top Balder, BCU, Top SN11.4, Top SN10.4 and Top SN10.1. In addition to these six horizons 5 more were interpreted using Statoil's interpretation report as a guide. The five horizons interpreted in this thesis are the

Seabottom, Top Utsira Fm, Top Shetland Group, Top SN9.3, and Top SN Lower Lunde. In OBC-data the seabottom reflection is very weak, but an estimated horizon has still been interpreted, as it is needed for the ray tracing modeling. The interpreted horizons and the corresponding trace pulse interpreted in are shown in Table 5-1, and the interpreted horizons, shown on one of the 2D-lines, are shown in Figure 5-3.

Table 5-1: The interpreted horizon with the corresponding pulse signal (Aga and Isdø 2006).

Horizons (from top to bottom)	Pulse signal (peak or trough)	Horizon color
Seabottom	Peak	Dark blue
Top Utsira Fm.	Trough	Purple
Top Hordaland Gp.	Trough	Turquoise
Top Balder Fm.	Peak	Red
Top Shetland Gp.	Trough	Pink
Base Cretaceous	(-/+)	Light green
Top SN 11.4	Peak	Yellow
Top SN 10.4	Peak	Light pink
Top SN 10.1	Trough	Light blue
Top SN 9.3	Trough	Orange
Top SN Lower Lunde	Peak	Green

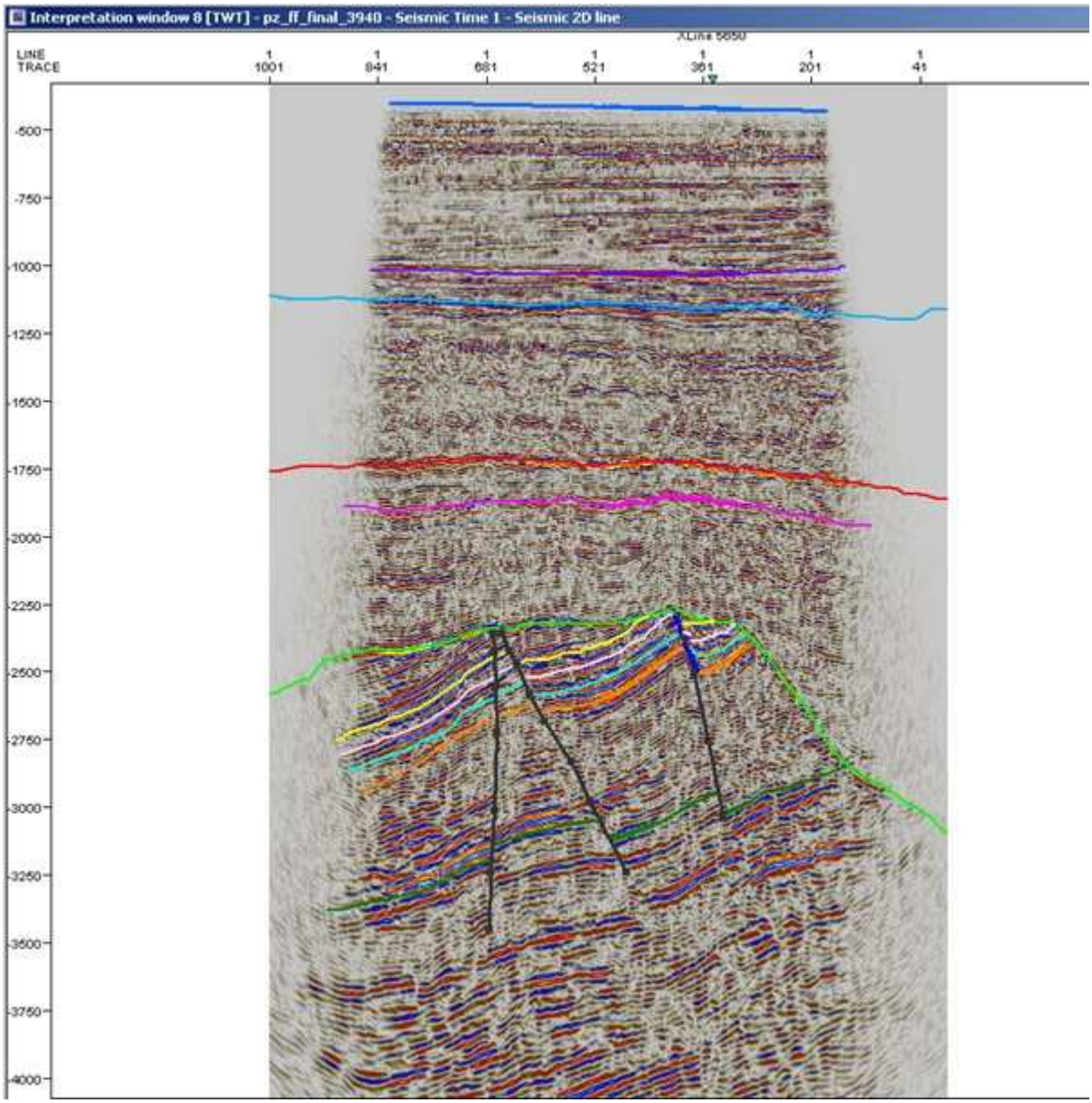

Figure 5-3: The 2-D line 3940 with interpreted horizons and faults.

The horizons Top SN9.3 to Top SN11.4 are the top of the different reservoir zones described in Chapter 2, belonging to the Upper Member of the Lunde Fm. and the Statfjord Fm.

Since the main goal of this thesis is correlating OBC with VSP, and improving an understanding of wave conversion in the subsurface, fault interpretation is not very important. However, the largest faults in the area have been interpreted in this thesis for better understanding of the horizons, and the corresponding layers.

After all the horizons and faults were interpreted, the horizons and faults were gridded into surfaces (see Figure 5-4), which were then smoothed.

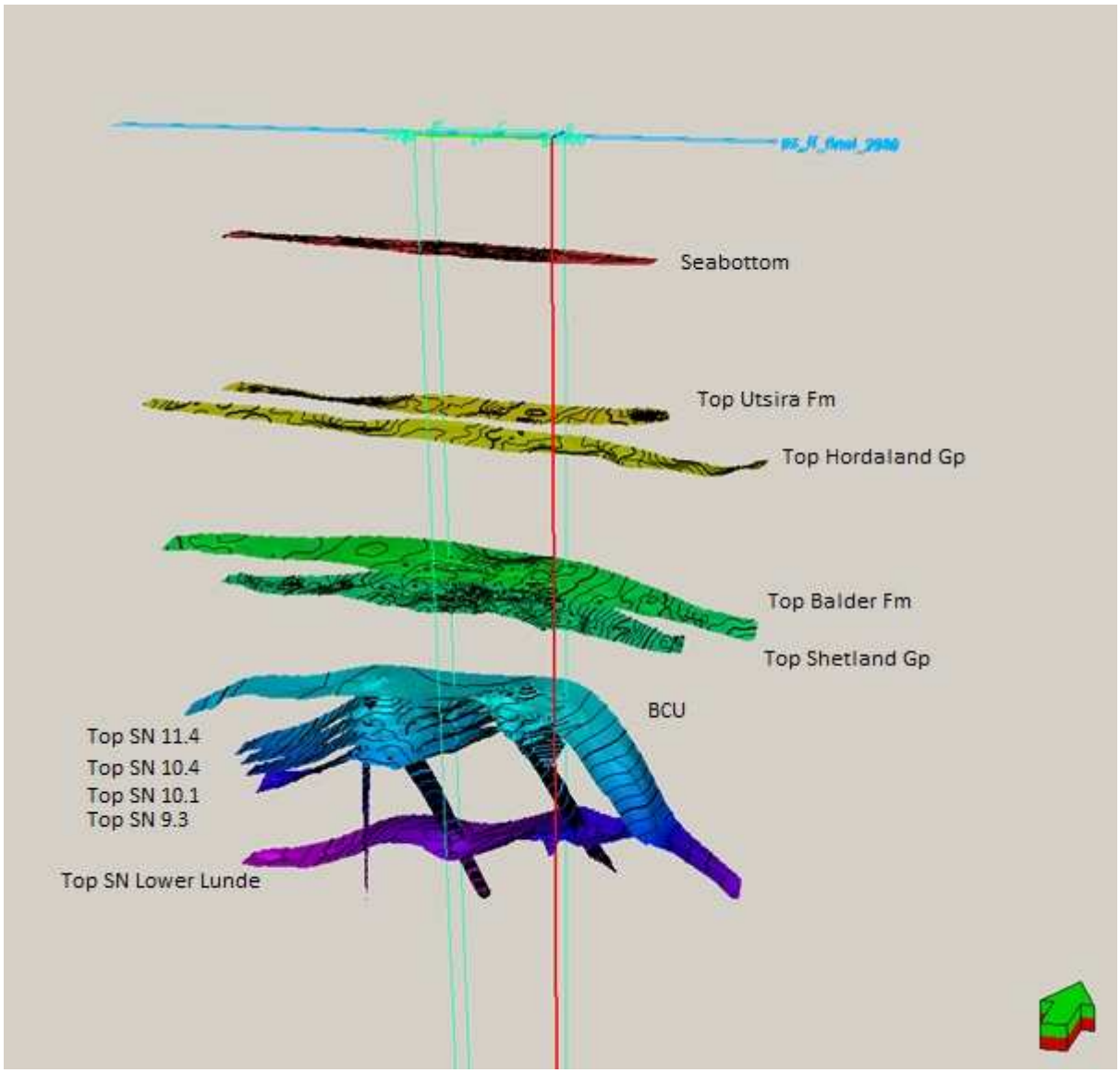

Figure 5-4: 3D-window from Petrel displaying the smoothed surfaces made from interpretation.

Then the 3D-cubes for S-wave were interpreted. First the PP-time cube was interpreted comparing with the P-wave cube. Then the S-wave cube in PS-time was interpreted, using both the P-wave cube and the PP-time S-wave cube for comparison. Displayed below are the interpretations on inline 3984 for all the cubes, with two-way-travel time (TWT) as the Z-axis (vertical scale) and inline/xline orientation as the horizontal scale.

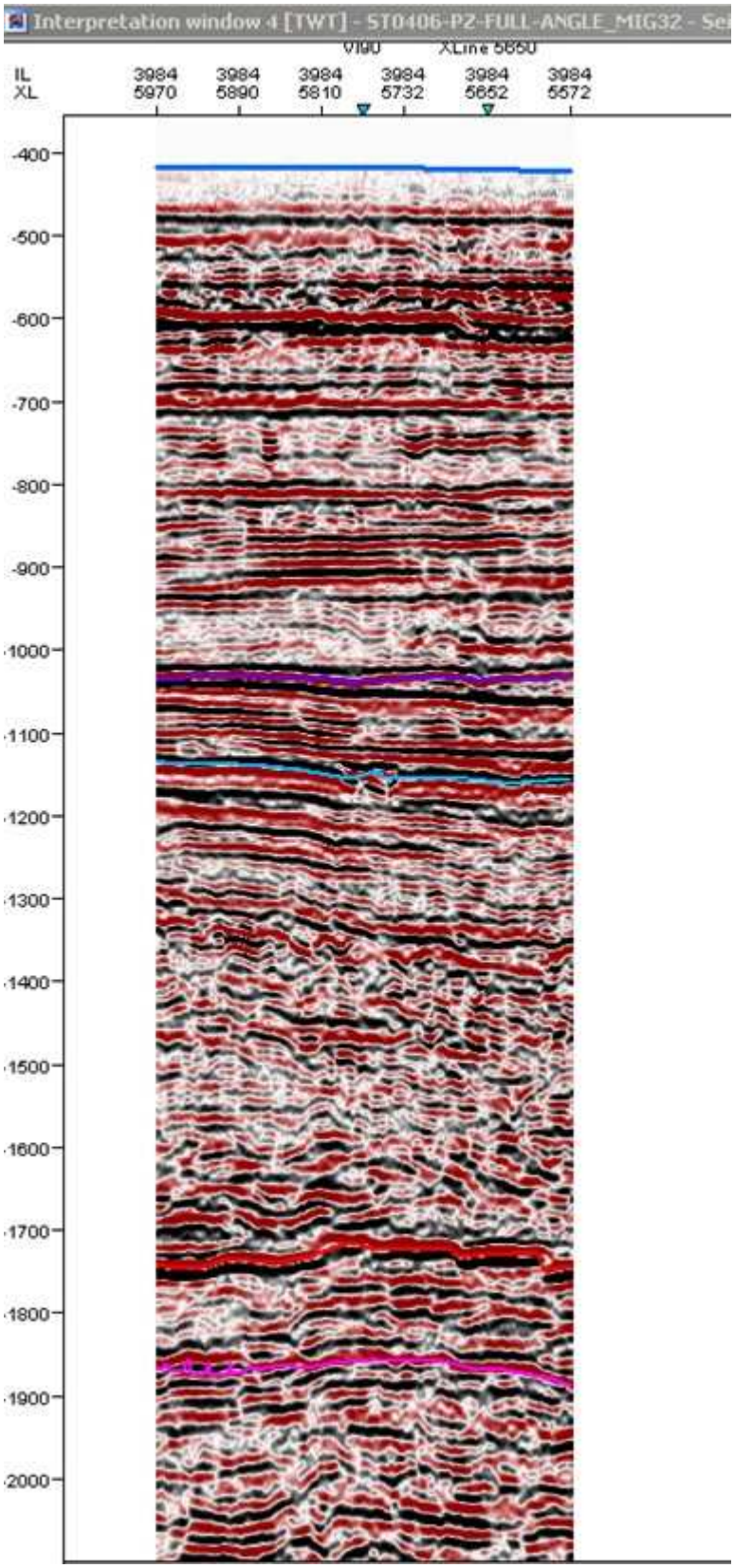

Figure 5-5: Interpretation on PZ 3D-cube, top layers

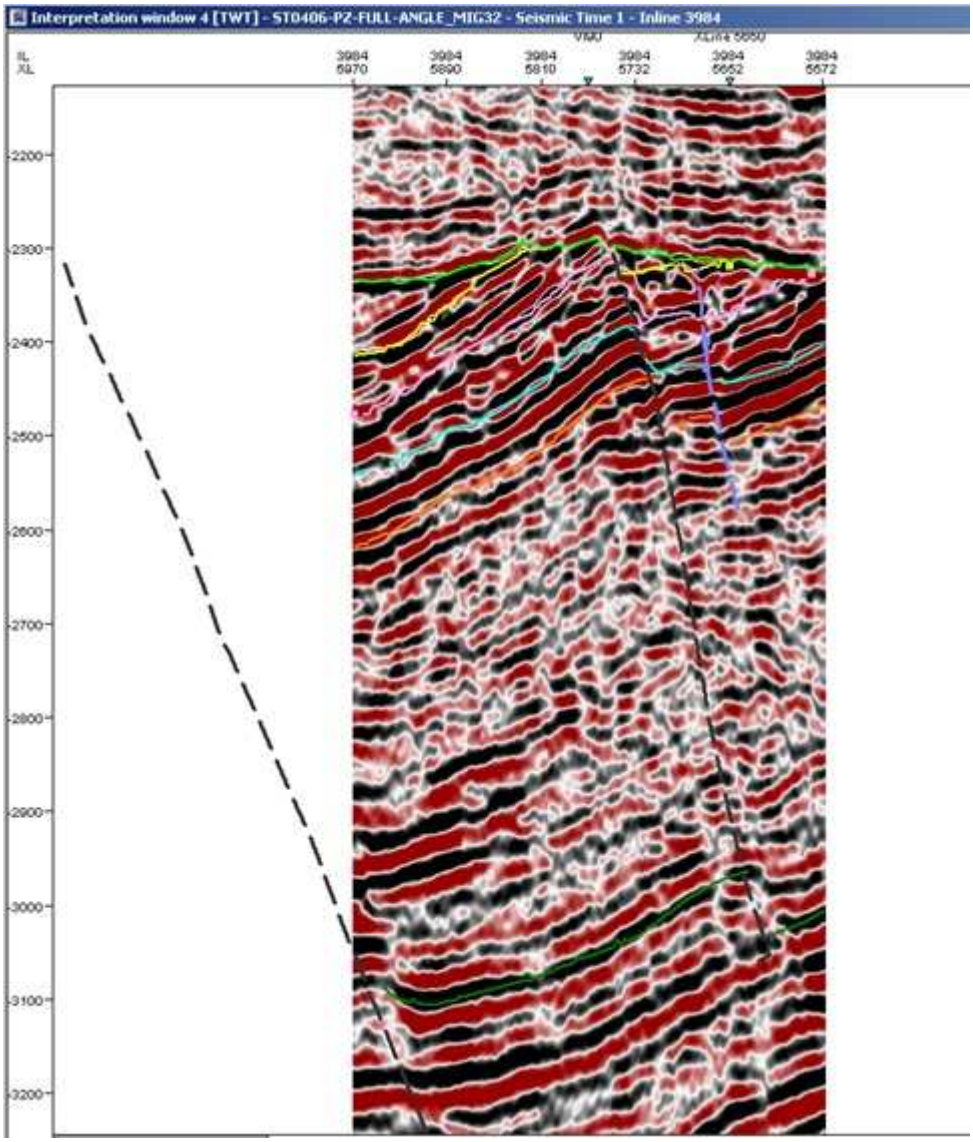

Figure 5-6: Interpretation on PZ 3D-cube, bottom layers

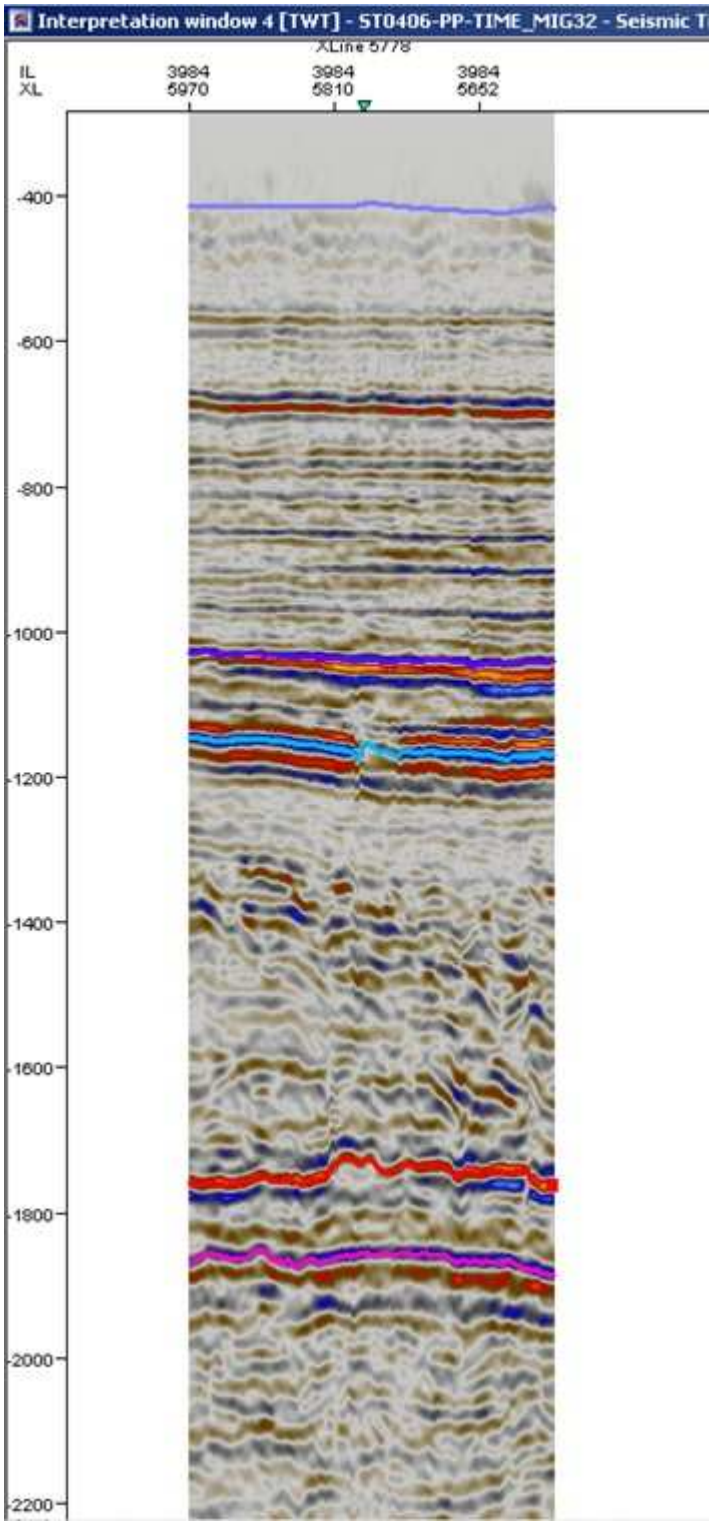

Figure 5-7: Interpretation on PS PP-time 3D-cube, top layers

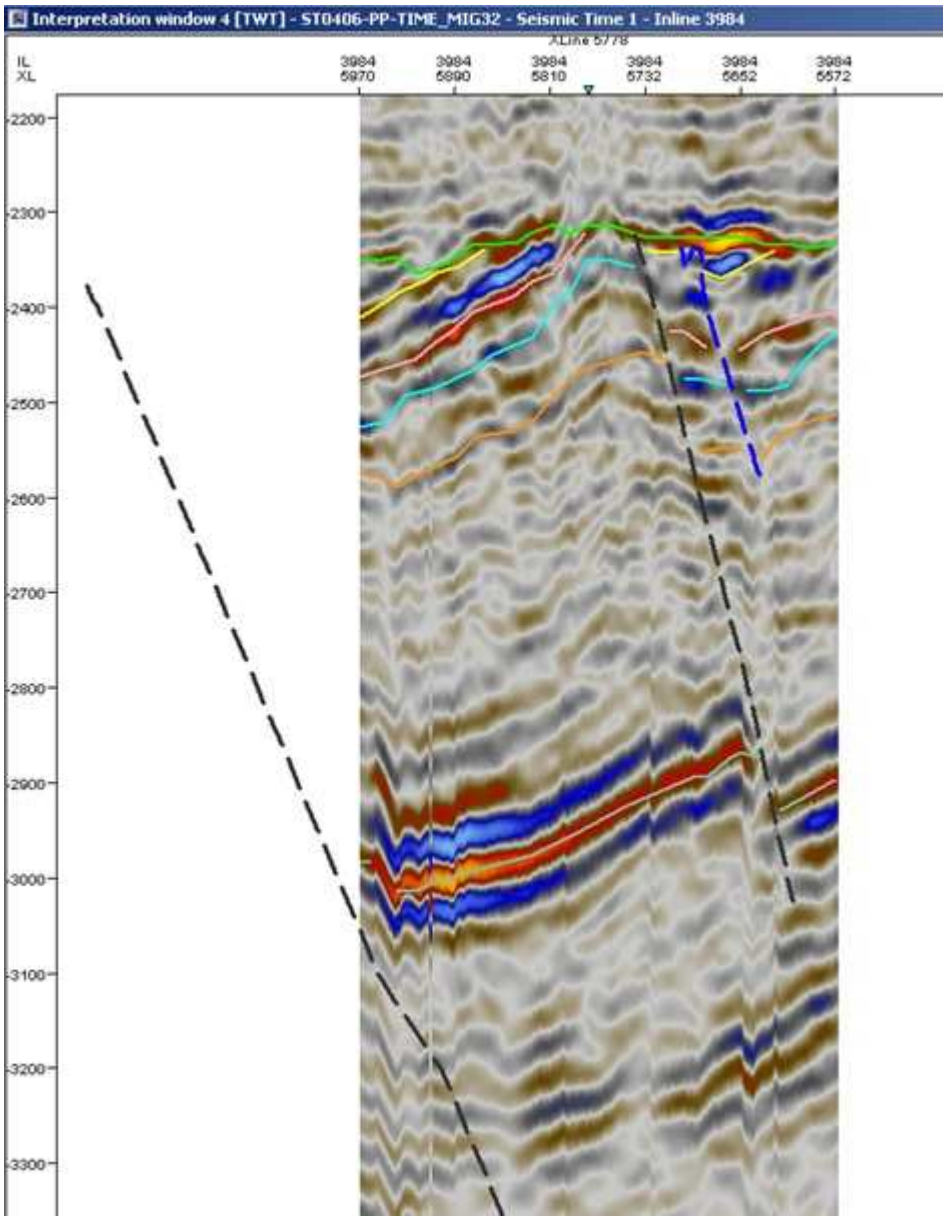

Figure 5-8: Interpretation on PS PP-time 3D-cube, bottom layers

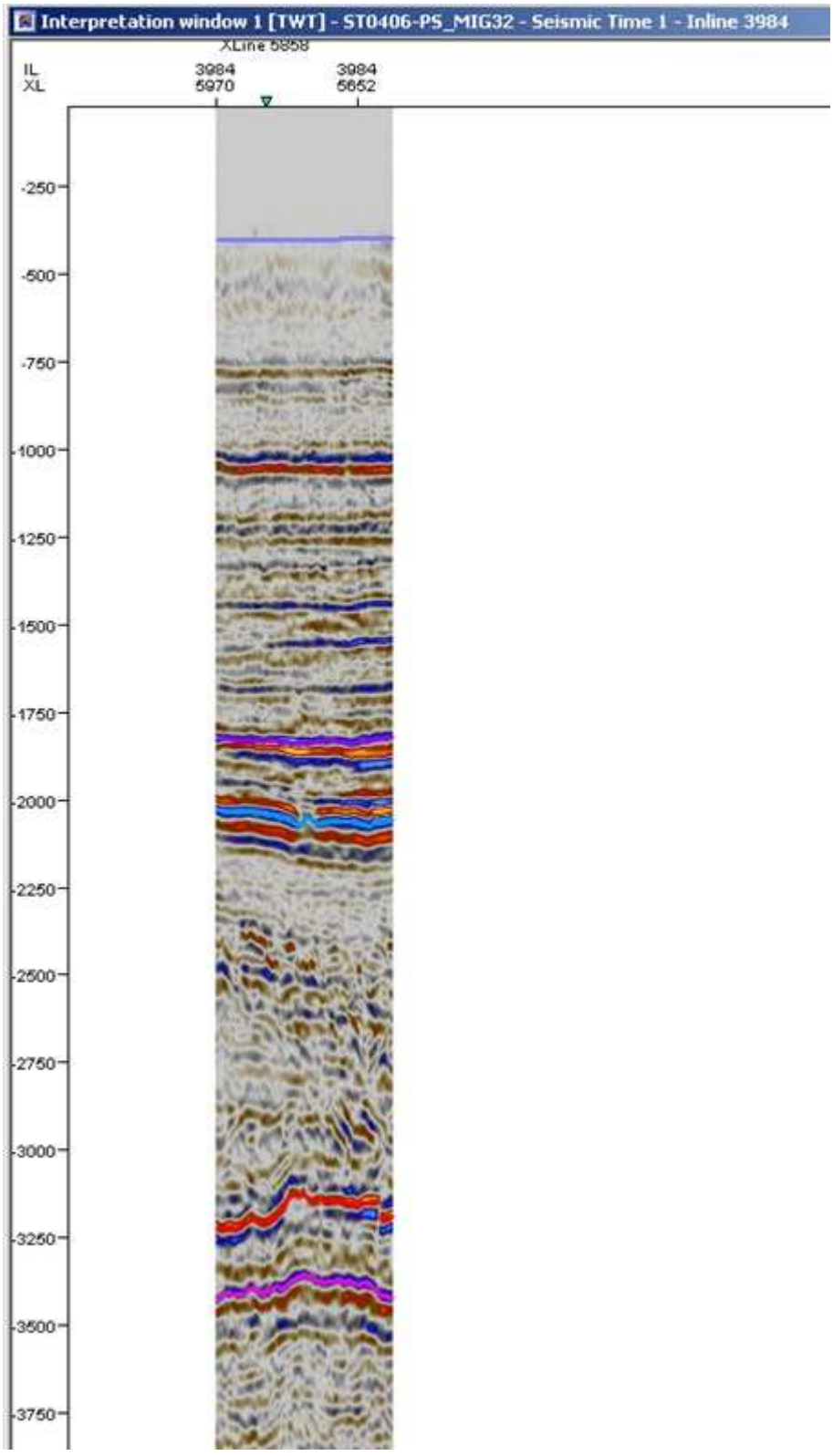

Figure 5-9: Interpretation on PS PS-time 3D-cube, top layers

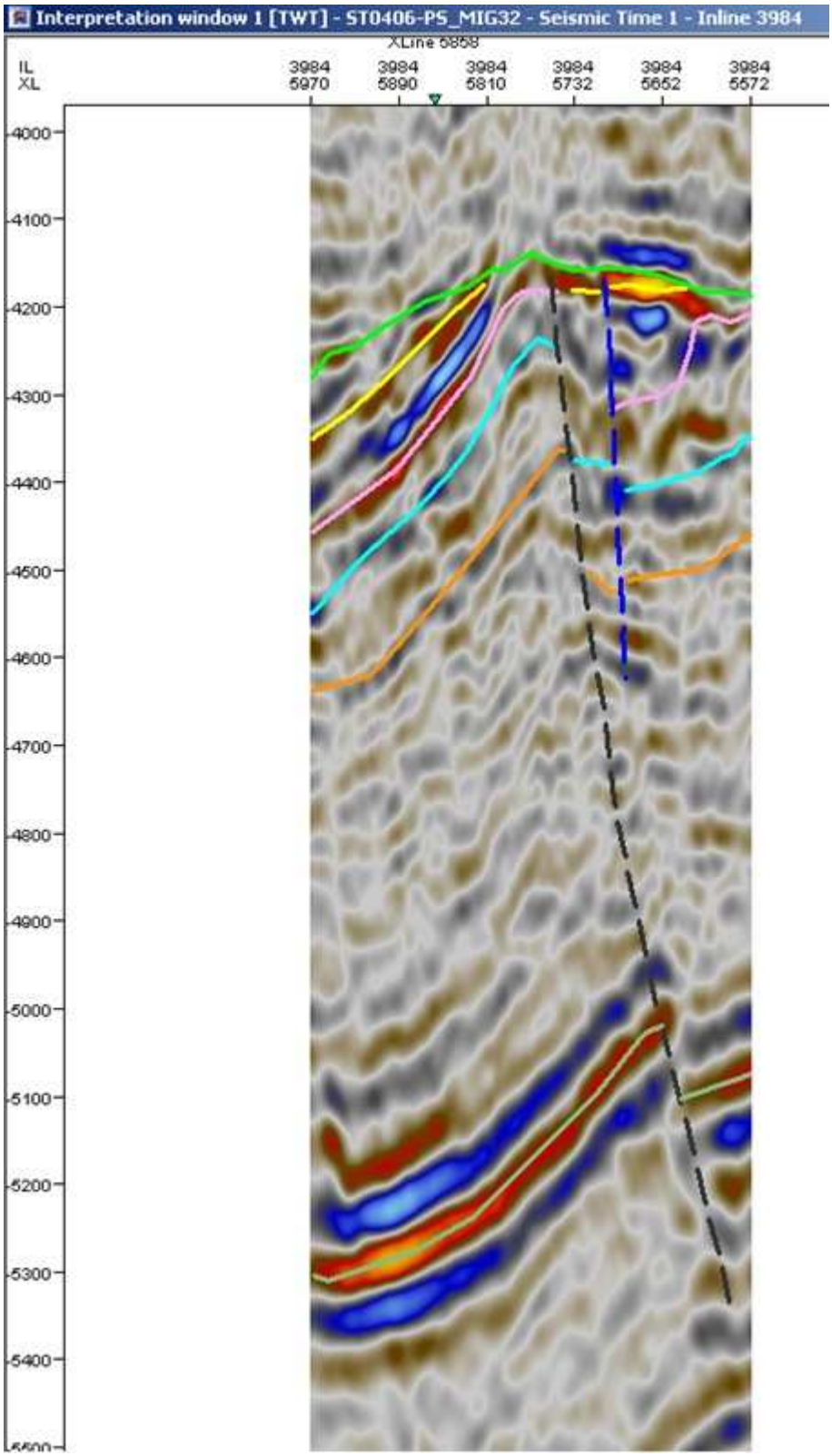

Figure 5-10: Interpretation on PS PS-time 3D-cube, bottom layers

When the interpretation of the 3D-cubes was complete, one of the Normal Incidence VSP SEGY-files (VSPNI-7 MPH Enhanced Deconvolved Upwave) were imported into Petrel, and then interpreted. The header values of the SEGY-file were missing the UTM positions, so these were made using the UTM coordinates of the well top and adding the coordinates for the receiver positions in ProMAX. When the SEGY-file was imported into Petrel we saw that the horizons from the OBC interpretation correlated well with the seismic pulses on the VSP profile (see Figure 5-11).

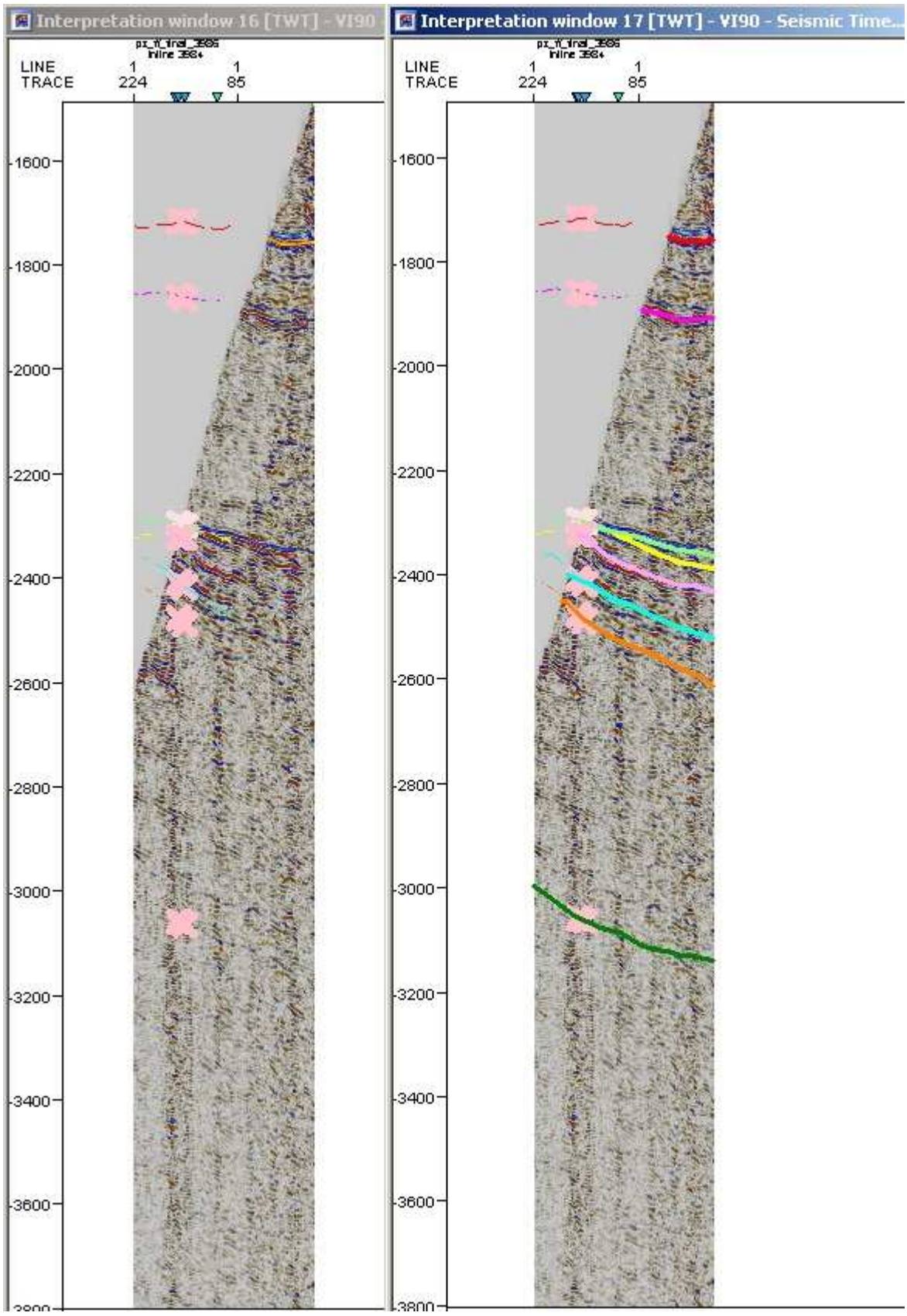

Figure 5-11: Interpretation of VSP profile; VSP profile with interpretation crosses and lines from the 2D and 3D interpretation (left), VSP profile with VSP interpretation.

5.4 Ray-trace modeling

A ray-trace model for a VSP survey was made with the NORSAR 3D modeling software. The surfaces made in Petrel were extrapolated as points, and imported into the modeling. First the surfaces were opened in the grid window, and stored as grids. The grids were then opened in the Model Builder window, where they were defined as horizons. The horizons were then cut in areas of cross-section between the horizons, and then placed into blocks. A horizon for the surface also had to be made for the modeling. This was used by using the grid for the seabottom, and changing the two-way travel time for all points to zero.

To model the Normal Incidence VSP the receiver locations, extracted from header values of the VSP SEGY-data, were imported. The shots were placed vertically above the receivers, at the surface (receiver and shot positions given in Appendix B). To include Rig Source VSP, a single shot point was added at the location given from the report, at UTM X: 454337, Y: 6813230.

First we concentrated on the Normal Incidence VSP modeling. After the horizons were imported, cut and blocked, velocities for each block had to be set. The P-wave velocities for the different layers were found from the NIVSP Report. A list of all the interval velocity with the corresponding depth and travel-times given in the report were used to make a graph (see Figure 5-12) (For full list of values for depth, traveltime and interval velocity, view Appendix B). The interval velocities were then blocked into the different layers, and the average values were found for each layer. These velocities were then put as the velocities of the different blocks in the model (see Table 5-2). The densities were kept standard for the program (ρ=2.0), since we first only needed a simple model. Then the horizons which are given in time are depth converted with the velocities given.

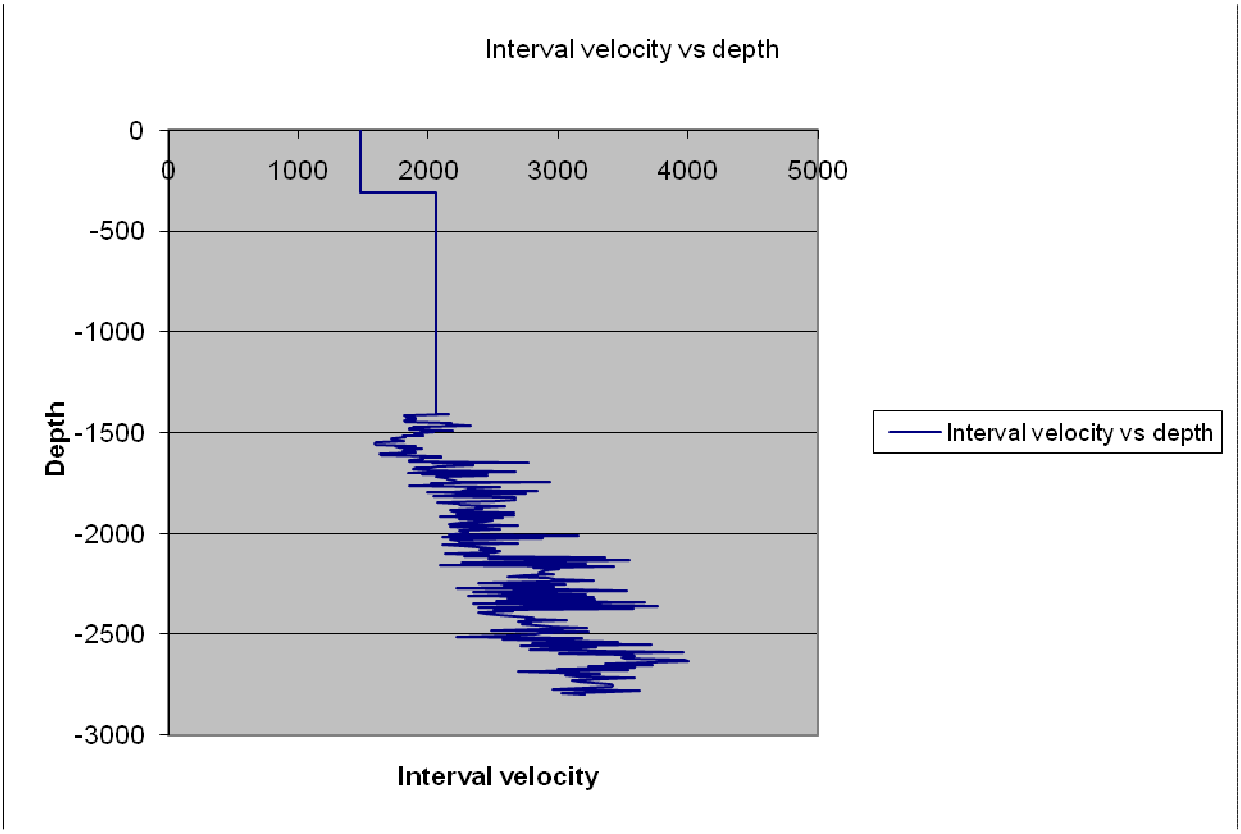

Figure 5-12: Interval P-wave velocities vs. depth, taken from NIVSP Report.

Table 5-2: Initial interval velocities given in ray-tracing model

Blocks	Interval velocity (P-wave)
Below Surface, above Seabottom	1478
Below Seabottom, above Utsira Fm	2062
Below Utsira, above Hordaland Gp	2000
Below Hordaland Gp, above Balder Fm	1948
Below Balder Fm, above Shetland Gp	2034
Below Shetland Gp, above BCU	2613
Below BCU, above SN11.4	2931
Below SN11.4, above SN10.4	3228
Below SN10.4, above SN10.1	3032
Below SN10.1, above SN9.3	3180
Below SN9.3, above SN Lower Lunde	3024

The ray-tracing was then performed in the Wave Tracer Window with a direct P-wave ray code selected. Because the horizons imported were smaller than the area of the well, some of the shot-receiver pairs were outside of the defined area, so only shot-receiver pairs 79 to 224 were included in this model. We concentrated however on these shots to correlate the direct wave given from the synthetic seismogram with the original vertical receiver VSP SEGY-file. By changing the velocities, in the time model, for the upper layers gradually, the arrival time of the direct wave was matched closer to that of the original SEGY-file (TC times from Interval Velocity-Time-Depth file in Appendix B). When doing this we only looked at the shot-receiver pairs; 80, 120, 150, 200, and 220. Shot-receiver pair means that for a specific shot number only the corresponding geophone number, located vertically below the shot point, is used in the ray-tracing. The seismogram generation of the shot-receiver pair 80 before velocity change is viewed in Figure 5-13, and the display of the seismogram is viewed in Figure 5-14. Table 5-3 and Table 5-4 show the final velocities decided on, and the arrival times for the direct wave in the report, in the initial model and the final model. The depth conversion of the model had to be redone after each velocity change.

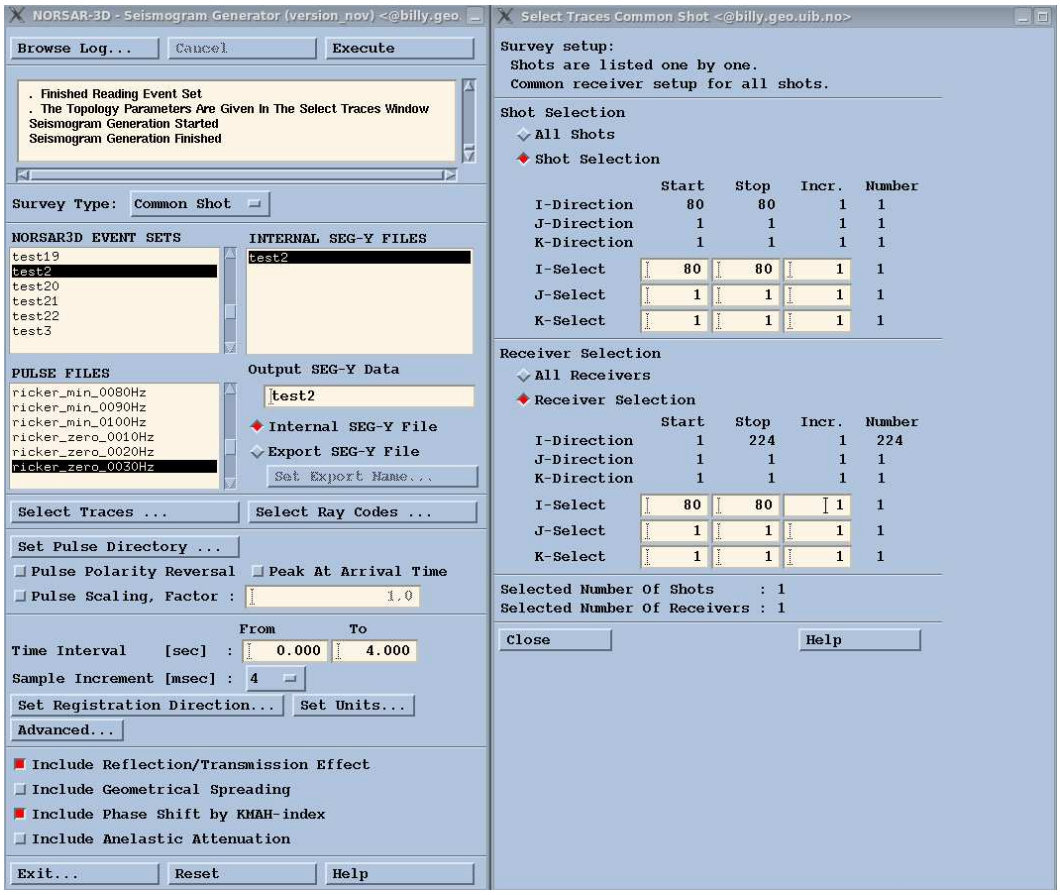

Figure 5-13: Generation of seismogram for shot-receiver pair 80.

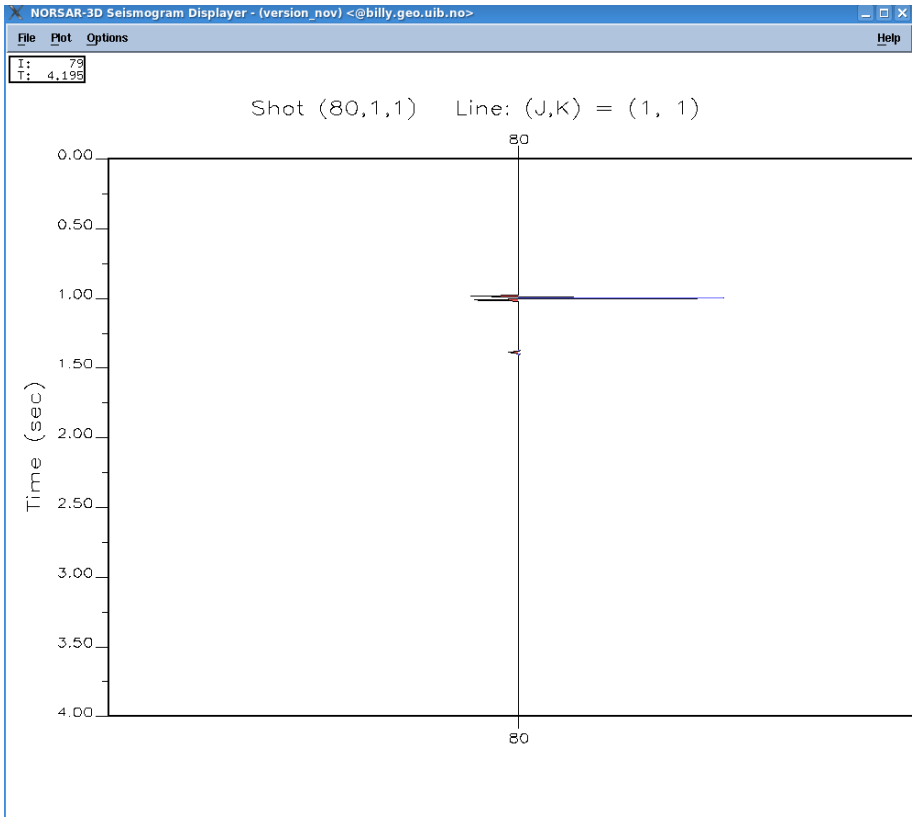

Figure 5-14: Display of seismogram for shot-receiver pair 80. The direct wave and a reflection can be viewed in the trace.

Table 5-3: Final interval velocities given in ray-tracing model

Blocks	Interval velocity (P-wave)
Below Surface, above Seabottom	1485
Below Seabottom, above Utsira Fm	2392
Below Utsira, above Hordaland Gp	2192
Below Hordaland Gp, above Balder Fm	1958
Below Balder Fm, above Shetland Gp	2044
Below Shetland Gp, above BCU	2613
Below BCU, above SN11.4	2931
Below SN11.4, above SN10.4	3228
Below SN10.4, above SN10.1	3101
Below SN10.1, above SN9.3	3180
Below SN9.3, above SN Lower Lunde	3024

Table 5-4: Shot-receiver pairs and the corresponding arrival times (TC), original times, and before and after velocity changes.

Shot-receiver pair	Arrival times from NIVSP report (TC)	First seismogram	Final Seismogram
80	940	996	951
120	1045	1090	1049
150	1125	1176	1133
200	1249	1288	1252
220	1294	1339	1298

The model was then ray-traced with all of the ray codes, direct P-wave and P-wave reflection on each interface. The ray-tracing was first done with the original velocity values, and then with the final velocity values. When ray-tracing in NORSAR all of the receivers are in use for each shot. In a NIVSP survey, only the receiver vertically below the shot point will be used. In order to get a synthetic seismogram with just the shot-receiver pairs, we had to generate separate seismograms for each shot-receiver pair, and then add these traces together to get the traces of the NIVSP. So for this model the traces 79-224 were made into 146 seismograms that were added together to make the full seismogram. This was done by using the Linux command window, and making a program adding the traces (shown below for adding of 5 traces).

Combine script

```
segyread tape=001.sgy endian=0 | segyclean > 001.su
segyread tape=002.sgy endian=0 | segyclean > 002.su
segyread tape=003.sgy endian=0 | segyclean > 003.su
segyread tape=004.sgy endian=0 | segyclean > 004.su
segyread tape=005.sgy endian=0 | segyclean > 005.su

cat 001.su \
002.su \
003.su \
004.su \
005.su > 1-005.su

segyhdrs < 1-005.su
segywrite < 1-005.su endian=0 tape=1-005.sgy

rm *.su

exit
```

The result of the first seismogram, one for the direct wave and one for the reflections, and the result of the final seismogram, both the direct and reflected in one seismogram, are given in Figure 5-15, Figure 5-16 and Figure 5-17. The arrivals were easier to view in the density display, than in the wiggle display, so all the seismograms were viewed in the density display.

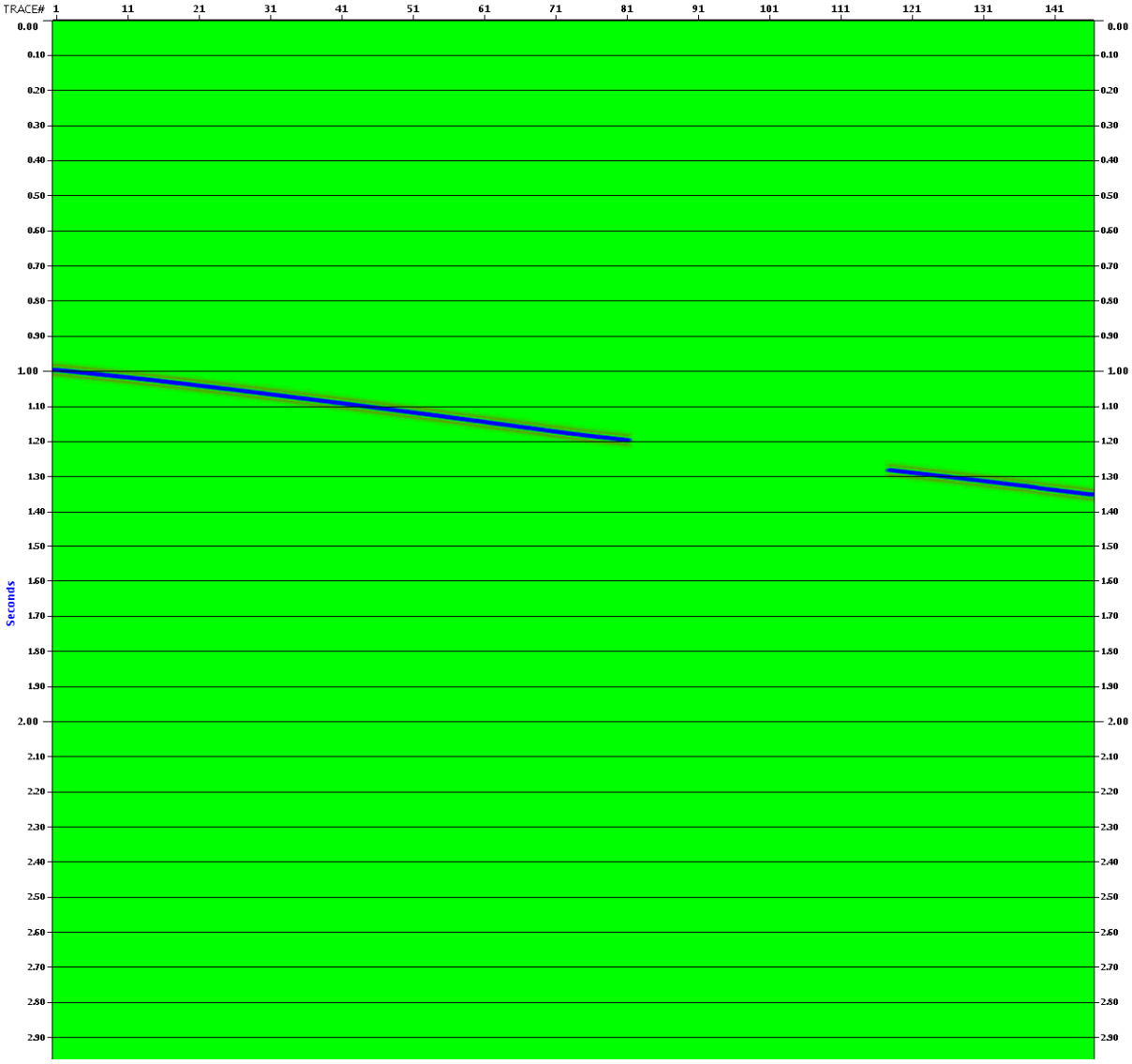

Figure 5-15: First seismogram for shot-receiver pair 79-224, direct wave

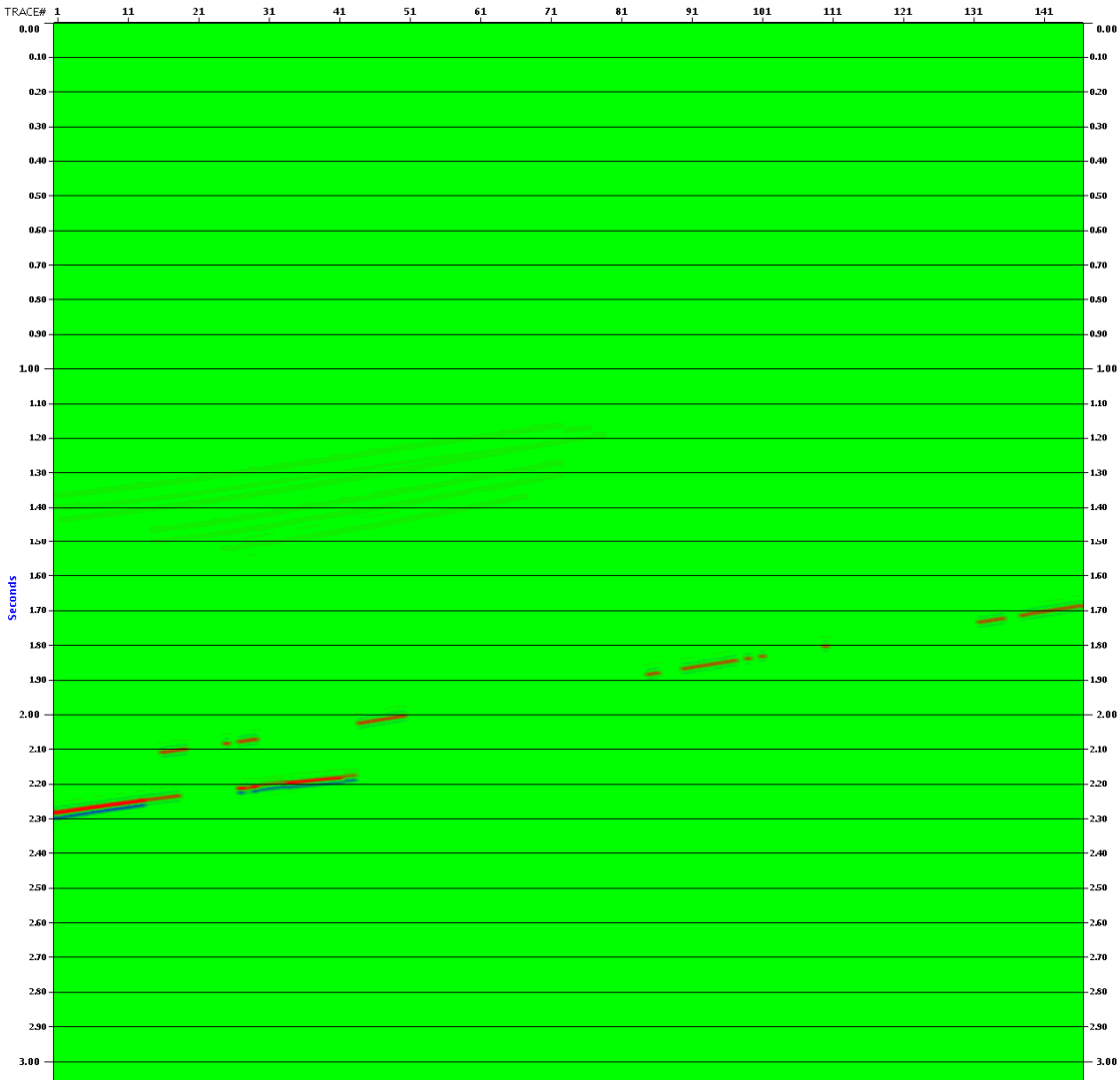

Figure 5-16: First seismogram for shot-receiver pair 79-224, reflected waves

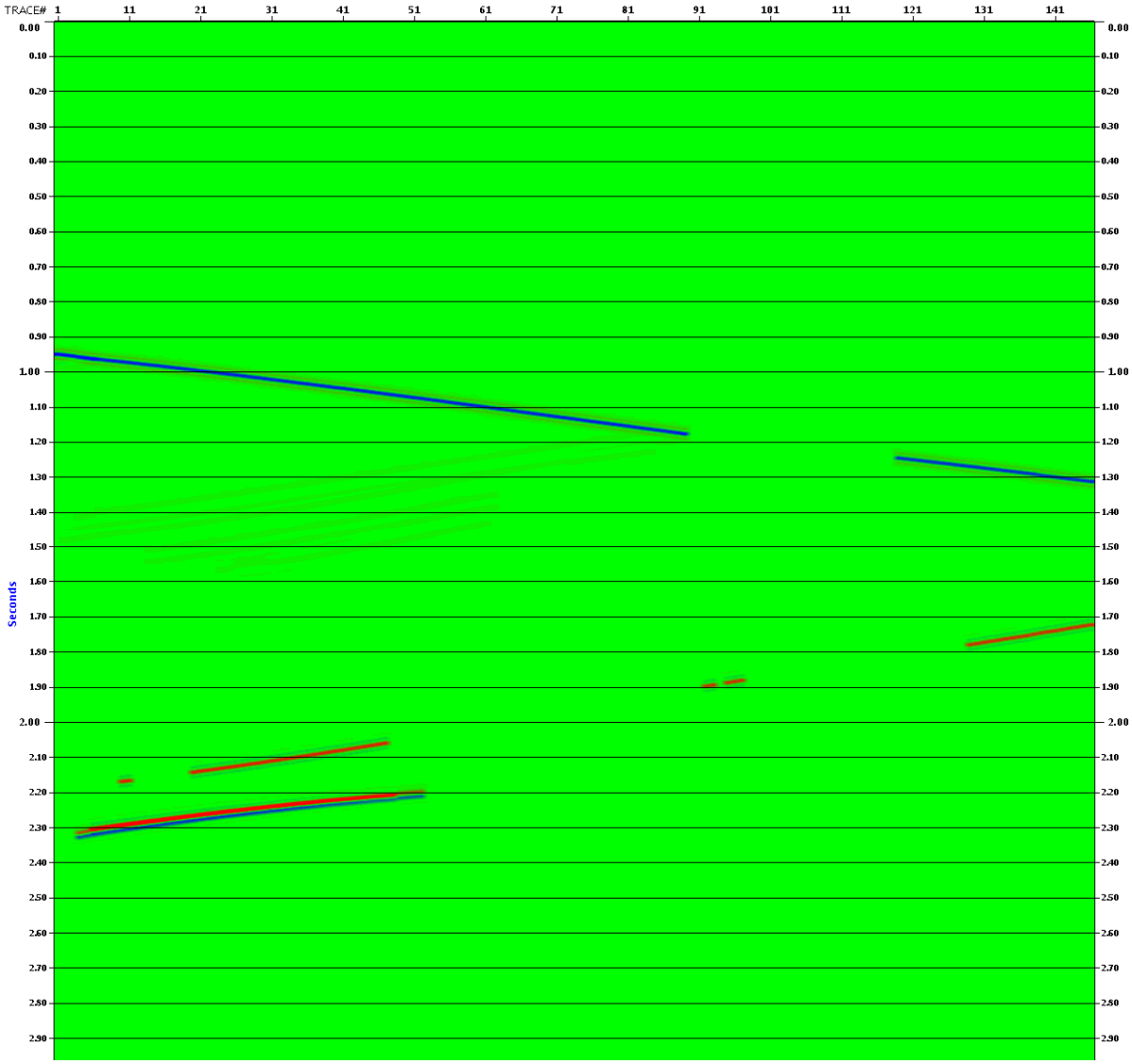

Figure 5-17: Final synthetic seismogram for shot-receiver pair 79-224

Some of the reflected waves can be hard to view, but by changing the scaling, this can be improved. In the seismograms displayed above there are gaps in the direct wave arrival, traces with no pulse signal. These indicated that the model had to be improved in the area with no traces.

To include all of the shots for the Normal Incidence, and also Rig Source VSP the top horizons in the model had to be extrapolated. This was done in the Model Builder window. The blocks remained the same, but some extra cutting had to be done on the lowest layer which was also extrapolated, due to loss of points after depth conversion. Also the gap in the data was treated by some more cutting and block definition of the model (see Figure 5-18).

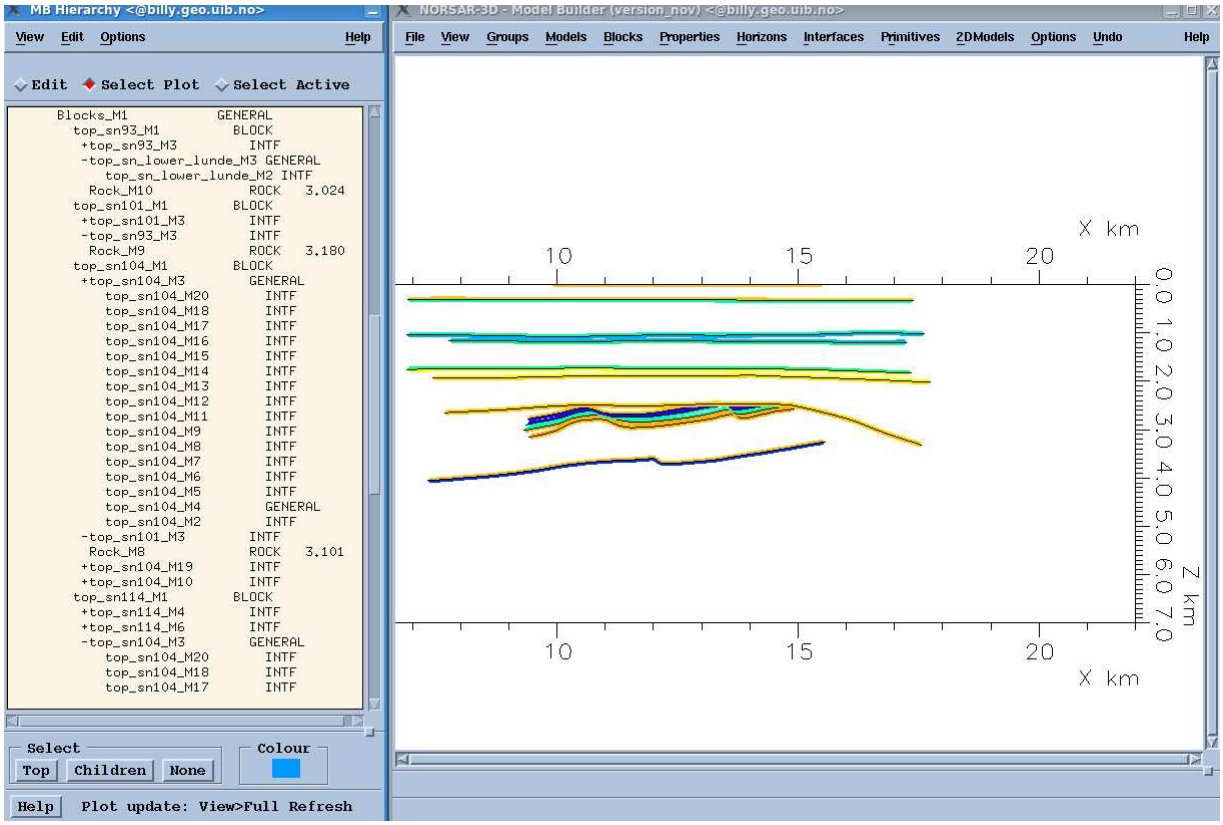

Figure 5-18: Model defined into block (different colors), with different velocities in the different blocks

Then the ray-tracing was performed for all of the shot-receiver pairs for Normal Incidence, and for the one shot point in the Rig Source VSP modeling. As mentioned above NORSAR includes all receivers for each shot. The direct P-wave for one shot for the NIVSP is displayed in Figure 5-19. For this shot we only want the direct arrival for the geophone located vertically below, when generating the Normal Incidence VSP synthetic seismogram.

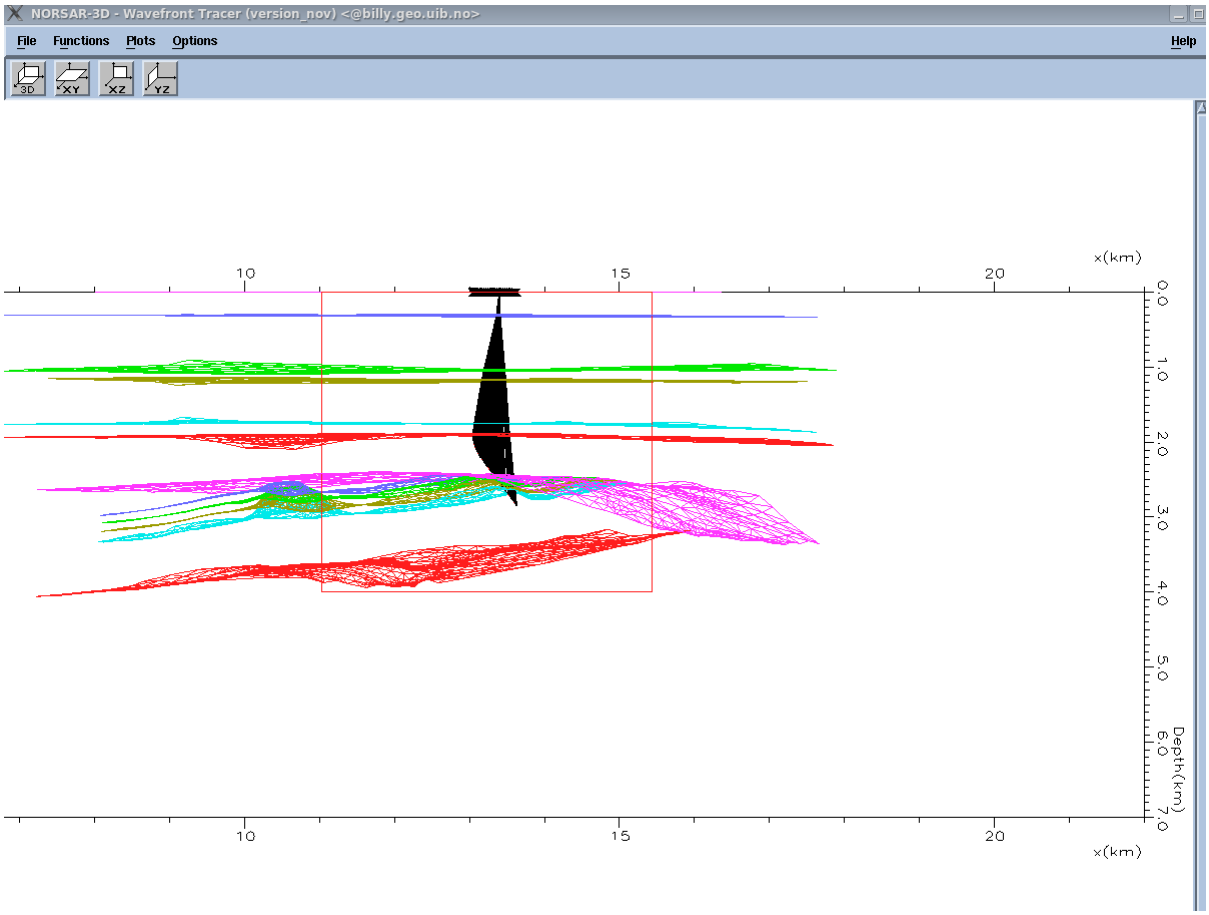

Figure 5-19: Direct P-wave for one shot in the NIVSP ray-tracing model. Arrivals at all the geophones are included.

To get the synthetic seismogram for the NIVSP seismograms for all of the 224 shot-receiver pairs had to be processed separately as before, and then added together using the combine script. The result of the NIVSP seismogram is shown in Figure 5-20, and the seismogram for the RSVSP is shown in Figure 5-21. The scaling was increased to a ratio of 15, to display the arrivals better. We also compared the P-wave arrival times of the direct wave on the Rig Source synthetic seismogram, with the observed arrival time of the survey. These also seemed to be closely matched with the final velocity model.

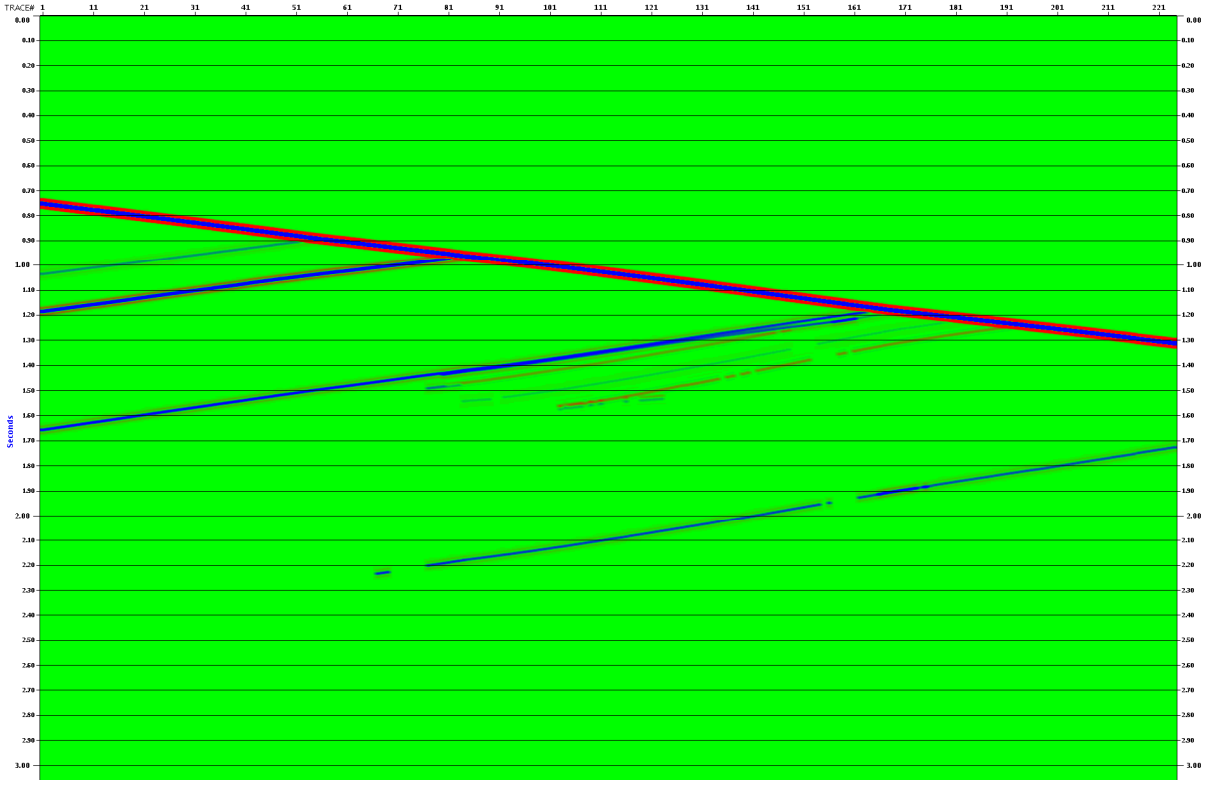

Figure 5-20: Synthetic seismogram for NIVSP with only direct P and reflected P (with a scaling ratio of 15)

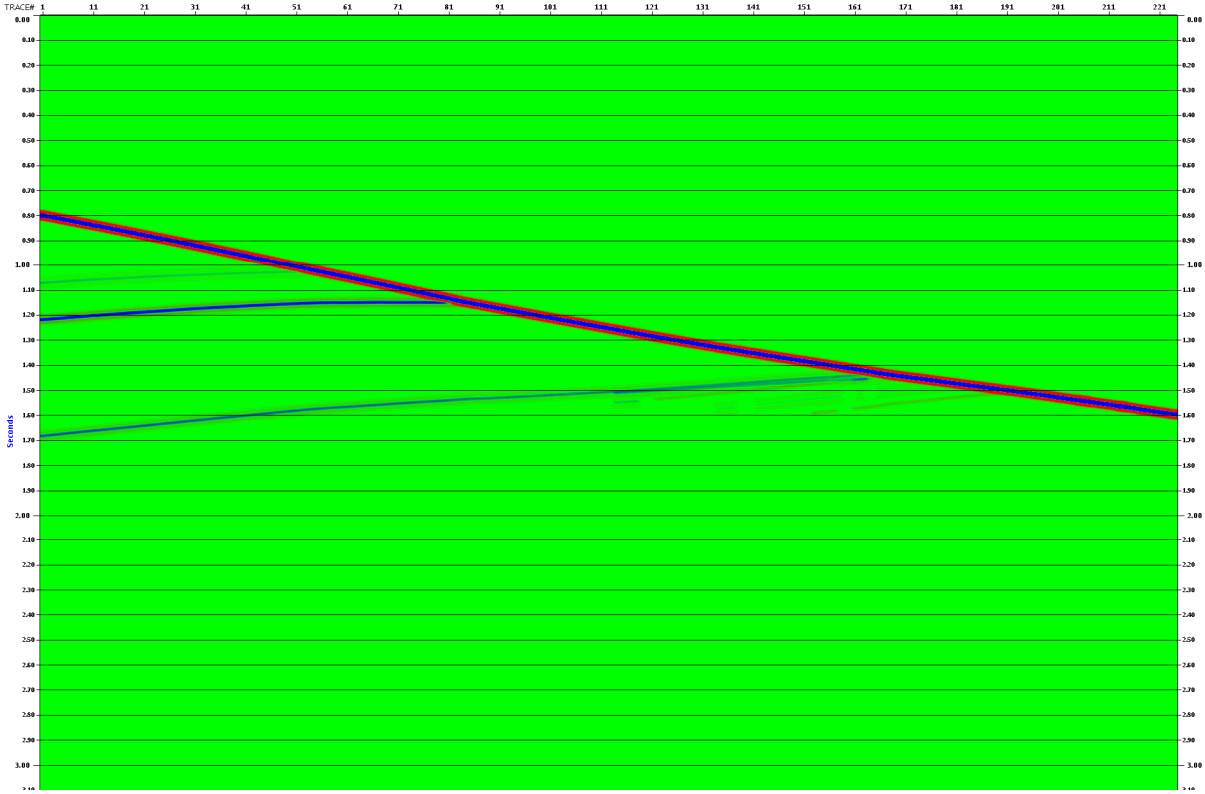

Figure 5-21: Synthetic seismogram for RSVSP with only direct P and reflected P (with a scaling ratio of 15)

Then S-wave conversion was taken into the models. The V_s/V_p ratio used was 0.55. This was calculated from looking at the up- and downgoing S-waves found in the VSP SEGY-files. The ray-codes chosen were direct P, P to P reflection from each horizon and P to S reflections from each horizon. The ray-tracing was run for both NIVSP (see Figure 5-22, Figure 5-23 and Figure 5-24) and RSVSP (see Figure 5-25, Figure 5-26 and Figure 5-27) with reflected S-wave conversion included. Three seismograms were made for each of the surveys; the H1 component, H2 component and the Vertical component. The previous seismograms displayed were only from the Vertical component.

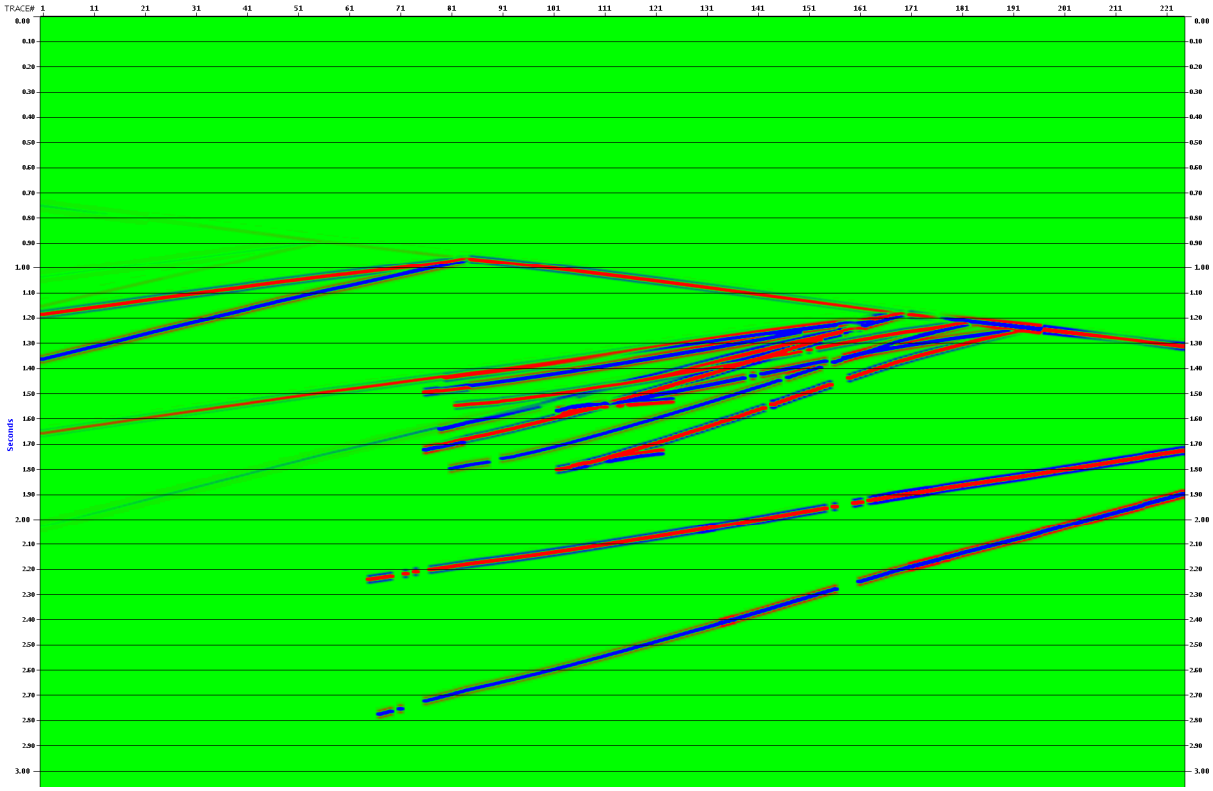

Figure 5-22: Synthetic seismogram for the H1 (X) component of NIVSP with reflected S-wave conversion in addition to direct P and reflected P (with scaling ratio of 15)

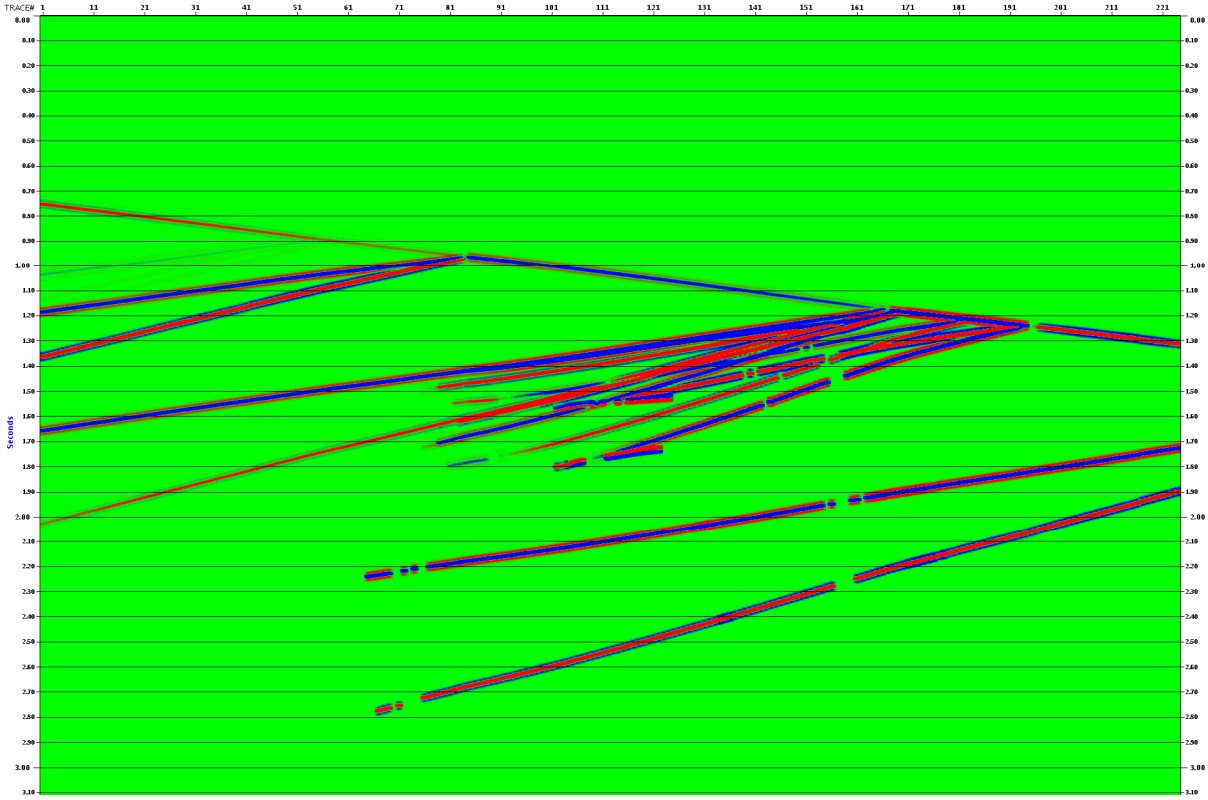

Figure 5-23: Synthetic seismogram for the H2 (Y) component of NIVSP with reflected S-wave conversion in addition to direct P and reflected P (with scaling ratio of 15)

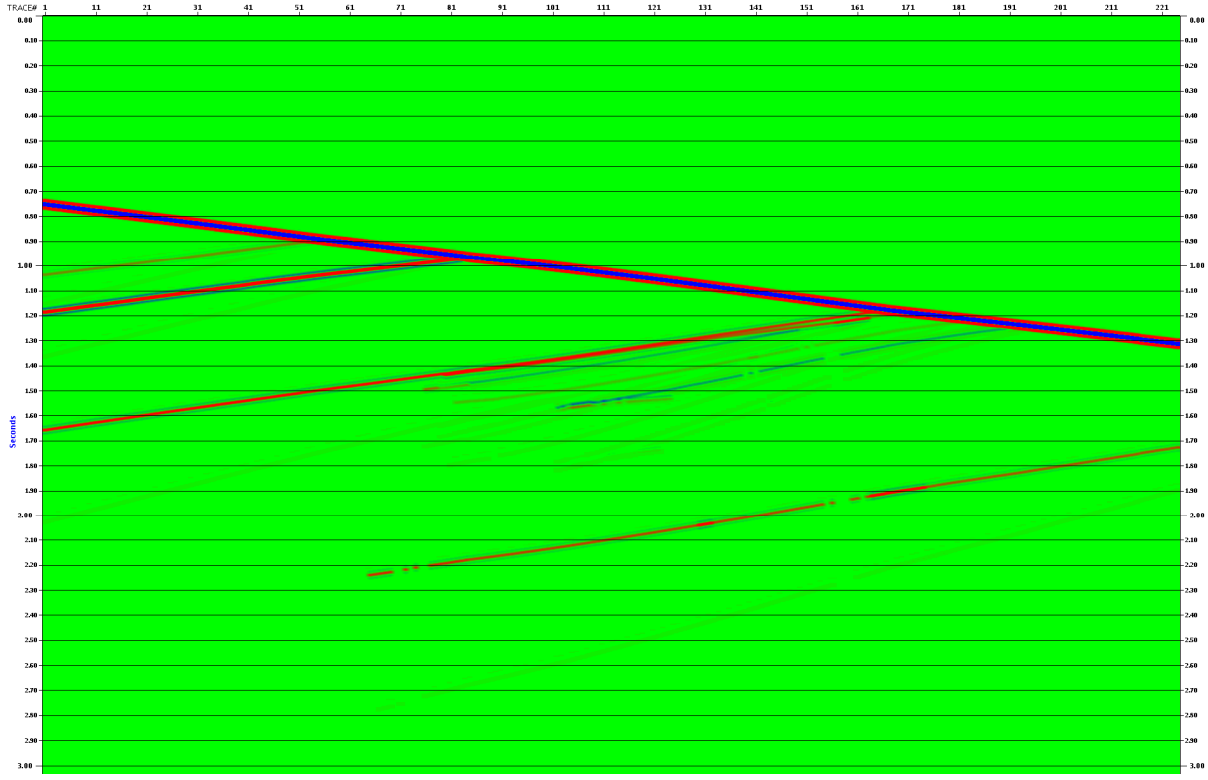

Figure 5-24:Synthetic seismogram for the Vertical (Z) component of NIVSP with reflected S-wave conversion in addition to direct P and reflected P (with scaling ratio of 15)

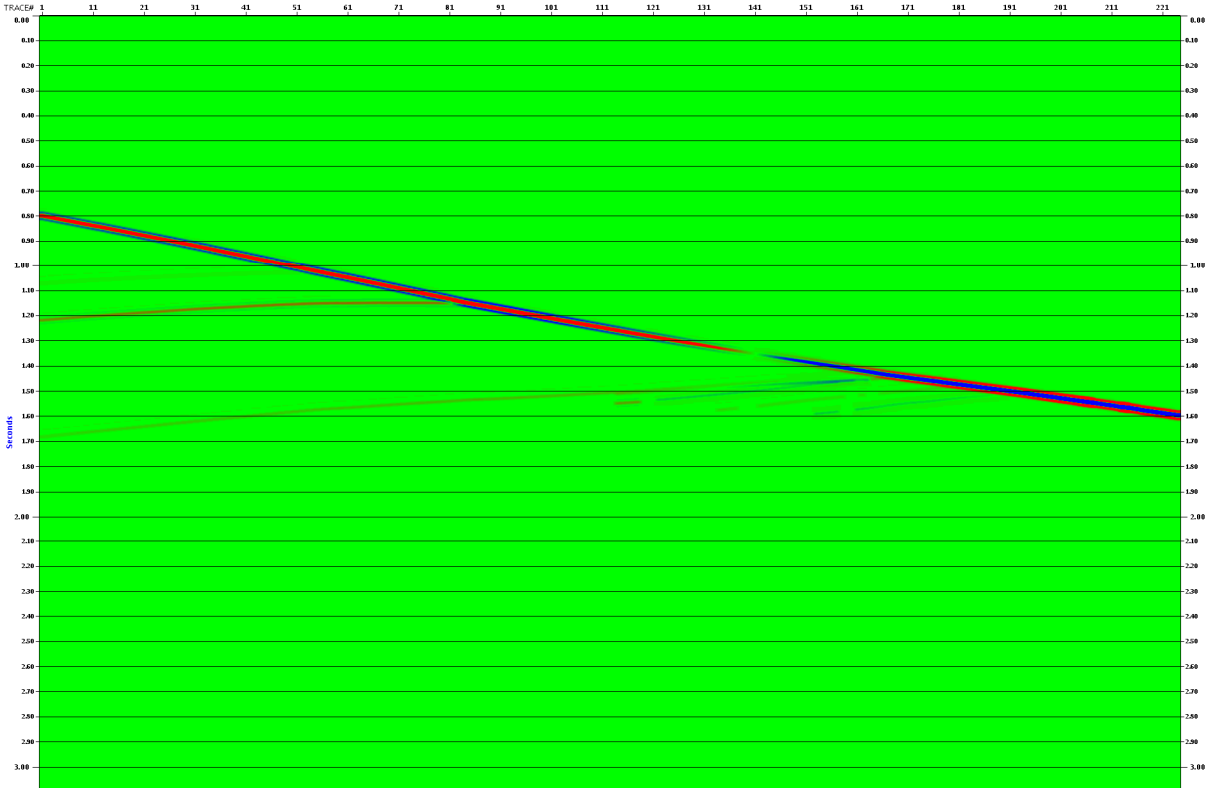

Figure 5-25: Synthetic seismogram for the H1 (X) component of RSVSP with reflected S-wave conversion in addition to direct P and reflected P (with scaling ratio of 15)

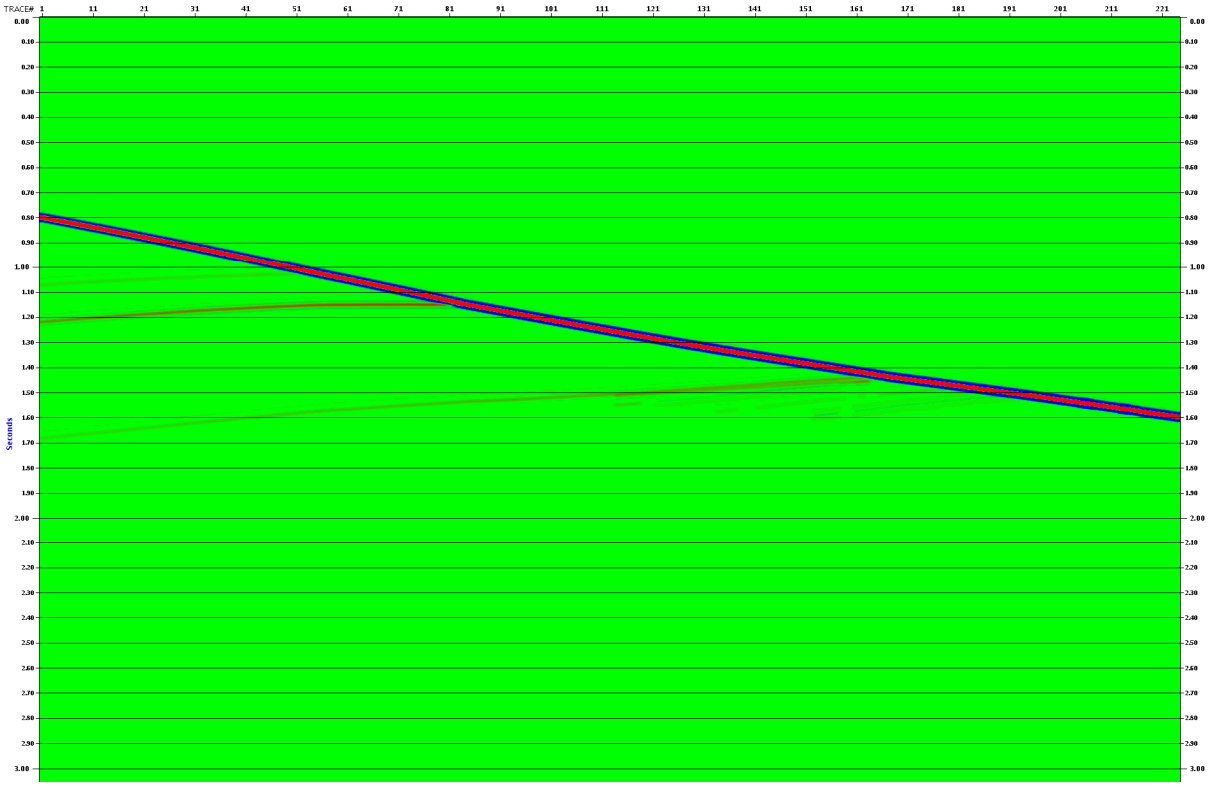

Figure 5-26: Synthetic seismogram for the H2 (Y) component of RSVSP with reflected S-wave conversion in addition to direct P and reflected P (with scaling ratio of 15)

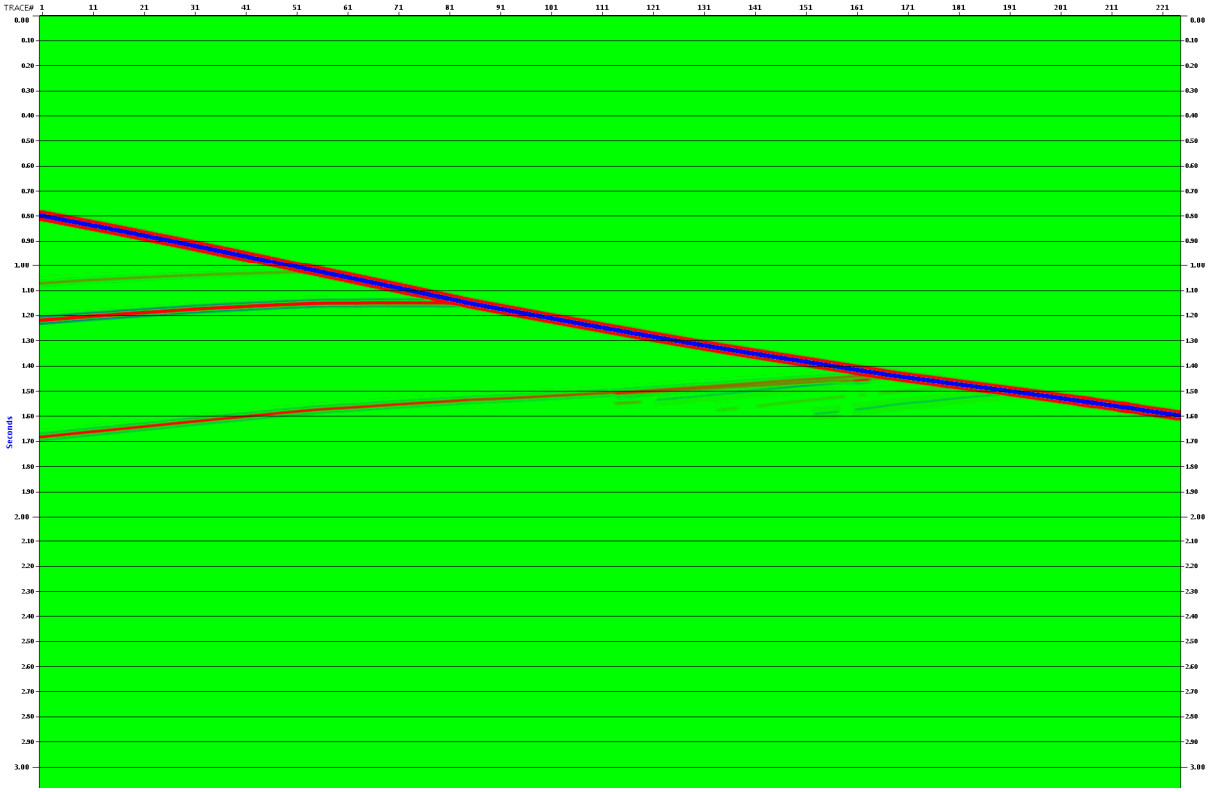

Figure 5-27: Synthetic seismogram for the Vertical (Z) component of RSVSP with reflected S-wave conversion in addition to direct P and reflected P (with scaling ratio of 15)

The modeling of the NIVSP was quite successful, demonstrating that both P- and PS- arrivals would be recorded even in the situation of approximately zero offset difference between source and receiver. In theory only P-waves would be recorded at zero offset. We do believe that the reason for the PS-arrivals being recorded is formation tops with structure above the receivers. The raypaths are therefore not truly vertical, giving rise to mode-conversions at certain interfaces.

Three issues should be emphasized:

- From the observed data it is possible to pick both the P first break and the PS first breaks. Picking the PS first breaks takes place on the background of noise and secondary arrivals as reflections and refractions.
- Based upon the first break picks it is possible to work out vertical times for both the P- and the PS-arrivals. Further, the Vs/Vp ratio may be computed. This Vs/Vp ratio (0,55) was fed into the modeling program to obtain a velocity model for the PS events.
- Defining the true PS-arrival is not easy. Some deviation and uncertainty to the result must be expected. However, there are no assumptions made to the data inside the VSP interval. We are looking at observations, which is unique to VSP.

It would be possible to discuss characteristics of the VSP using the observed data. However, the PS-events being of lower S/N-ratio would make this unnecessarily difficult. We therefore prefer to carry out the modeling exercise as it is easier to visualize NIVSP results by displaying synthetic seismograms with a selected and higher S/N ratio.

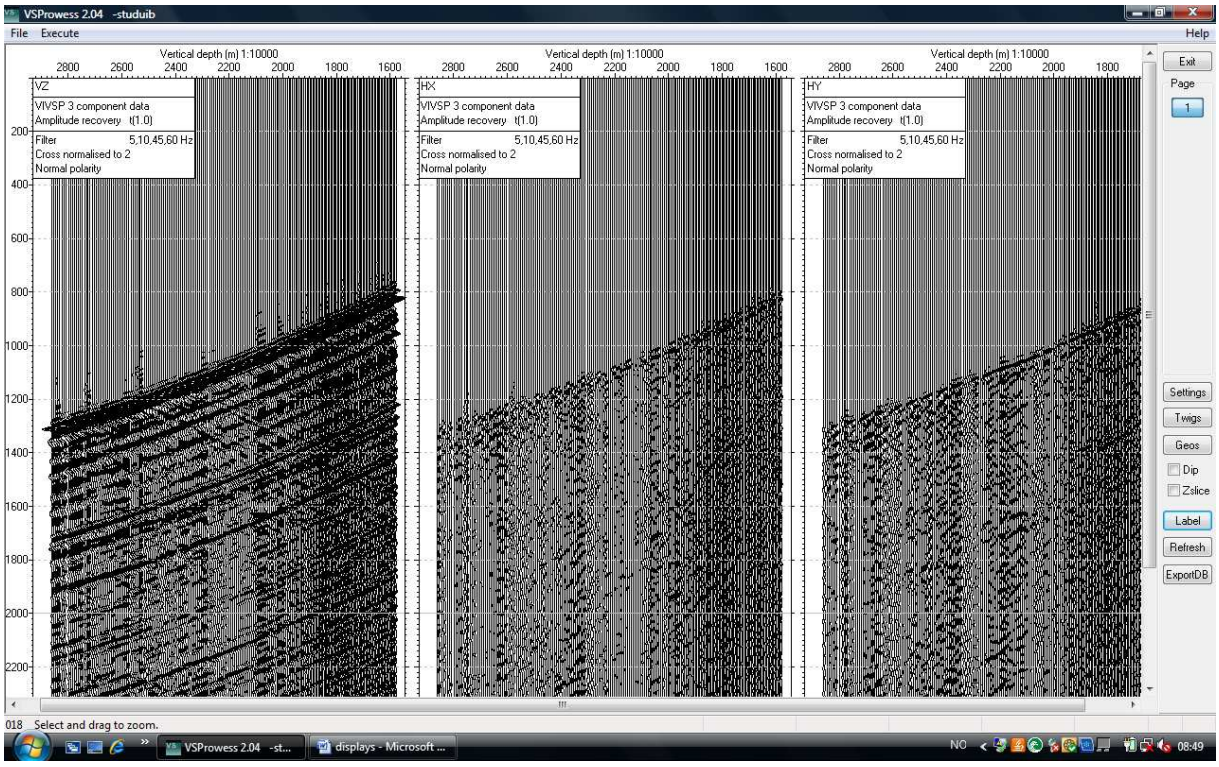

Figure 5-28: The three recorded components of the NIVSP survey.

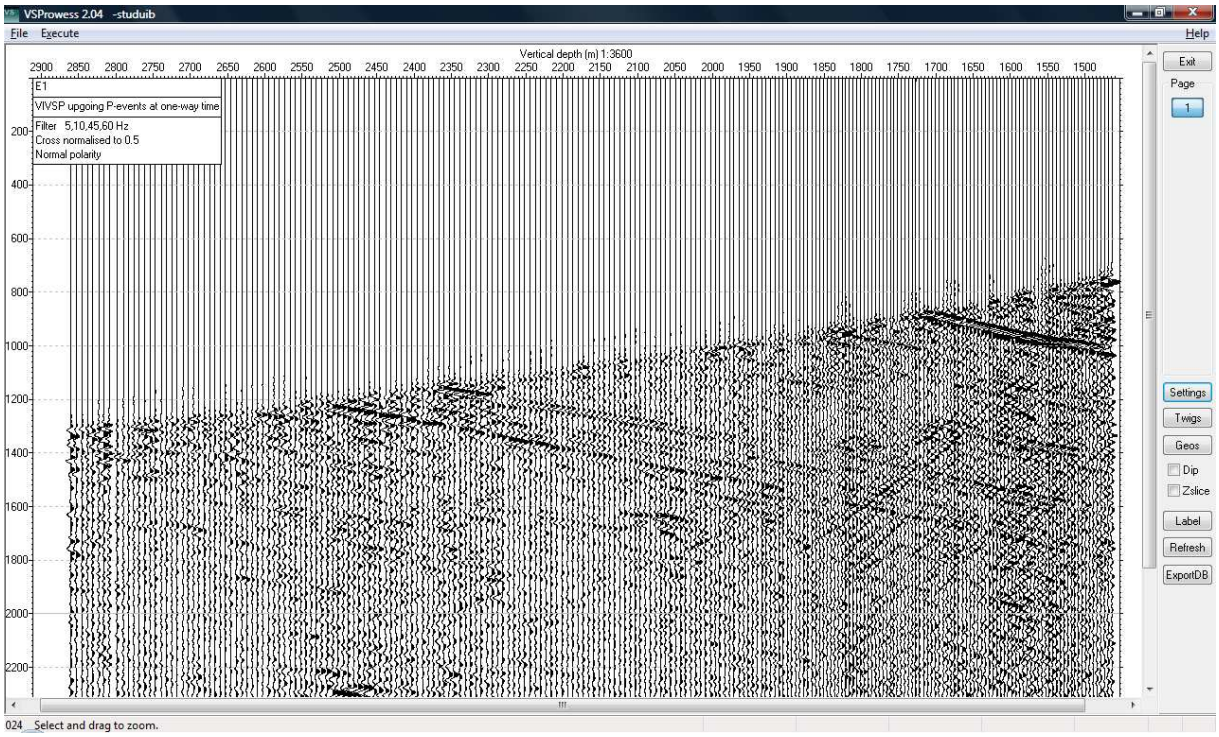

Figure 5-29: Upgoing P-events at one way traveltime recorded in NIVSP survey

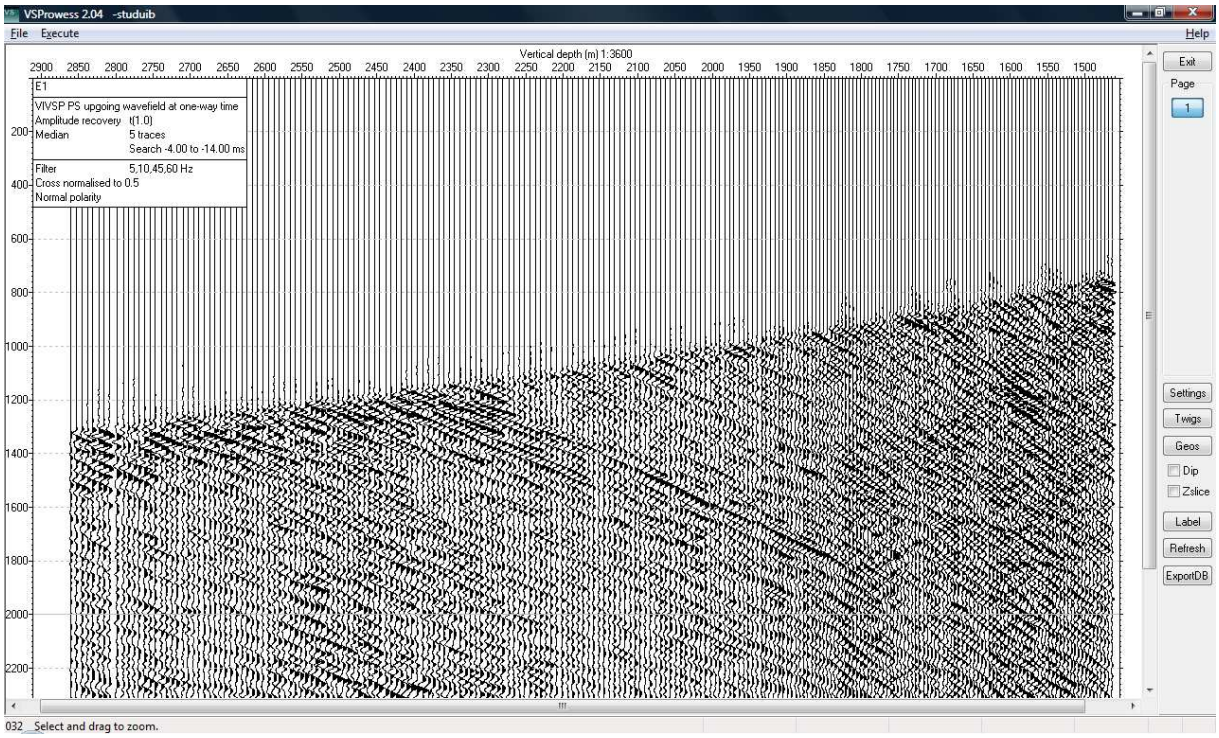

Figure 5-30: Upgoing PS-events at one-way traveltime recorded in the NIVSP survey.

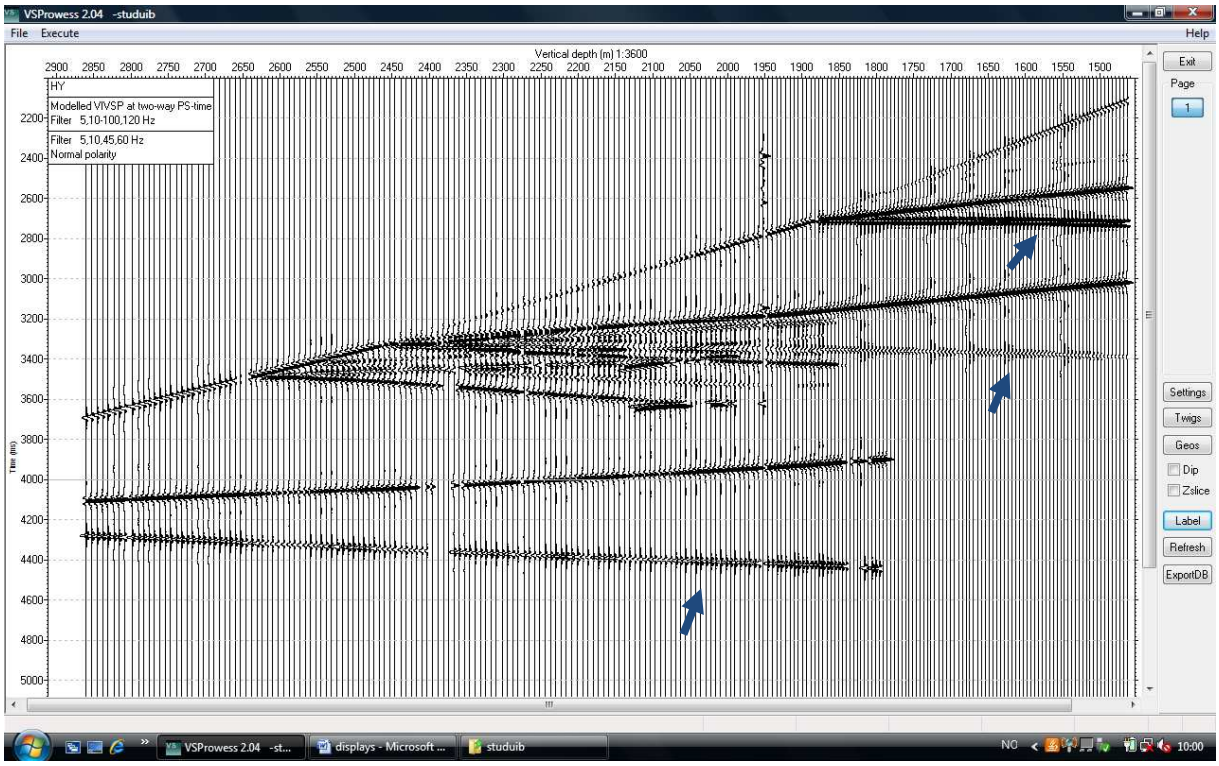

Figure 5-31: Modeled NIVSP at two-way PS time. Blue arrows indicate the PS reflections.

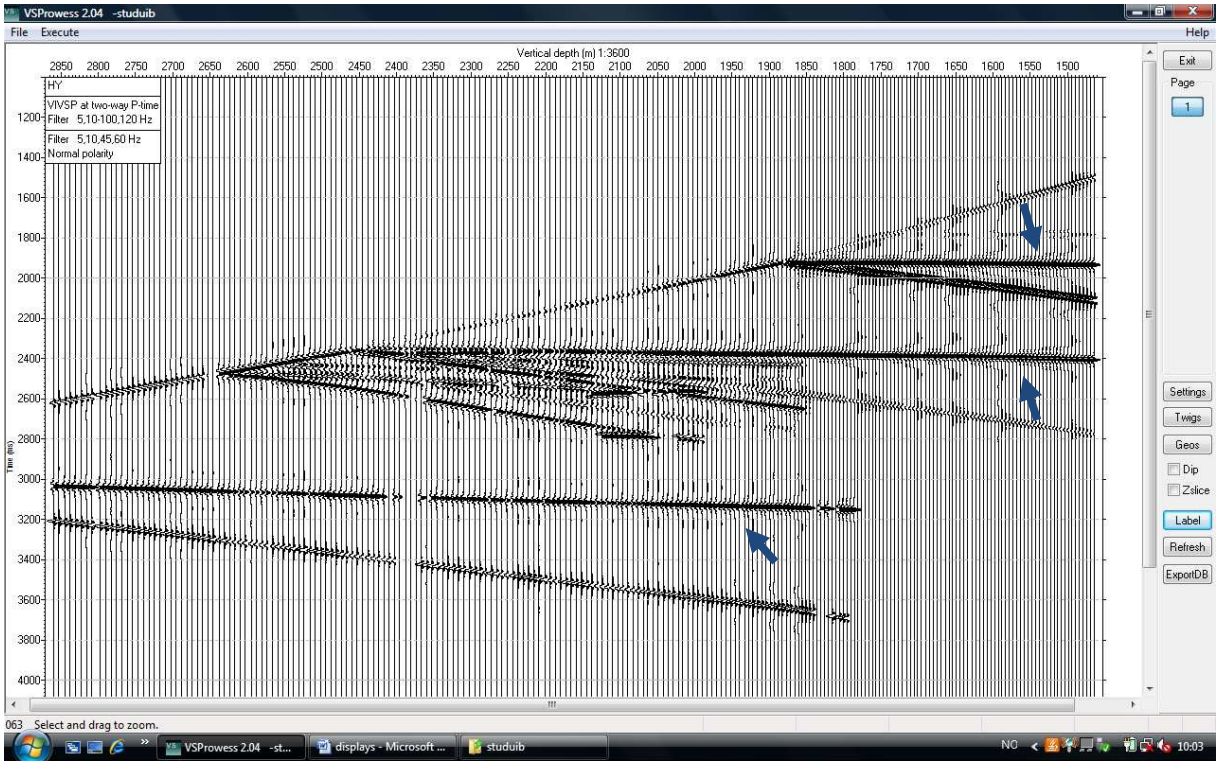

Figure 5-32: Modeled NIVSP at two-way P-time. Blue arrows indicate the P reflectors.

6 Discussion

6.1 OBC and VSP interpretation correlation

Importing the processed VSP SEGY-file into Petrel, gave us the possibility to see how well the data collected from a VSP survey correlates with previous surveys done in the area (OBC and MCS). As a result we saw that the interpreted lines from the OBC 3D-cube correlates well with the VSP file. This shows how well VSP can improve the interpretation of an area.

While processing the OBC data interpreted horizons from the MCS survey was used as control points for the velocity analysis on the PZ-cube. When the PS-cube was processed, these horizons were not available in S-wave time, so there were no control points. For VSP we can generate a SEGY-file from the S-wave wavefield measured on the H1 and H2 component through processing. This can then be used as control points for a more accurate velocity analysis of the PS-cubes from OBC surveys.

6.2 Ray-trace modeling

For VSP surveys the velocities in the layers above the top geophones in the borehole are unknown. Therefore using a ray-tracing model, we try to estimate the velocities in these layers. By changing the P-wave velocities until we have matched the direct P-wave arrival times to the observed arrival times in the VSP. Also the S-wave conversions and velocities can be found from this method. This can be done for both Normal Incidence VSP and Rig Source VSP. This was the main goal with this thesis.

The V_s/V_p-ratio we used in the modeling was 0.55. In the OBC processing PGS used the ratio $V_s/V_p = 1/(2.5)=0.4$. However, the ratio found from the VSP seismic is more reliable since the V_p/V_s-ratio can't be calculated directly from just ocean bottom seismic.

From ray-tracing of the models, we got three synthetic seismograms for each survey. This corresponds to the wavefield measured in the Vertical, H1 and H2 component in the survey performed in the area. So these seismograms can be compared to the SEGY-data received from Statoil. In our model however, we have only included the direct wave and the up-going wavefields. P-to-P transmission and P-to-S transmissions are not included. Therefore some difference will be showed in the comparison. Also due to time-limit, the S-wave velocities weren't changed to fit better with the original data. This would be a logical next step in working with these models. The seismograms made in this thesis are, however, compared with the SEGY-data, and some similarities in the S-waves are still possible to see.

First the synthetic seismograms from the Normal Incidence VSP survey model are compared to the original SEGY-files. The vertical (z) component from the model is compared with the file VSPNI-2 Raw Stack Vertical Component. The H1 (x) component from the model is compared with the file VSPNI-3 Raw Stack H1 Component. The H2 (y) component from the model is compared with the file VSPNI-4 Raw Stack H2 Component. The scaling of each seismogram was adjusted to give a best possible view of the arrivals for the comparison.

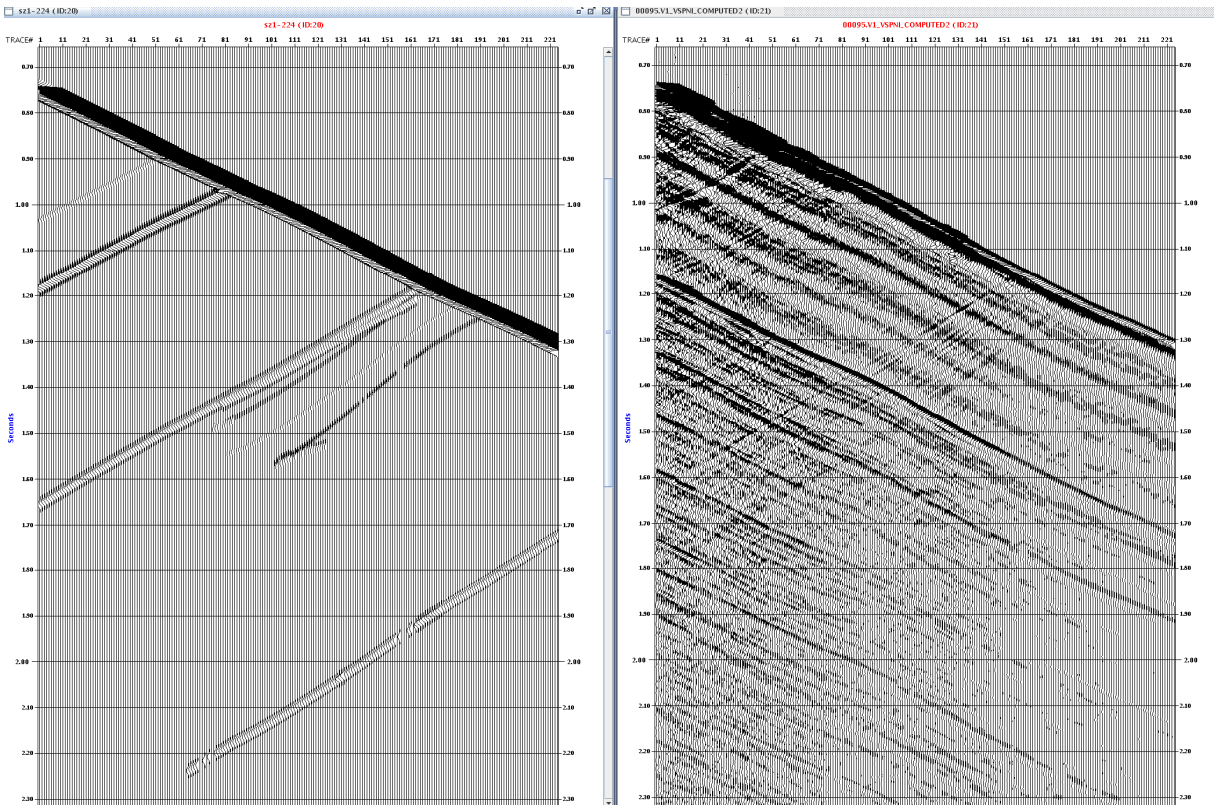

Figure 6-1: Vertical component from NIVSP model compared with original Vertical Component NIVSP SEGY file.

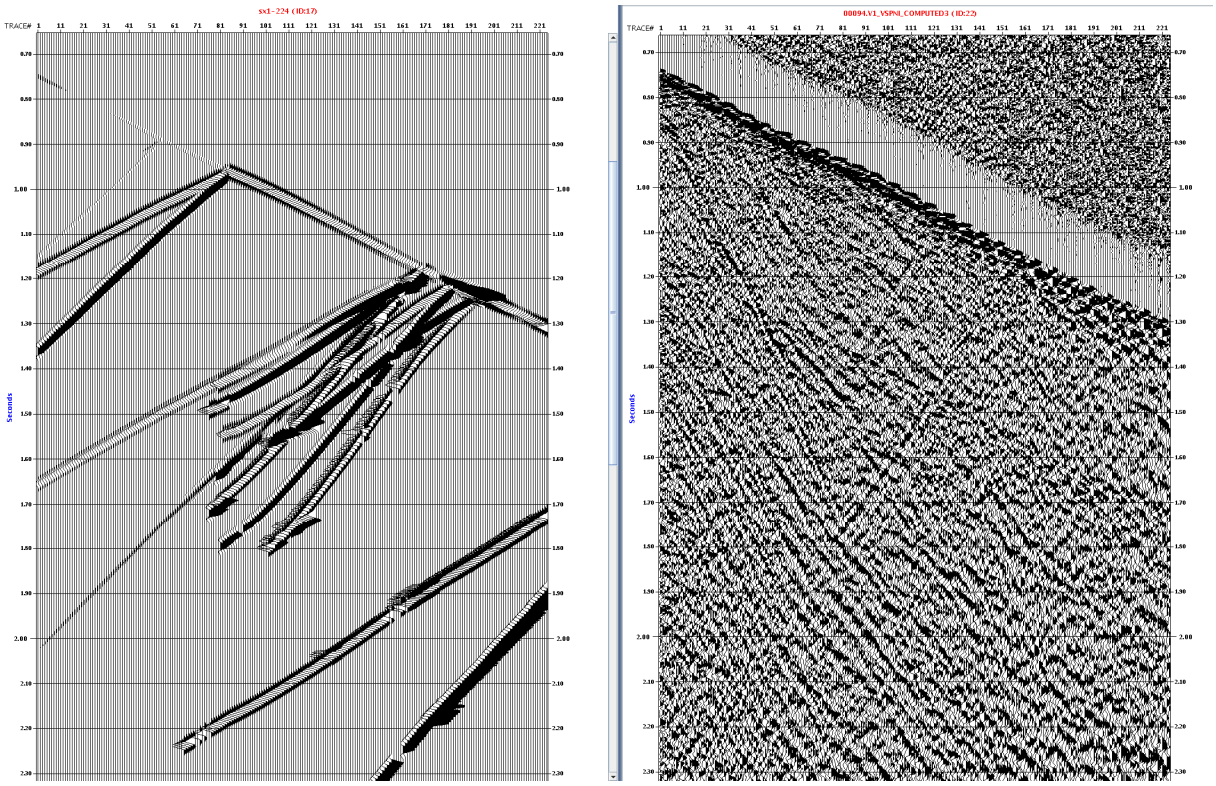

Figure 6-2: H1 Component from NIVSP model compared with original H1 Component NIVSP SEGY-file.

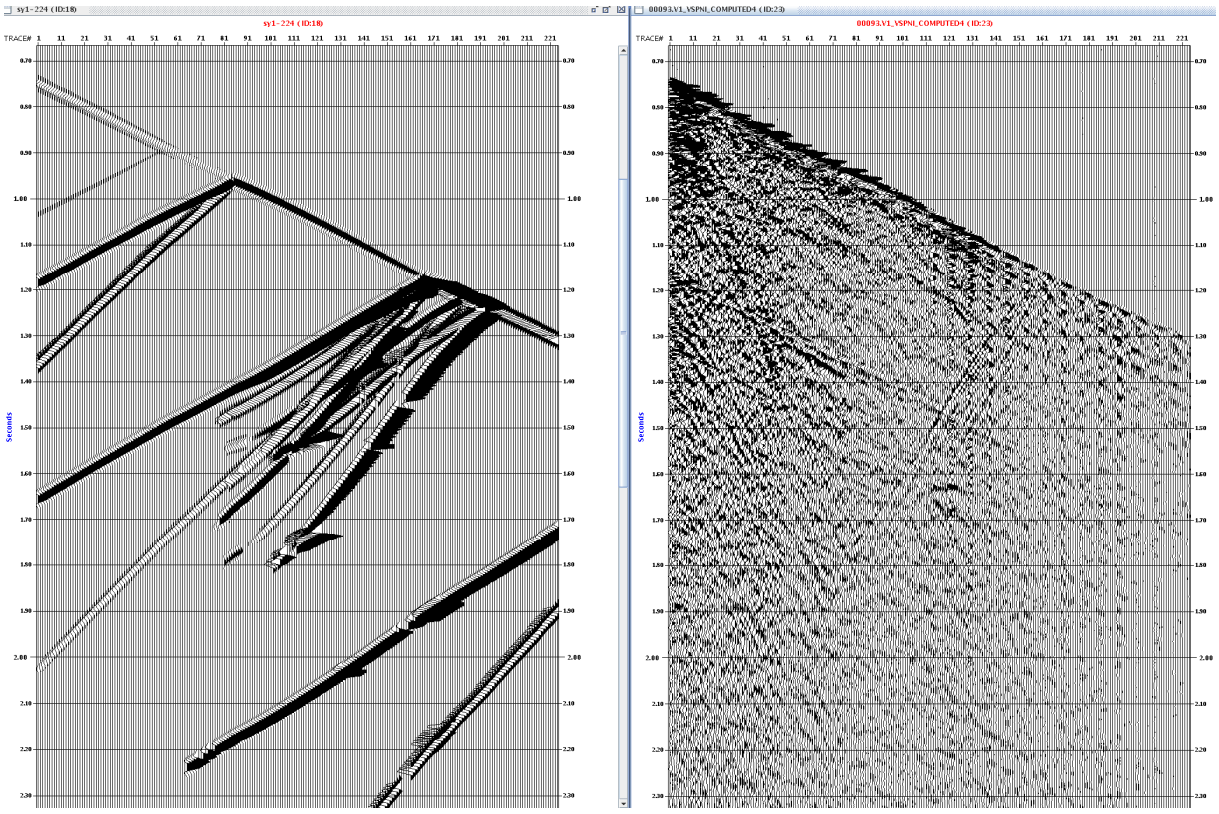

Figure 6-3: H2 Component from NIVSP model compared with original H2 Component NIVSP SEGY-file.

From the comparison we can see that the direct arrival in the model is closely matched to the observed direct arrival. We can also recognize some of the up-going P- and S-waves. Some of the S-waves have a different dip for the model than for the observed. This could be improved by more investigation of the S-wave velocities in the model. In this model we have a constant V_p/V_s-ratio for all the layers. The ratio is probably different for each of the layers, so finding the reflections in the observed dataset, and then changing the ratio in the layer reflected from, and the layers reflected in, could have an effect on the dips of the S-waves in the synthetic seismogram. Also densities from well logs can be used to improve the model.

Then the synthetic seismograms from the Rig Source VSP survey model are compared to the original SEGY-files. The vertical (z) component from the model is compared with the file VSPRS-1 Raw Stack Vertical Component. The H1 (x) component from the model is compared with the file VSPRS-2 Raw Stack H1 Component. The H2 (y) component from the model is compared with the file VSPRS-3 Raw Stack H2 Component.

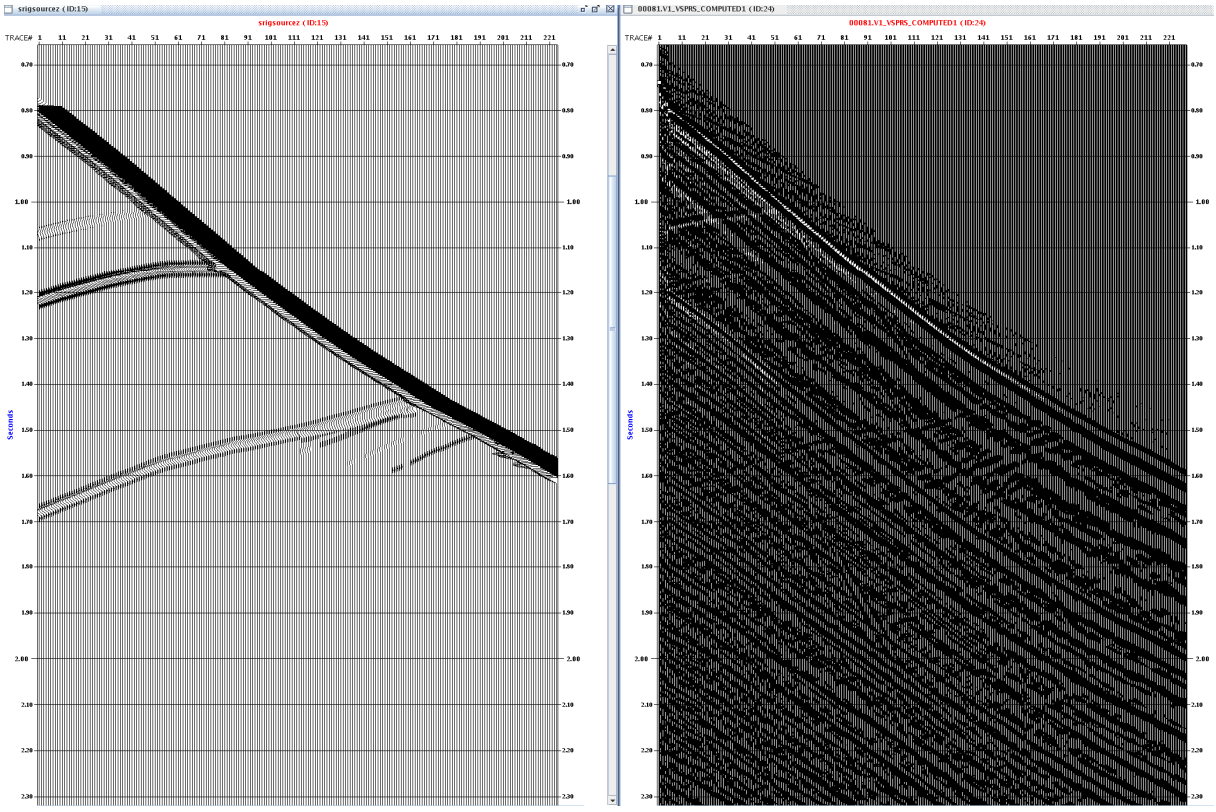

Figure 6-4: Vertical component from RSVSP model compared to original Vertical Component VSP SEGY-file.

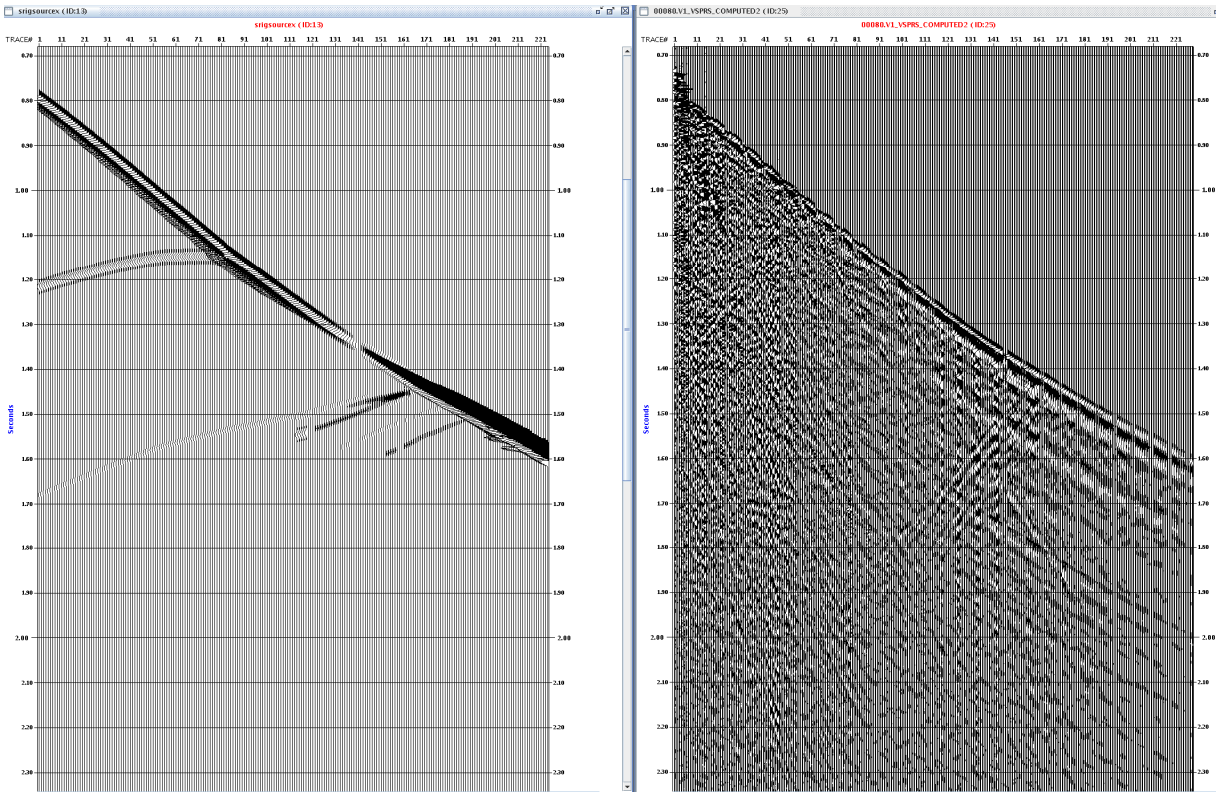

Figure 6-5: H1 Component from RSVSP model compared to original H1 Component RSVSP SEGY-file.

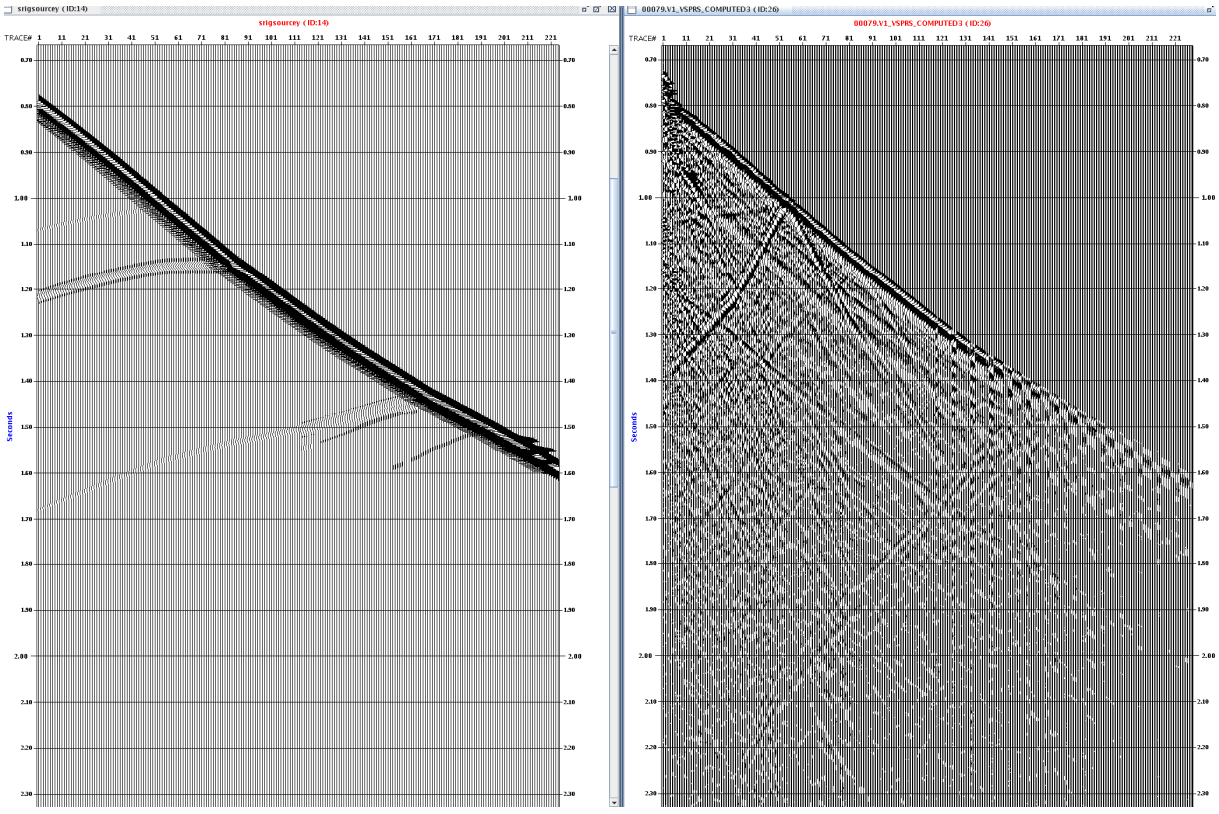

Figure 6-6: H2 Component from RSVSP model compared with original H2 Component RSVSP SEGY-file.

In the Rig Source VSP comparison we can also see that the direct arrival is closely matched to that of the observed direct arrival. We can also recognize some of the upgoing P- and S-waves on the RSVSP comparison, but the S-waves in the two seismograms have differences in dip.

It is a fundamental characteristic with Offset VSPs (including long-offset Rig Source VSPs) that the arrival times are not reliable for two-way time conversions. This means going from recorded (one-way) time to two-way time normally introduces errors. The VSP may not be compared to the surface seismic directly. A migration of the data must be carried out.

A migration may be done for the P-image. However for the PS-image it is not meaningful as the knowledge of the S-wave velocity field is uncertain. The modeling of the RSVSP was carried out to demonstrate that the events are readily visible both for the P- and the PS-waves. The results have been displayed. Further work on the RSVSP has not been done.

6.3 Uncertainties

When making the ray-tracing model, we have kept the model as simple as possible. This means that the results are simplified, and not a real indication of an actual survey. This means that there are uncertainties with the results. With VSP surveys the velocities of the layers above the top geophone in the borehole are unknown, and this means that the velocities estimated in this model for these layers are uncertain. The P-wave velocities for the lower layers were taken from the VSP Report, and these velocities are only valid in proximity of the well.

Other uncertainties in the modeling are the densities and the S-wave velocities. Considering that the well is deviated, the V_p/V_s-ratio read from the SEGY-files are also uncertain. Another uncertainty is that the layers in the area have lateral velocity changes, seen from the OBC processing. The model in this thesis does not have lateral velocity changes. The reason we didn't include this is given in the next subchapter.

The Rig Source VSP modeling is also uncertain, as an actual Rig Source survey in the area will be affected by anisotropy. The models we have made have been kept isotropic for simplicity, so variations in the results of the Rig Source VSP are partly due to this.

Above top VSP we have no information, and hence an uncertainty of the mode conversion exists. It is not possible to obtain reasonable information about the Vs/Vp ratio in this interval. This information is normally needed in order to compute the PS arrival times in this interval and should be taken into account for modeling exercises if possible.

Such information would be the stacking velocities from the OBC data, which could not be used in the modeling program.

6.4 Problems encountered

The three 3-D cubes I first received from Statoil turned out to be corrupted. There was something wrong with the amplitude values, so the data displayed when loaded into Petrel was not possible to work with. Some work was done to try to fix the data, but in the end we had to ask Statoil for new data. One of the corrupted 3-D cubes received is displayed in Figure 6-7.

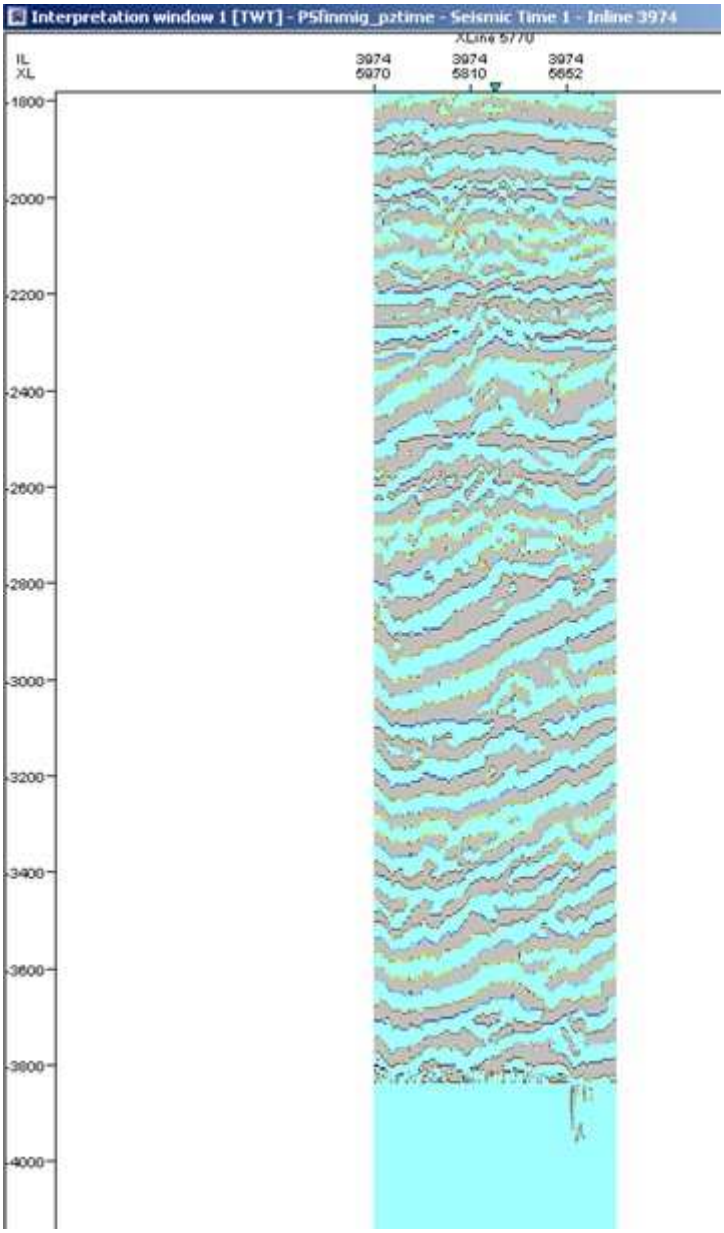

Figure 6-7: Corrupted PS PP-time cube first received from Statoil.

The next problem we encountered was that the header values in the VSP SEGY-files were incomplete. This required a bit of work to fix. We managed to fix the Normal Incidence VSP-

file that was imported into Petrel. The Rig Source files, however, we didn't get the time to fix, as these required more work. The plan was to use the Raw Reflected S-wave file from the RSVSP, and process this so we could import it into Petrel to compare with the PS PS-time 3D-cube.

We also had a lot of problem with the NORSAR software, and the configurations on how to use this program for VSP surveys, as no one had good knowledge on how to make this type of model. Another problem in NORSAR was the determination of the velocity. We had originally planned to import stacking velocities from the OBC processing. But the software only supports interval velocities. We did convert these stacking velocities using Geovecteur, but the resulting velocity field needed more work, and also had velocity changes within the layers defined in the model. We would then have to make a model using the velocity changes as layers, instead of the layers interpreted. The reason we wanted to use these velocities originally is because there are lateral velocity changes in the layers of the model area. So there is likely to be velocity variations along the deviated well, and also the lateral variations of the velocities above top VSP are hard to determine without the stacking velocities from the OBC. Since these velocities were problematic to include in the model, it was decided to use the interval velocities from the NIVSP processing report, and ignore the lateral velocity changes.

We also planned to extract a random line from the OBC 3D-cubes, to directly compare with the processed VSP SEGY-files. We originally intended to do this in Petrel, but it turned out to be impossible. We then tried using Geovecteur, but also here we couldn't quite figure out how to do it.

The recurring problem in this thesis is lack of knowledge about VSP, and using the software for this type of work. So a lot of time has been wasted trying to figure out how to proceed, resulting in too little time to work on the models.

6.5 Future work

With more time, and fewer technical problems, we could have achieved more results in this thesis. However, the can still be used for further work on the Snorre reservoir. The synthetic seismograms could be improved by more information on densities, S-wave velocities, and lateral velocity changes, giving a more accurate result of a Normal Incidence and Rig Source VSP survey in the area.

The next step when the model is improved would be to compare these results with the OBC data sets. This would give us even more insight to the area interpreted, especially the S-wave conversions in the subsurface.

No attempt has been made to determine the magnitude ratio of the P- versus the PS-events. This may be done by careful 3-component processing of the VSP in order to virtually orientate the receivers with respect to the arriving energy, but is outside the scope of this thesis.

7 Conclusion

In VSP we record both P- and S-waves, which give more information about mode-conversion taking place in the subsurface than surface and ocean bottom seismic. With the use of VSP seismic we are able to tell whether the conversion has taken place as a reflected or a transmitted conversion (up- or downgoing wave), and we can identify the formation tops acting as converting interfaces, and compute the formation interval S-wave velocity with confidence.

With more time and less technical problems, more results could have been achieved. There was not enough time to really inspect the wave conversion from the ray-tracing models made. The results can, however, be used for continuous work in the area. By changing the V_p/V_s-ratio, and include lateral velocity changes and more accurate densities in the layers, the synthetic seismograms can be improved, and be used for correlation with the ocean bottom seismic, and the acquired VSP seismic. Then inspection of the wave conversion in the model can be done, and the converting interfaces can be determined.

The reasons for S-waves being an important factor in acquiring more knowledge about a reservoir is that the resolution of S-wave images are superior to that of P-waves. Ocean bottom seismic (or multi-component seabed) surveys also record and process S-waves, but the quality is often poor, so additional information is needed to make a proper correlation between an S-event and the corresponding P-event on the multi-component data. This information is found by using VSP data.

This thesis shows how VSP surveys can improve interpretation and knowledge of a reservoir. The VSP seismic can be used to help determine stacking velocities in the processing of the OBC S-wave cube and also improve the interpretation of seismic, by comparing the VSP with the OBC seismic sections.

A ray tracing-model gives information on the travel paths of the rays, and the wave conversion points in the subsurface. Getting a better understanding on wave conversion improves the knowledge of the area, and is especially useful in oil/gas detection. By calculating S-wave velocities and the V_p/V_s-ratio from VSP seismic, we can get information about the lithologies (sand/shale ratio).

The modeling of the VIVSP was quite successful, demonstrating that both P- and PS- arrivals would be recorded even in the situation of approximately zero offset difference between source and receiver, and the results have been displayed. The RSVSP dataset was available, and a modeling exercise using that geometry was also carried out. The modeling of the RSVSP was carried out to demonstrate that the events are readily visible both for the P- and the PS-waves. The results have been displayed. Further work on the RSVSP has not been done.

The events which are interpreted, it being P- or PS-events will arrive on the same depth but not the same time. Defining the P-time is fairly easy both on VSP, OBC and regular surface seismic. However, defining the PS-time is the challenge.

It should be noted that all seismograms are a function of time, not depth. Therefore, performing depth conversion is meaningless if the time or velocity functions are not known. An uncertainty exists on OBC data with respect to the relationship time-depth.

Using information from VSP data would reduce this uncertainty to a minimum, as the time-depth relationship is directly observed and require no computation.

Comparing VSP P-data and PS-data will reveal the relationship between the P-time, the depth and the PS-time, see displays 1 and 2 of the modeling results. For each interpretable arrival, at each depth, it is possible to identify the times for both the P and the PS upcoming events.

In the industry today, among geophysicists, there are generally too little knowledge about VSP, and the information this type of survey can give. Because VSP is an expensive and complex survey, many companies choose other, simpler methods when possible. In order to get more information of the reservoirs and to improve oil and gas recovery in mature areas, converted wave energy is important, and therefore VSP can play an important part for optimizing producing fields.

8 References

Aga, K. and Isdø, D. (2006). “Interpretation of the OBS pz data ST0406 on the Snorre Field”. Statoil internal. 87 p.

Bacon, M., Simm, R., Redshaw, T. (2003). *3-D Seismic Interpretation.* Cambridge University Press, 212 p.

CGG Veritas (2006). *Geocluster Release Notes*.

Dahl, N, Solli, T. (1993). Structural evolution of the Snorre Field and the surrounding areas. *Petroleum Geology of the Northwest Europe: Proceedings of the 4th Conference*. The Geological Society, London, pp. 1159-1166.

Fowler, C. M. R. (2005). *The Solid Earth: An Introduction to Global Geophysics.* Cambridge University Press, 685 p.

Glennie, K. W. (1998). *Petroleum Geology of the North Sea: Basic concepts and recent advances.* Blackwell Science, Oxford, 636 p.

Hardage, B. A. (2000). *Vertical Seismic Profiling: Principles.* Pergamon, Amsterdam, New York. 552 p.

Hart, B. (2000). *3-D Seismic Interpretation: A Primer for Geologists*. SEPM Short Course. Notes 48, 124 p.

Karlsson, W. (1986). The Snorre, Statfjord and Gullfaks oilfields and the habitat of hydrocarbons on the Tampen Spur, offshore Norway. *In:* SPENCER, A. M. *ET AL.* (eds) *Habitat of Hydrocarbons on the Norwegian Continental Shelf.* Graham & Trotman, London, 181-197.

Keary,P., Brooks, M., Hill, I. (2002). *An Introduction to Geophysical Exploration.* Blackwell Publishing, 262 p.

Landmark (1997). *ProMAX 3D Reference Guide, Vol.1*, Landmark Graphics Corporation, Houston, TX, 1142 p.

Lervik, K. S. (2006). Triassic lithostratigraphy of the Northern North Sea Basin. *Norwegian Journal of Geology*, Vol. 86, pp. 93-116.

Mitchum, R. M., Vail, P. R. & Thompson, I. (1977). Seismic Stratigraphy and Global Changes of Sea Level, Part 2: The Depositional Sequence as a basic Unit for Stratigraphic Analysis. Seismic Stratigraphy-application to hydrocarbon exploration, *AAPG*, 26, 53-62.

Mjelde, R. (2003). ”Seismic acquisition: Geophysical Principles”, e-learning module from www.lg.eage.net.

Mjelde, R. (2003). ”Seismic Processing”, e-learning module from www.lg.eage.net.

Mjelde, R. (2008). ”4-C Seismic”, e-learning module from www.lg.eage.net.

Mjelde, R. (2008). ”VSP Data: Applications”, e-learning module from www.lg.eage.net.

Mjelde, R. (2009). ”VSP Data: Principles”, e-learning module from www.lg.eage.net.

Mjelde, R. (2010). ”Seismic Equipment”, e-learning module from www.lg.eage.net.

NORSAR (2008). NORSAR Ray Modelling Software (Help and Introduction Notes).

NPD. (2011). *NPD Fact-pages.* Available: http://www.npd.no/engelsk/cwi/pbl/en/index.htm. Last accessed 14.02.2011.

NPD. (2011). *NPD FactMaps.* Available: https://npdmap1.npd.no/website/NPDGIS/viewer.htm. Last accessed 14.02.2011.

Nystuen, J. P. and Fält, L-M. (1989), Correlation of Triassic to Lower Jurassic sequences, Snorre Field and adjacent areas, northern North Sea: In Collinson, J. D. (ed), *Correlation in Hydrocarbon Exploration*, Graham & Trotman, London, 273-289.

PGS Geophysical A.S. (2005). “Data Processing Report: Snorre 3D4C-Processing Statoil”, 109 p.

Saga Petroleum A.S. (1993). “VSP Processing Report: Normal Incidence VSP 34/7-P-8”, Read Well Service A/S, 226 p.

Saga Petroleum A.S. (1993). “VSP Processing Report: Rig Source VSP 34/7-P-8”, Read Well Service A/S, 150 p.

Schlumberger (2008). *Petrel, Seismic-to Simulation Software. Seismic Visualization and Interpretation Course,* 380 p.

Seldal, M. et al (Nov. 2008). “Snorre Reservoir Development Plan 2008”, internal report, Statoil.

Sheriff, R. E. & Geldart, L. P. (1995). *Exploration Seismology,* Cambridge University Press, 592 p.

Yilmaz, O. (2001). *Seismic Data Analysis.* Doherty, S. M. (ed.), Society of Exporation Geophysicists, Tulsa, Oklahoma. 2027 p.

Ziegler, W. H., Doery, R., Scott, J. (1986). *Tectonic habitat of Norwegian oil and gas*. *In:* SPENCER, A. M. *ET AL.* (eds) *Habitat of Hydrocarbons on the Norwegian Continental Shelf.* Graham & Trotman, London, 181-197.

APPENDIX A

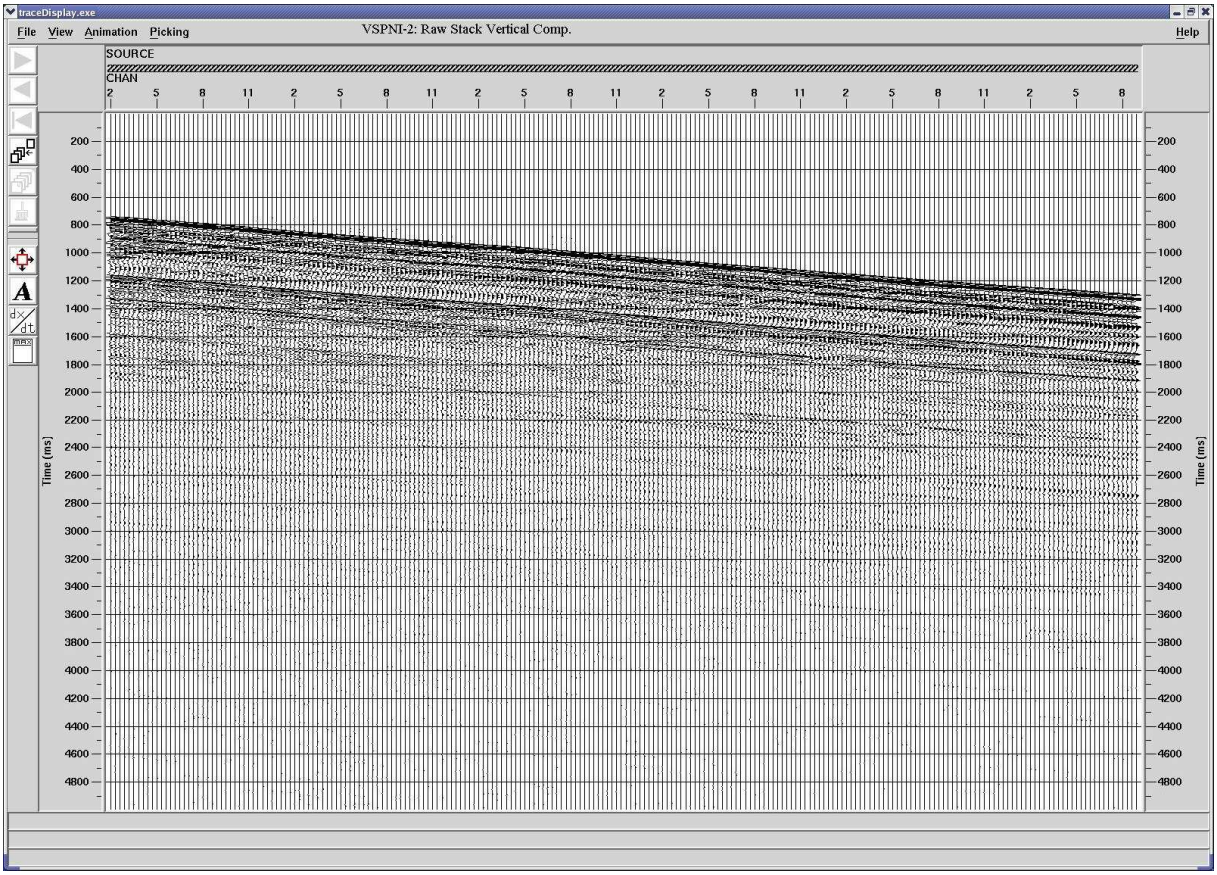
traceDisplay.exe
File View Animation Picking
VSPNI-2: Raw Stack Vertical Comp.
Help
SOURCE
CHAN
Time (ms)

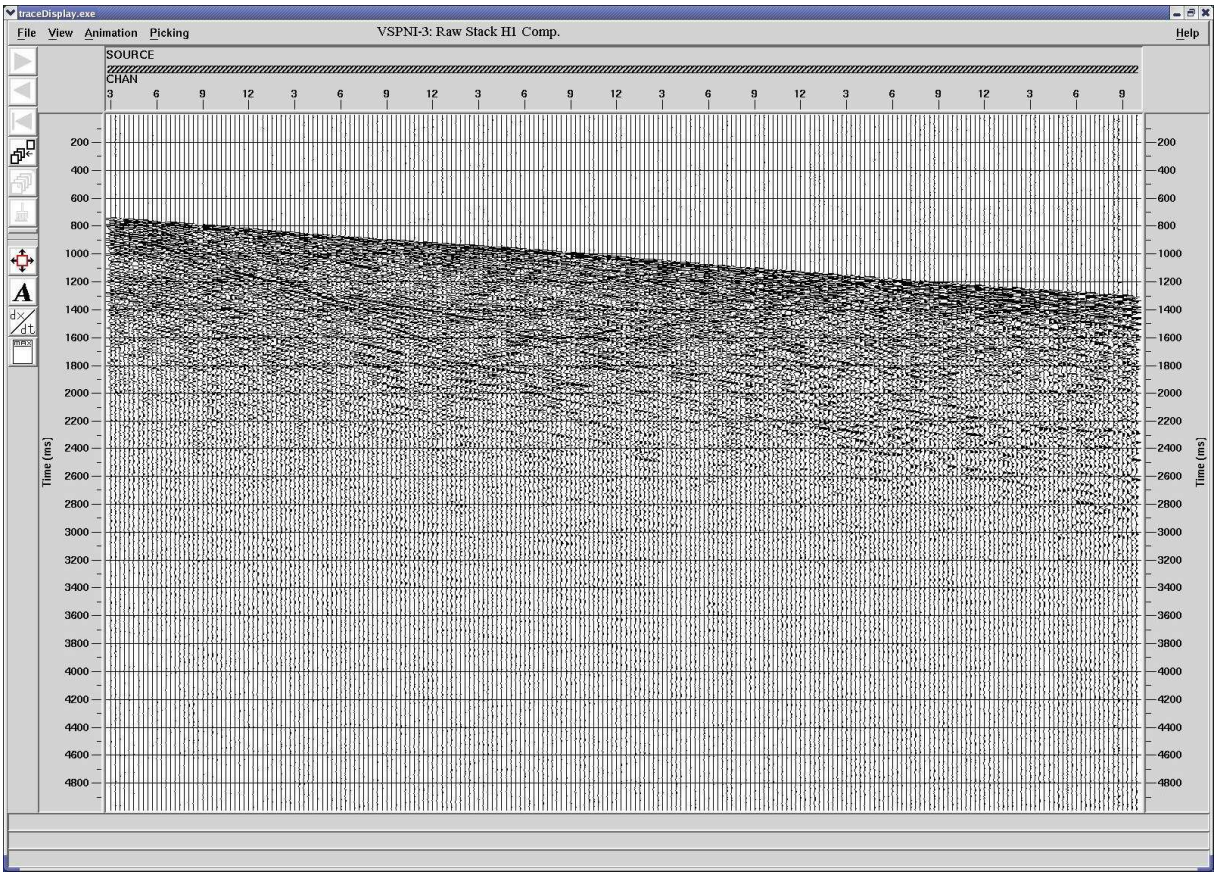
traceDisplay.exe
File View Animation Picking
VSPNI-3: Raw Stack H1 Comp.
Help
SOURCE
CHAN
Time (ms)

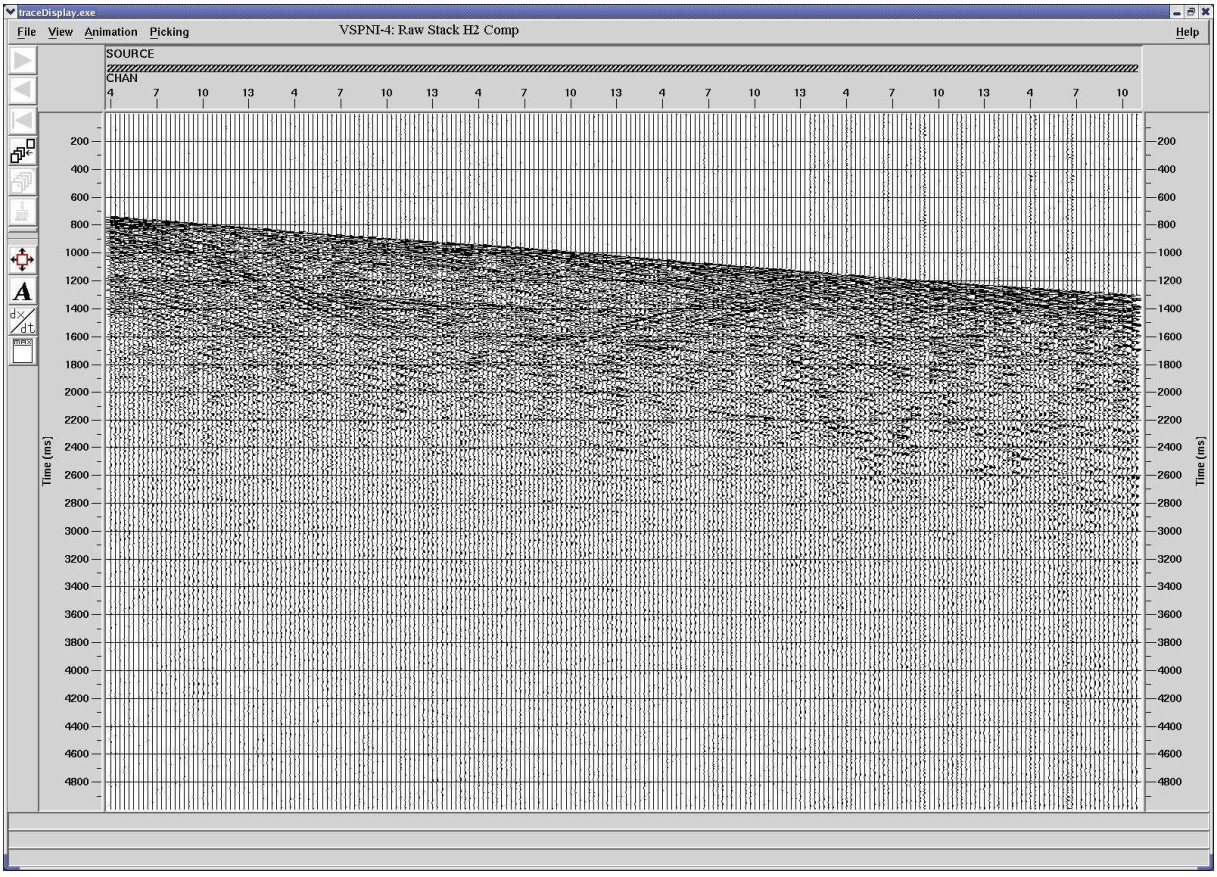
traceDisplay.exe
File View Animation Picking
VSPNI-4: Raw Stack H2 Comp
Help
SOURCE
CHAN
Time (ms)

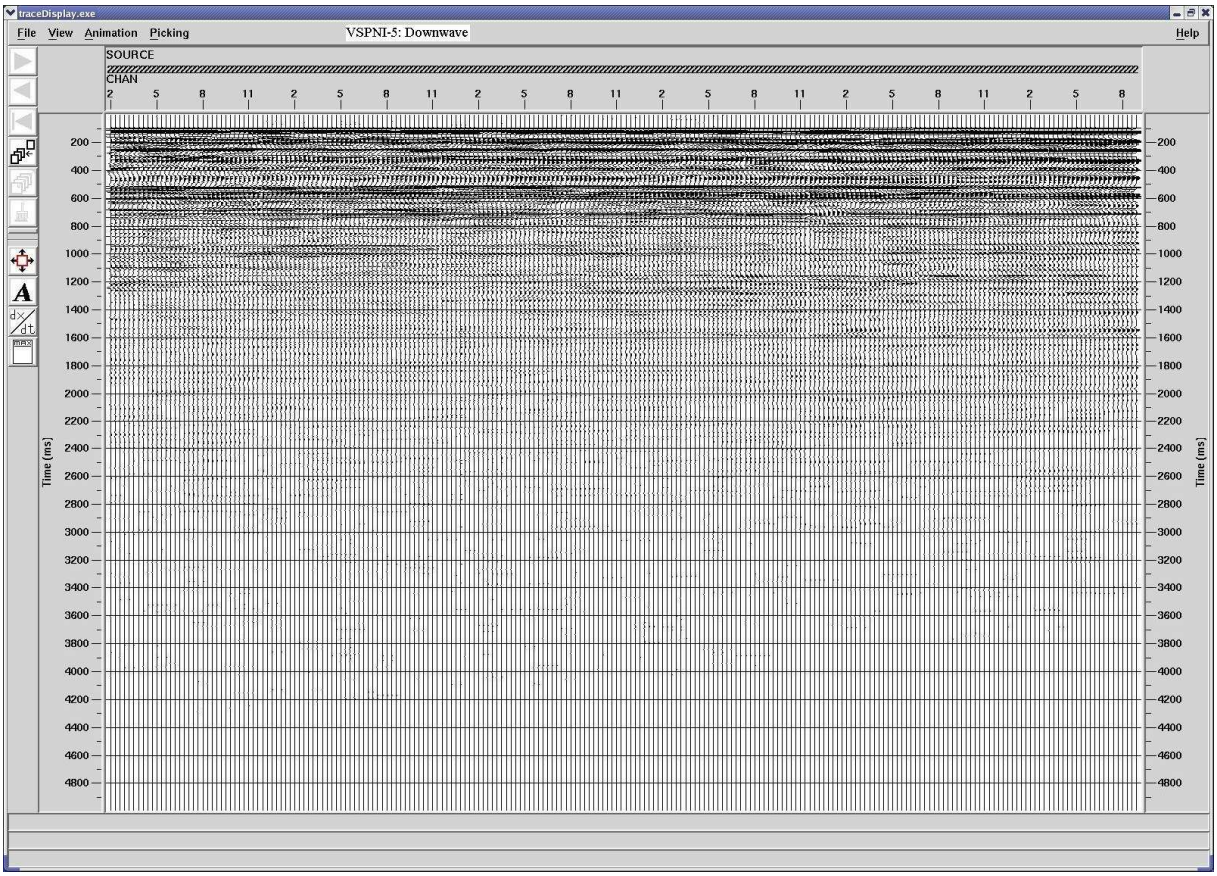
traceDisplay.exe
File View Animation Picking
VSPNI-5: Downwave
Help
SOURCE
CHAN
Time (ms)

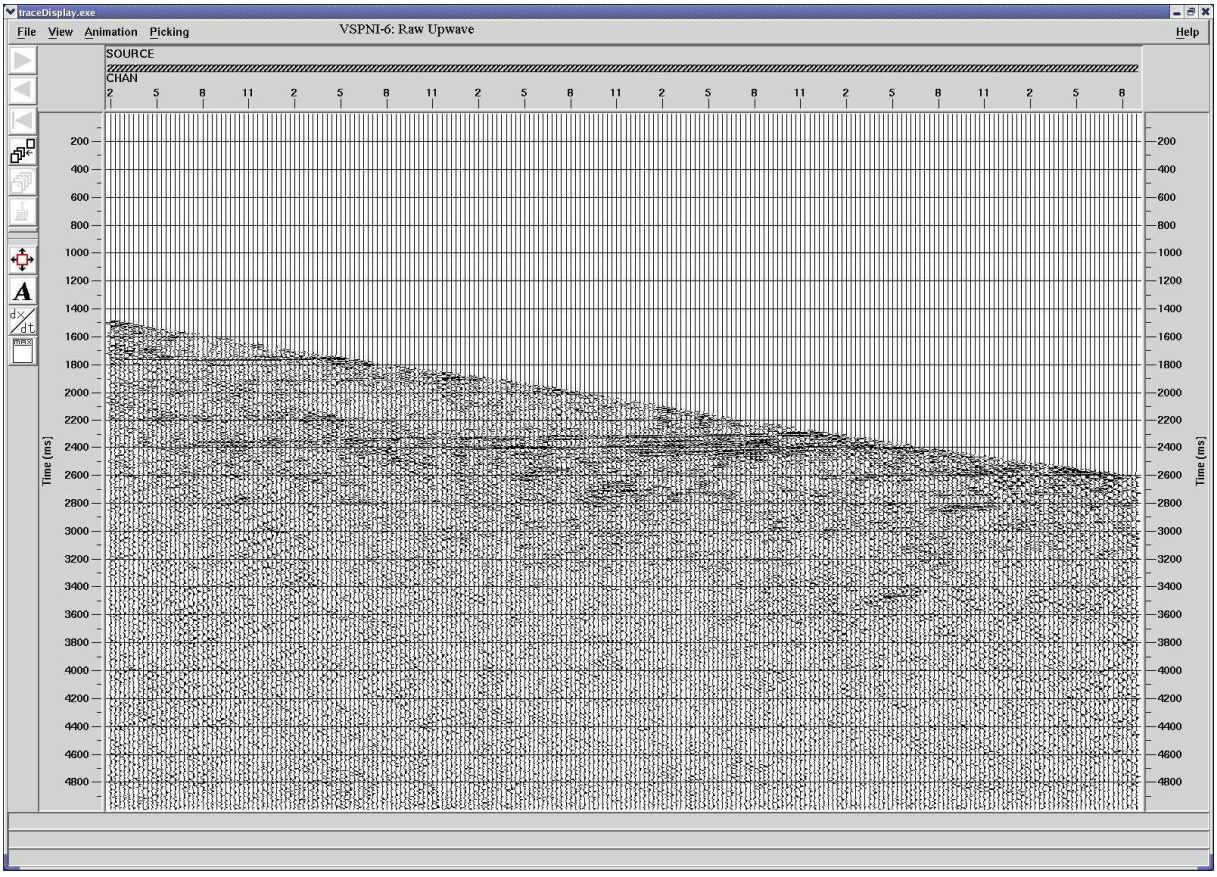
traceDisplay.exe
File View Animation Picking
VSPNI-6: Raw Upwave
Help
SOURCE
CHAN
Time (ms)

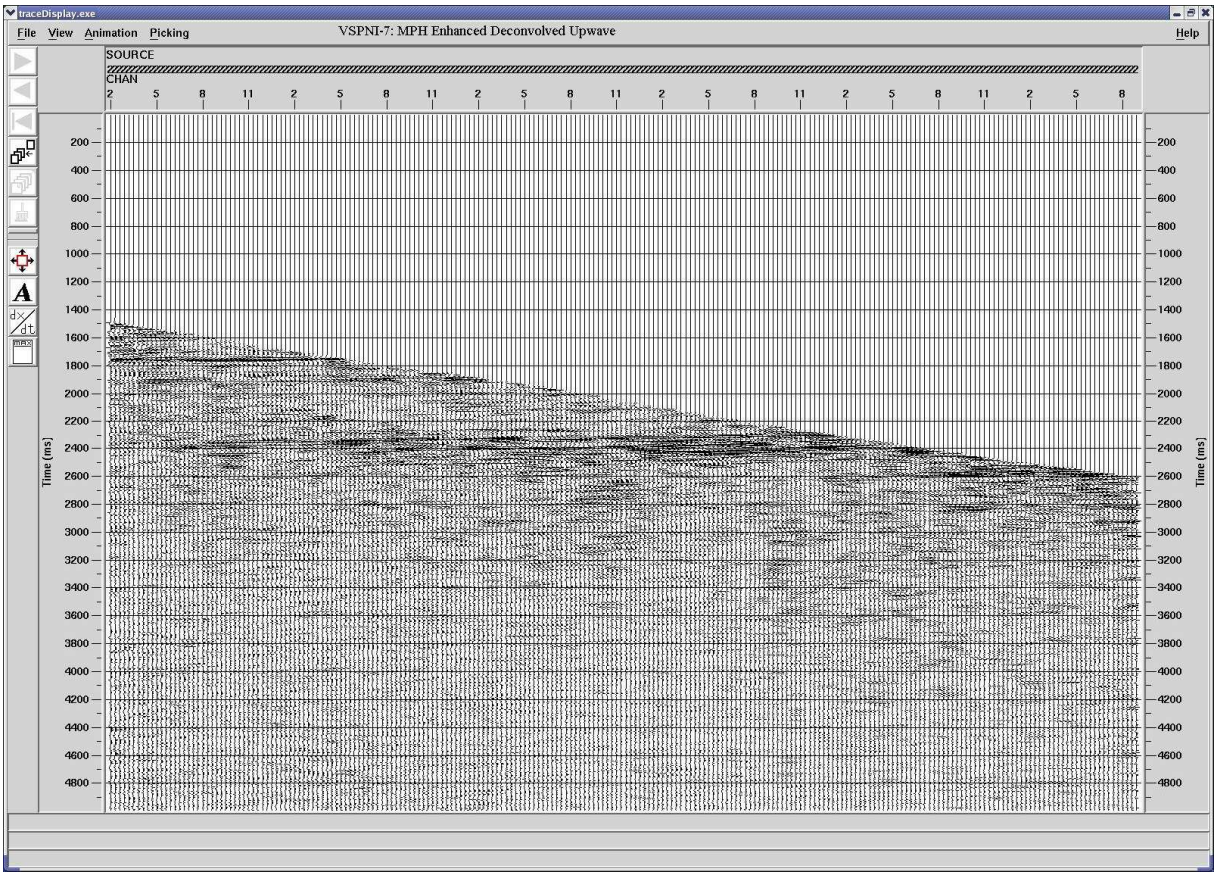
traceDisplay.exe
File View Animation Picking
VSPNI-7: MPH Enhanced Deconvolved Upwave
Help
SOURCE
CHAN
Time (ms)

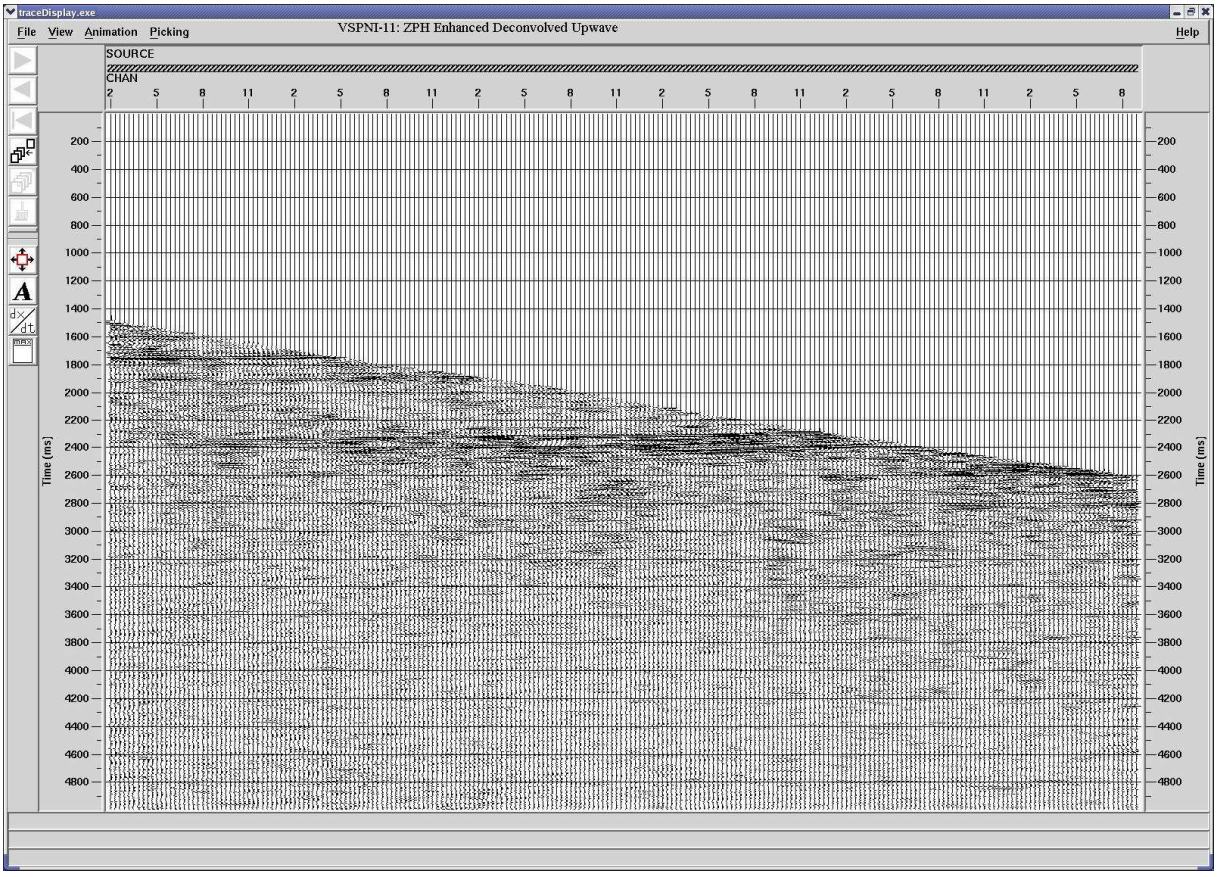
traceDisplay.exe
File View Animation Picking
VSPNI-11: ZPH Enhanced Deconvolved Upwave
Help
SOURCE
CHAN
Time (ms)

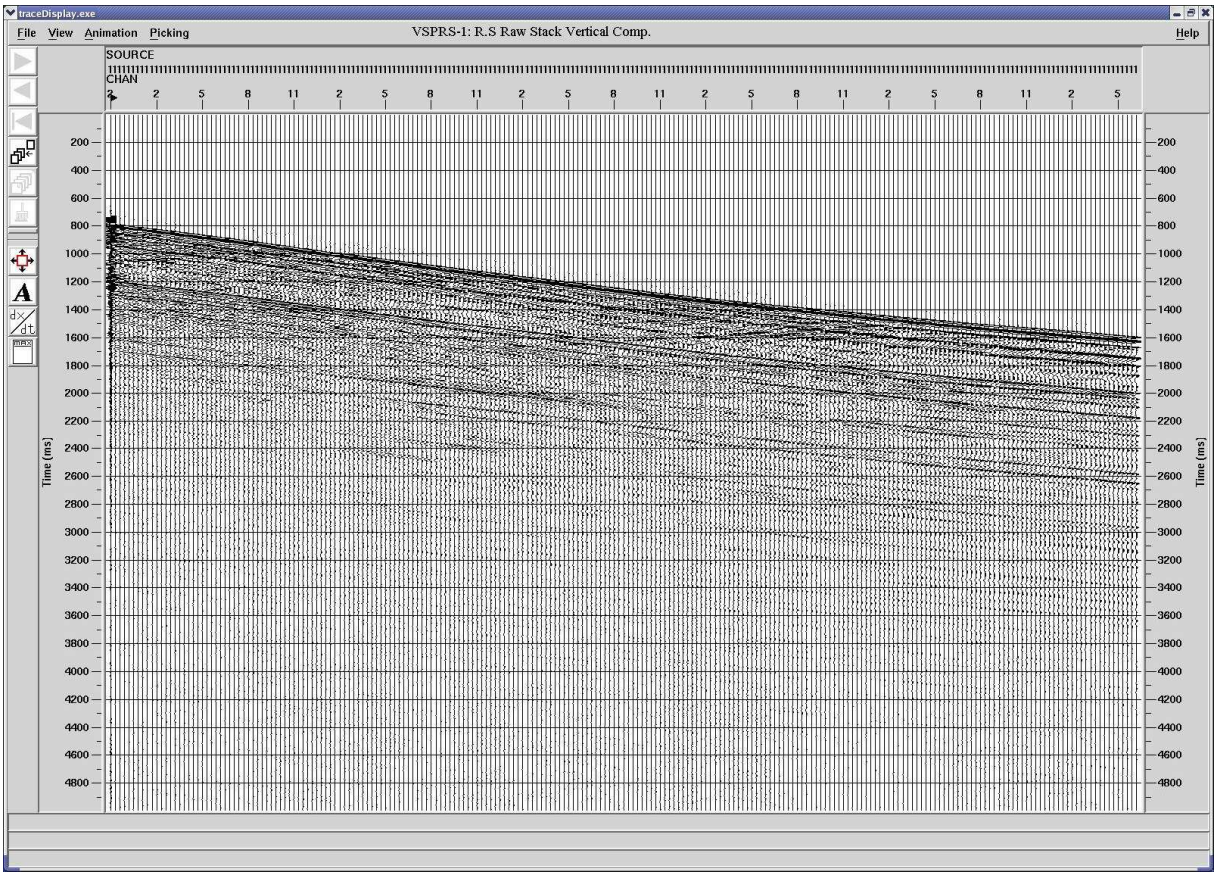
traceDisplay.exe
File View Animation Picking
VSPRS-1: R.S Raw Stack Vertical Comp.
Help
SOURCE
CHAN
Time (ms)

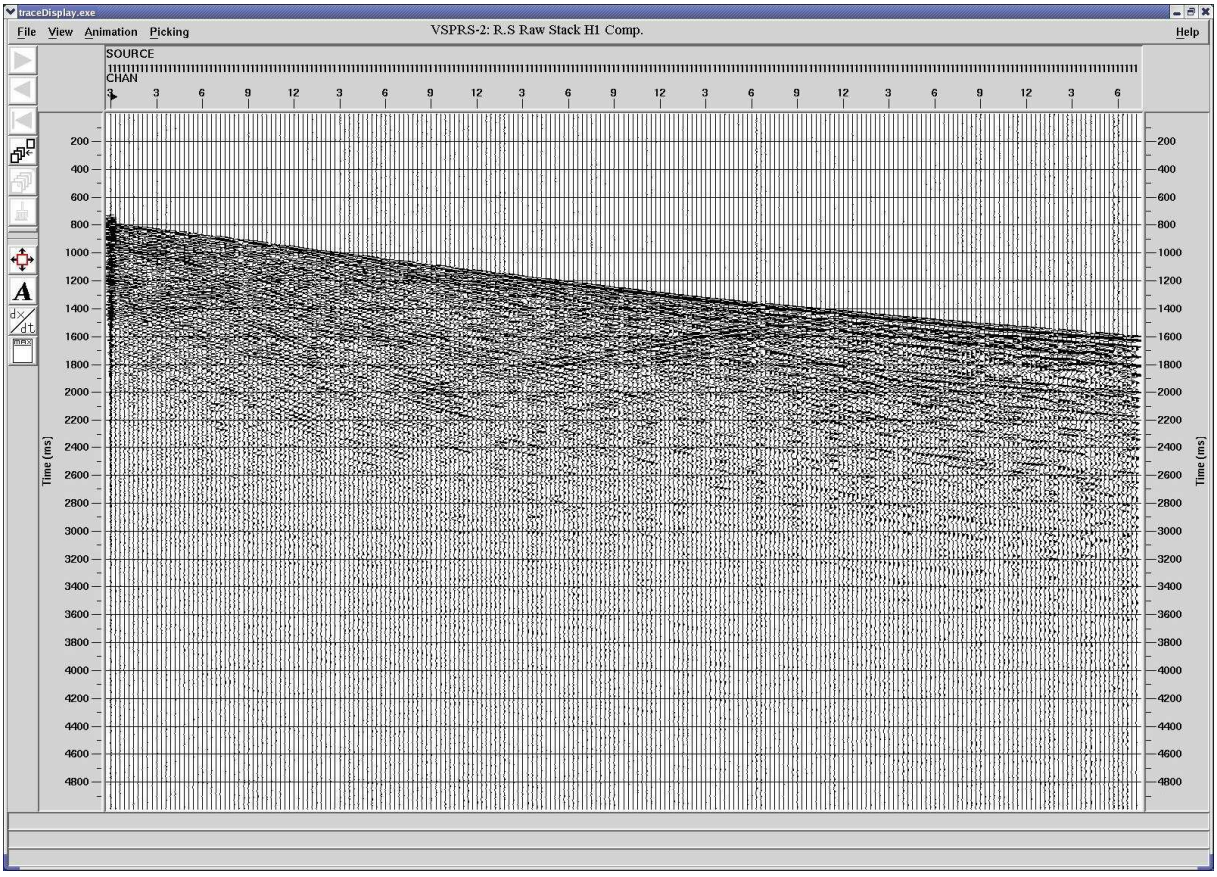
traceDisplay.exe
File View Animation Picking
VSPRS-2: R.S Raw Stack H1 Comp.
Help
SOURCE
CHAN
Time (ms)

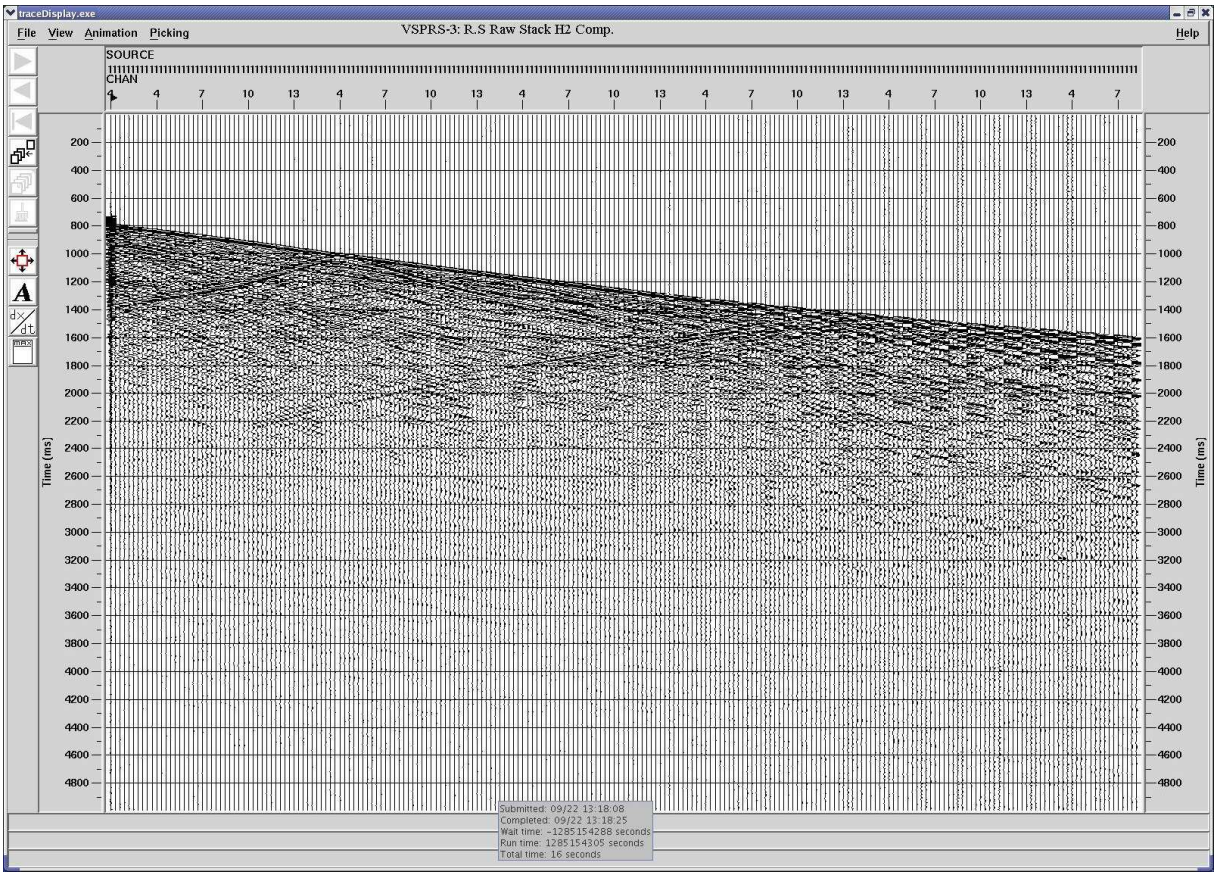
traceDisplay.exe
File View Animation Picking
VSPRS-3: R.S Raw Stack H2 Comp.
Help
SOURCE
CHAN
Time (ms)
Submitted: 09/22 13:18:08
Completed: 09/22 13:18:25
Wait time: -1285154288 seconds
Run time: 1285154305 seconds
Total time: 16 seconds

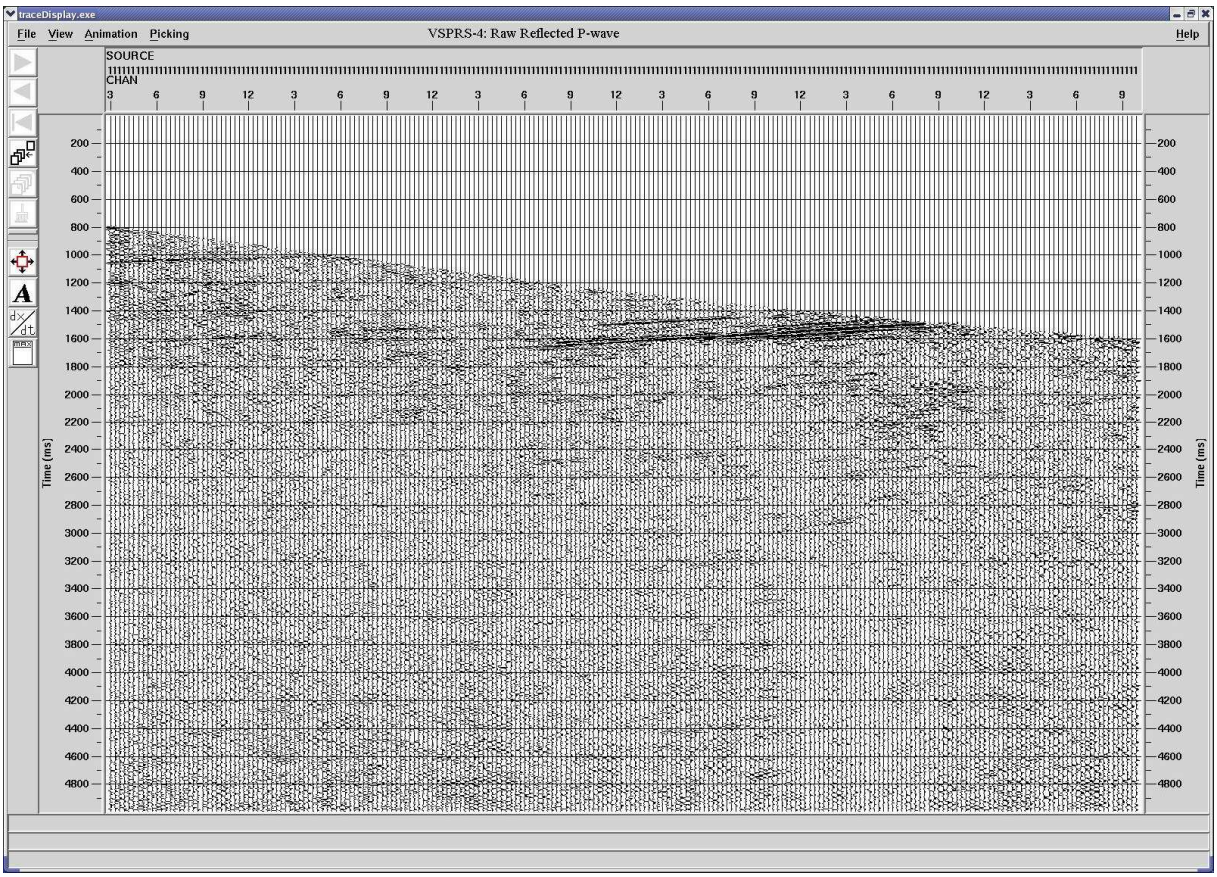
traceDisplay.exe
File View Animation Picking
VSPRS-4: Raw Reflected P-wave
Help
SOURCE
CHAN
Time (ms)

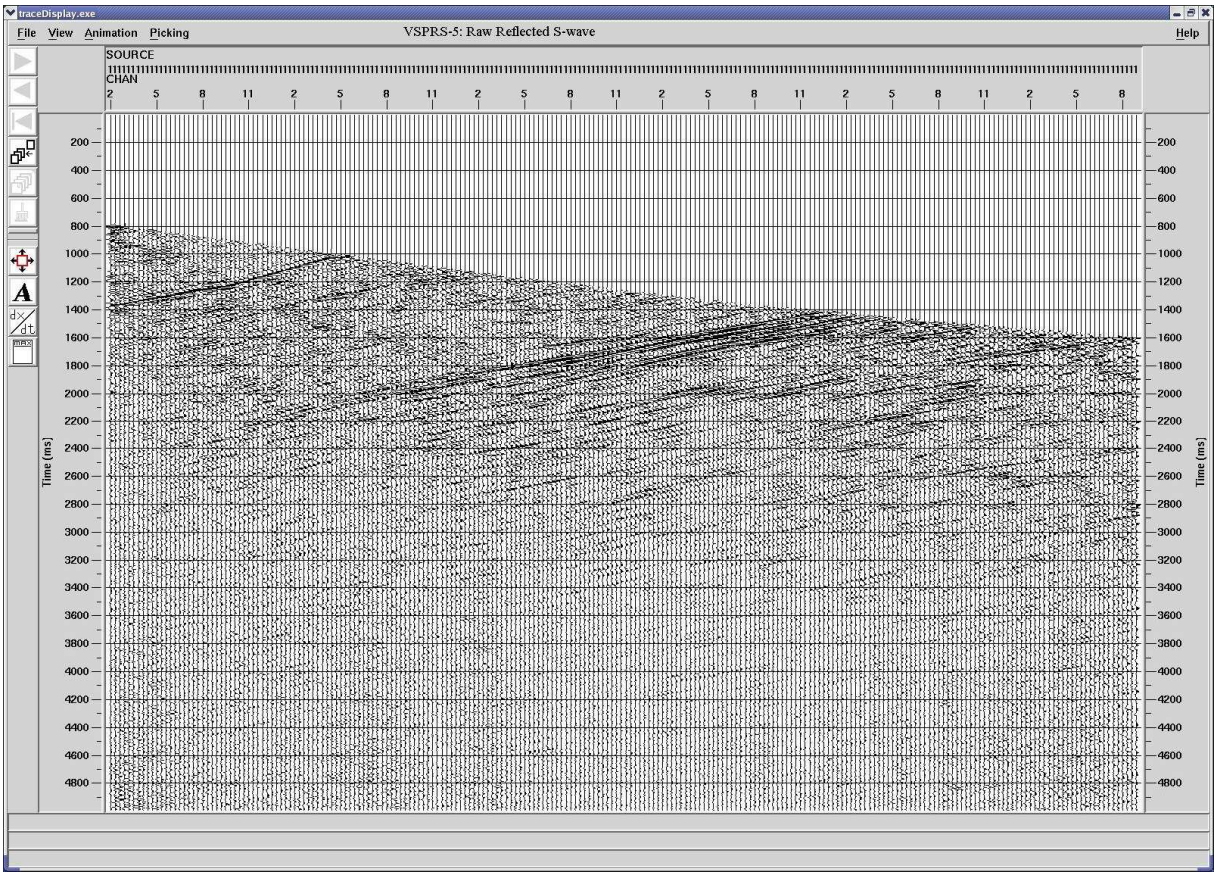
traceDisplay.exe
File View Animation Picking
VSPRS-5: Raw Reflected S-wave
Help
SOURCE
CHAN
Time (ms)

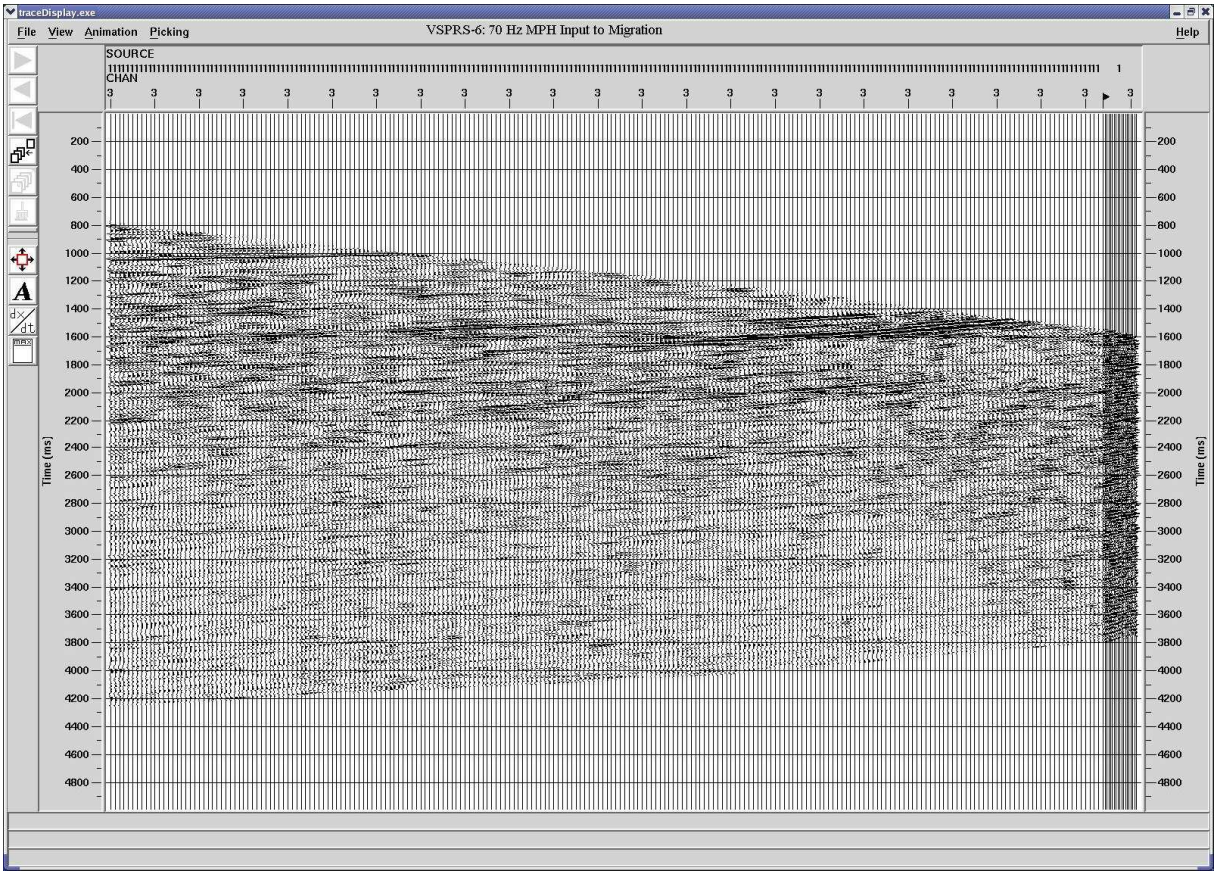
traceDisplay.exe
File View Animation Picking
VSPRS-6: 70 Hz MPH Input to Migration
Help
SOURCE
CHAN
Time (ms)

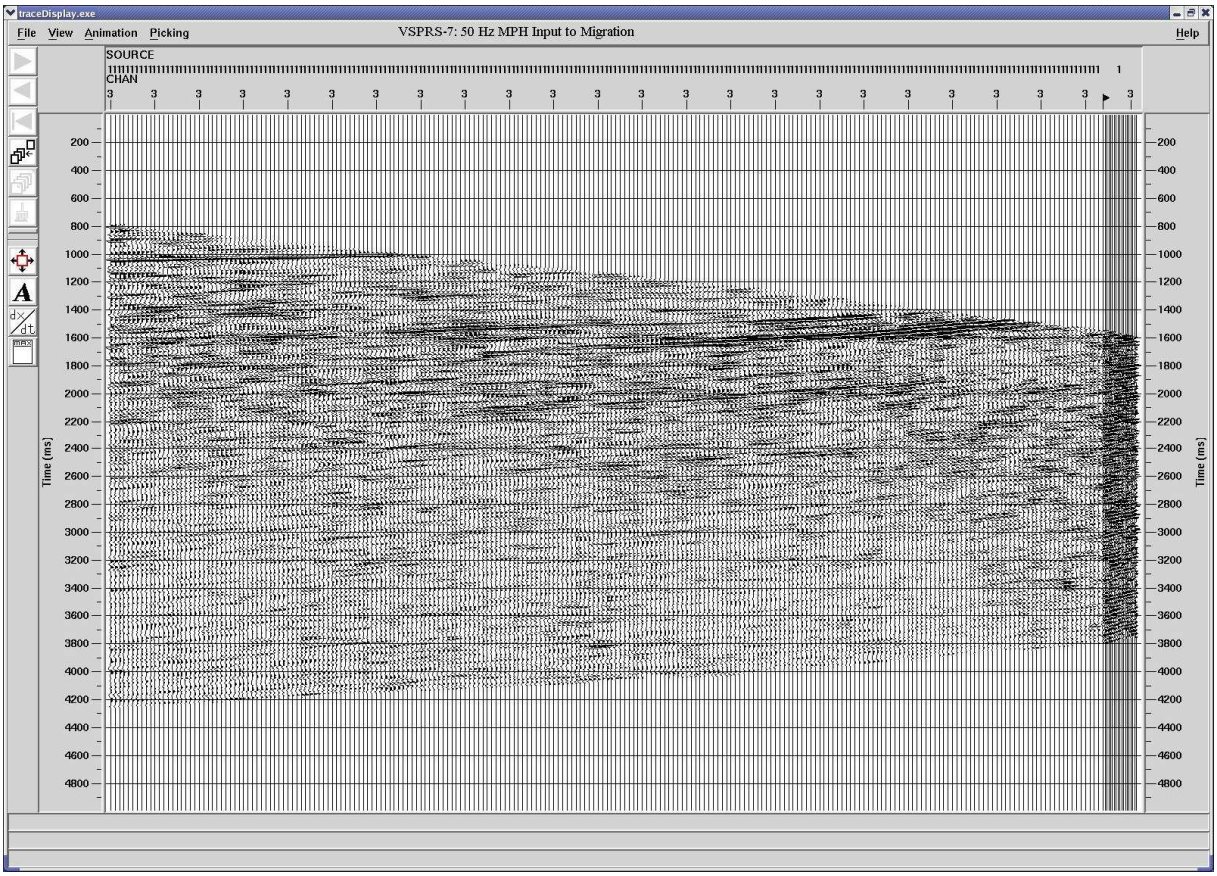
traceDisplay.exe
File View Animation Picking
VSPRS-7: 50 Hz MPH Input to Migration
Help
SOURCE
CHAN
Time (ms)

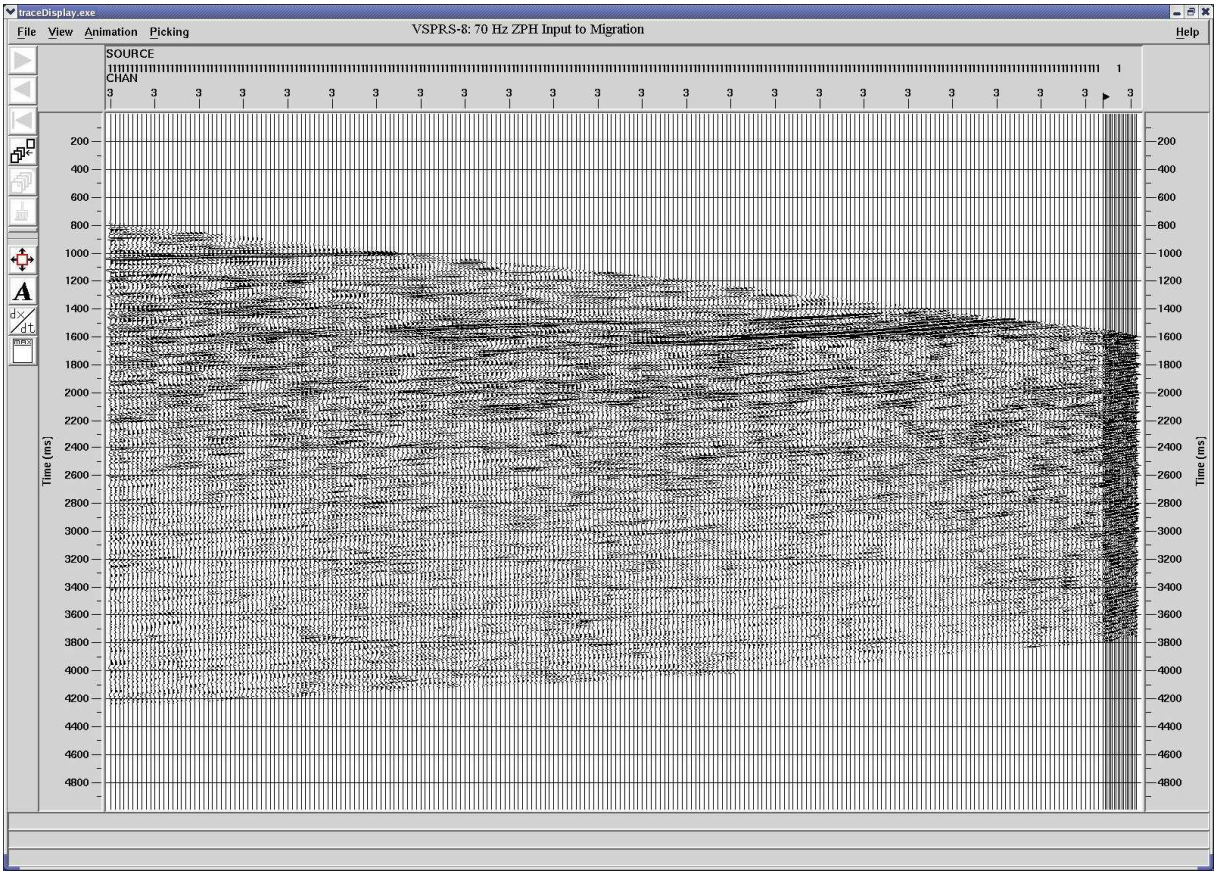
traceDisplay.exe
File View Animation Picking
VSPRS-8: 70 Hz ZPH Input to Migration
Help
SOURCE
CHAN
Time (ms)

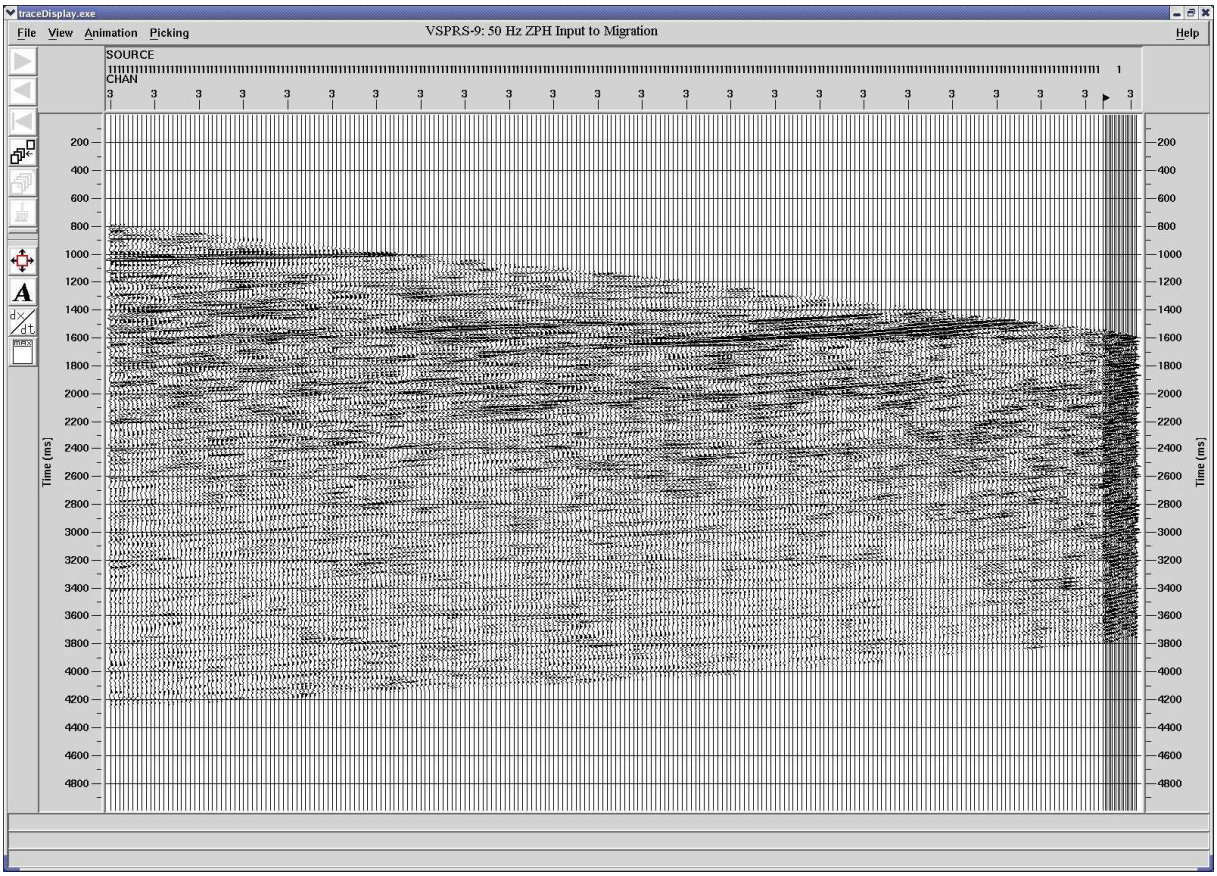
traceDisplay.exe
File View Animation Picking
VSPRS-9: 50 Hz ZPH Input to Migration
Help
SOURCE
CHAN
Time (ms)

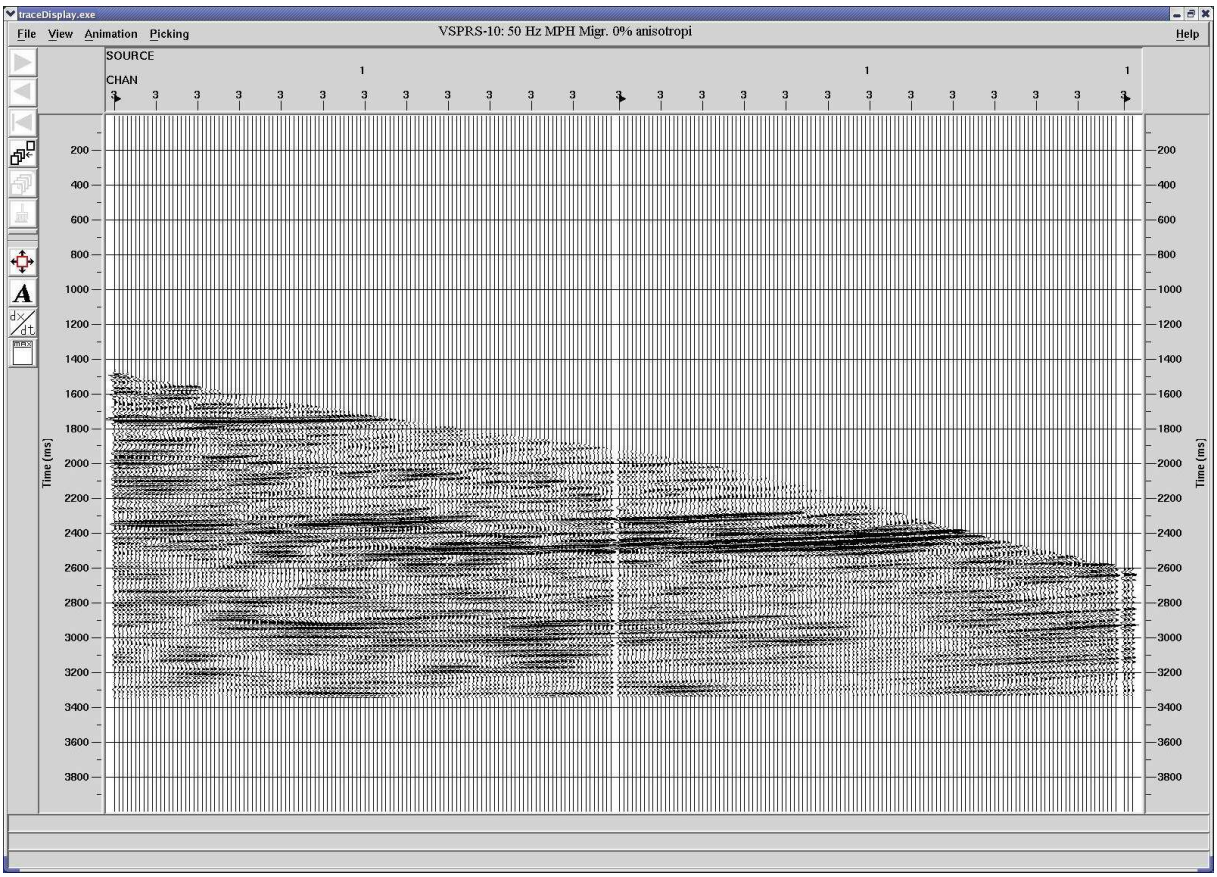
traceDisplay.exe
File View Animation Picking
VSPRS-10: 50 Hz MPH Migr. 0% anisotropi
Help
SOURCE
CHAN
Time (ms)

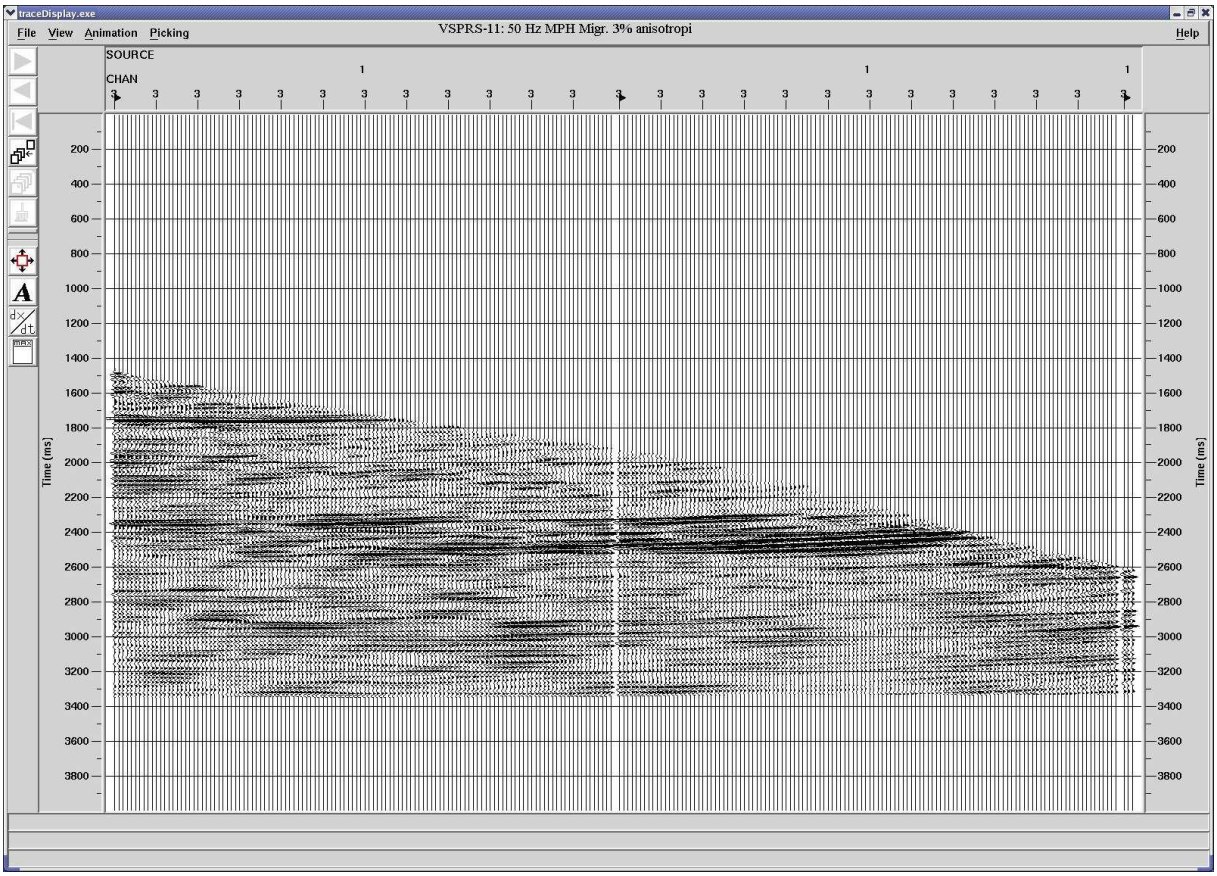
traceDisplay.exe
File View Animation Picking
VSPRS-11: 50 Hz MPH Migr. 3% anisotropi
Help
SOURCE
CHAN
Time (ms)

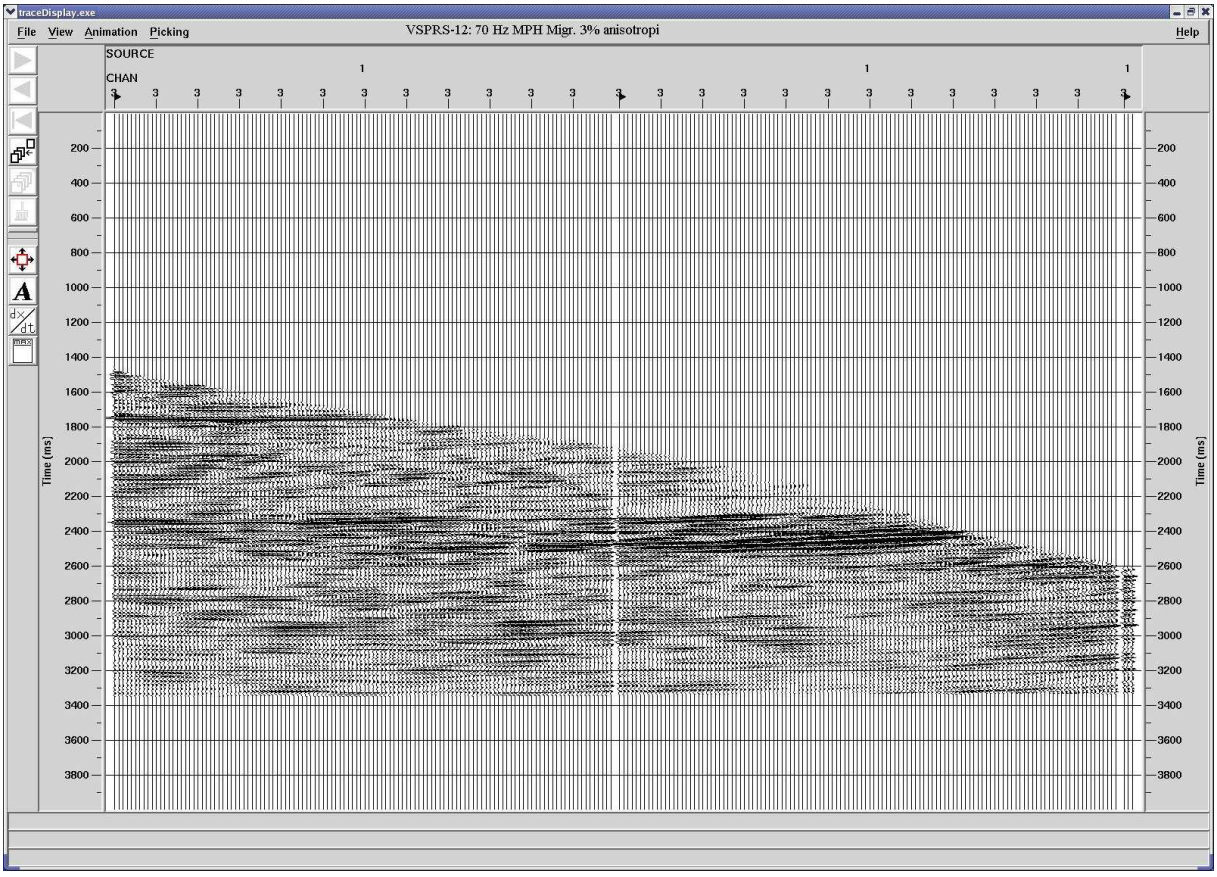
traceDisplay.exe
File View Animation Picking
VSPRS-12: 70 Hz MPH Migr. 3% anisotropi
Help
SOURCE
CHAN
Time (ms)

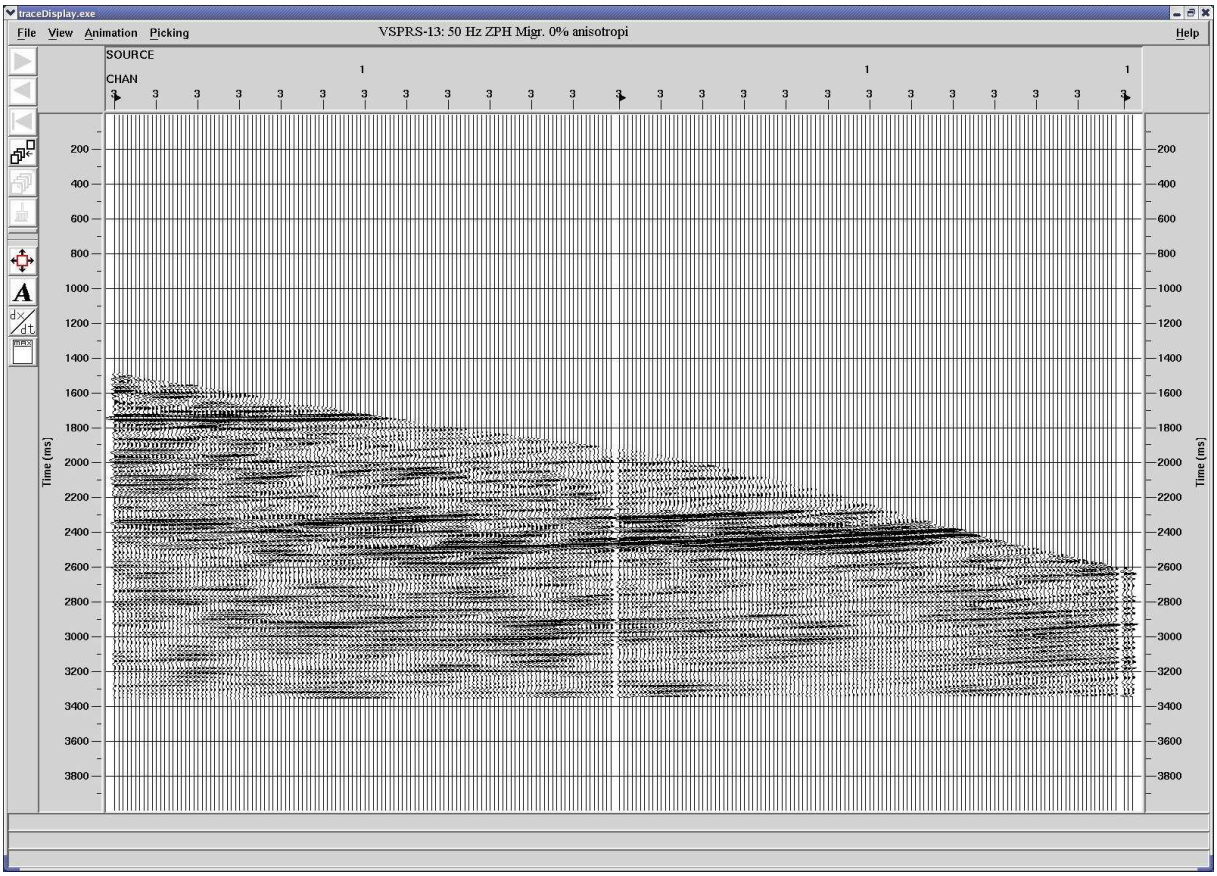
traceDisplay.exe
File View Animation Picking
VSPRS-13: 50 Hz ZPH Migr. 0% anisotropi
Help
SOURCE
CHAN
Time (ms)

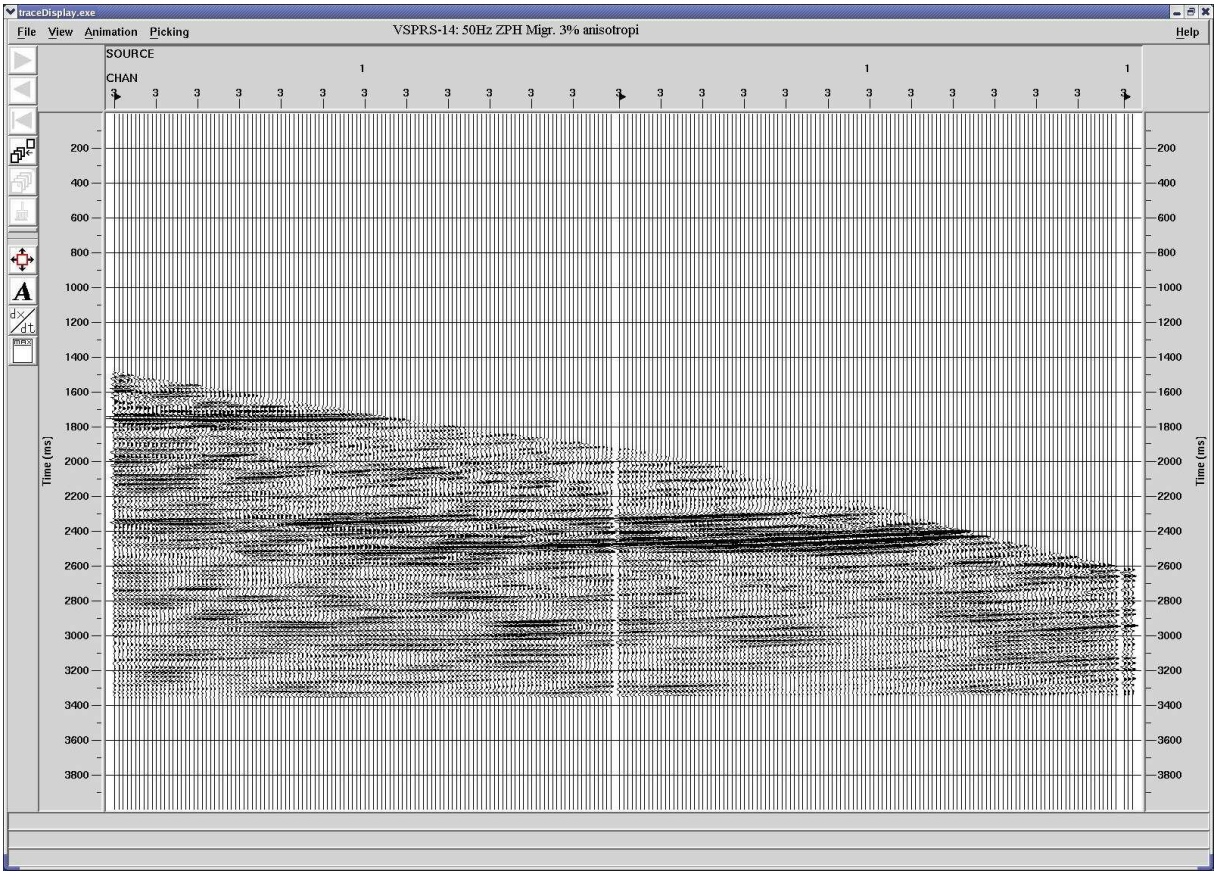
traceDisplay.exe
File View Animation Picking
VSPRS-14: 50Hz ZPH Migr. 3% anisotropi
Help
SOURCE
CHAN
Time (ms)

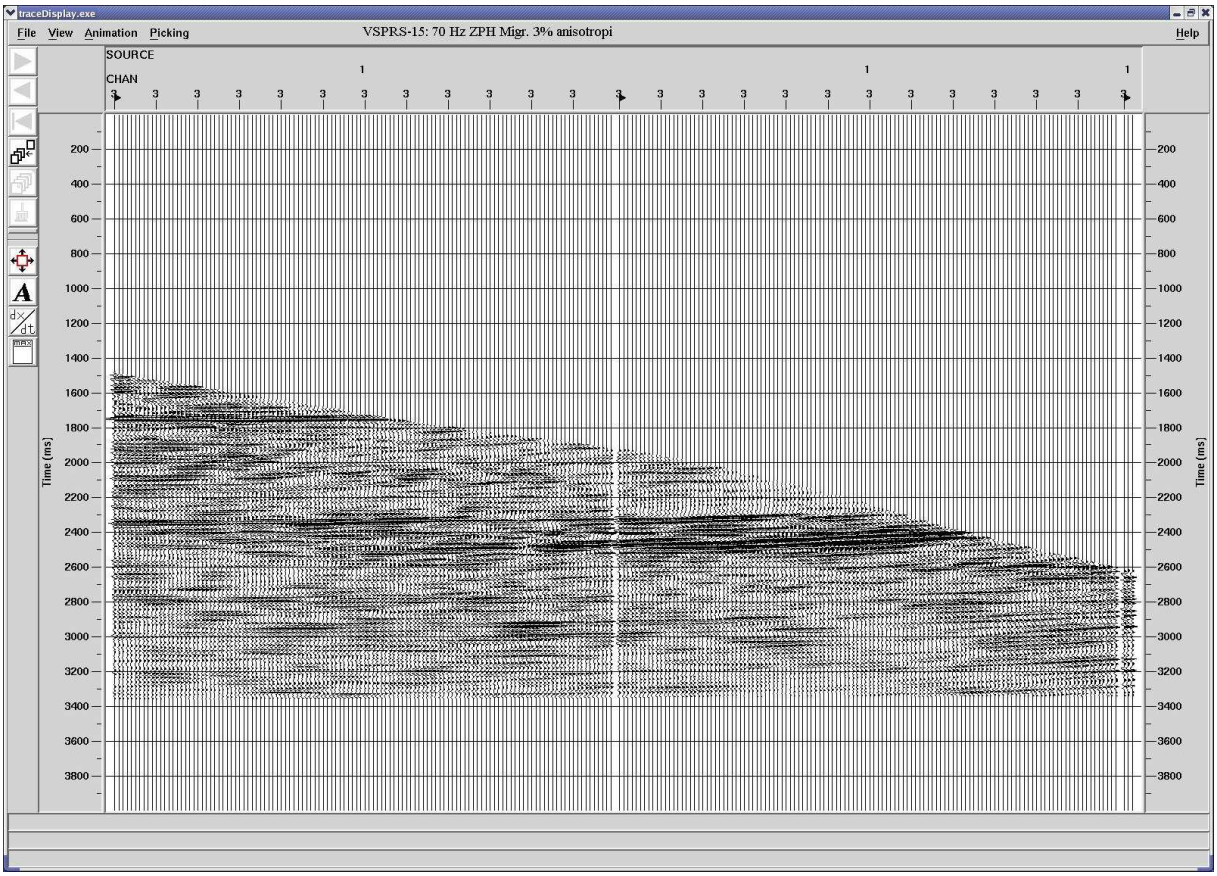
traceDisplay.exe
File View Animation Picking
VSPRS-15: 70 Hz ZPH Migr. 3% anisotropi
Help
SOURCE
CHAN
Time (ms)
200
400
600
800
1000
1200
1400
1600
1800
2000
2200
2400
2600
2800
3000
3200
3400
3600
3800

APPENDIX B

Receiver Positions

UTMx	UTMy	Depth
454269.0	6812690.0	1464.0
454268.0	6812682.0	1469.0
454267.0	6812673.0	1474.0
454266.0	6812664.0	1479.0
454265.0	6812656.0	1484.0
454264.0	6812647.0	1489.0
454263.0	6812639.0	1494.0
454261.0	6812630.0	1499.0
454260.0	6812621.0	1504.0
454259.0	6812613.0	1509.0
454258.0	6812604.0	1514.0
454257.0	6812595.0	1518.0
454256.0	6812587.0	1523.0
454255.0	6812578.0	1528.0
454254.0	6812569.0	1533.0
454253.0	6812561.0	1538.0
454252.0	6812552.0	1543.0
454251.0	6812544.0	1548.0
454249.0	6812535.0	1553.0
454248.0	6812526.0	1558.0
454247.0	6812518.0	1563.0
454246.0	6812509.0	1568.0
454245.0	6812500.0	1573.0
454244.0	6812492.0	1578.0
454243.0	6812483.0	1583.0
454242.0	6812475.0	1588.0
454241.0	6812466.0	1593.0
454240.0	6812458.0	1598.0
454239.0	6812449.0	1603.0
454238.0	6812441.0	1608.0
454237.0	6812432.0	1613.0
454236.0	6812423.0	1618.0
454235.0	6812415.0	1623.0
454234.0	6812406.0	1628.0
454233.0	6812398.0	1634.0
454232.0	6812389.0	1639.0
454231.0	6812381.0	1644.0
454230.0	6812372.0	1649.0
454229.0	6812364.0	1654.0
454228.0	6812355.0	1659.0

454227.0	6812347.0	1664.0
454226.0	6812338.0	1670.0
454225.0	6812330.0	1675.0
454224.0	6812321.0	1680.0
454223.0	6812313.0	1685.0
454222.0	6812304.0	1690.0
454221.0	6812296.0	1696.0
454220.0	6812287.0	1701.0
454219.0	6812279.0	1706.0
454218.0	6812270.0	1711.0
454217.0	6812262.0	1716.0
454216.0	6812253.0	1722.0
454215.0	6812245.0	1727.0
454215.0	6812236.0	1732.0
454214.0	6812228.0	1737.0
454213.0	6812219.0	1742.0
454212.0	6812210.0	1747.0
454211.0	6812202.0	1752.0
454210.0	6812193.0	1757.0
454209.0	6812184.0	1761.0
454208.0	6812176.0	1766.0
454207.0	6812167.0	1771.0
454207.0	6812158.0	1776.0
454206.0	6812150.0	1781.0
454205.0	6812141.0	1786.0
454204.0	6812132.0	1791.0
454203.0	6812124.0	1796.0
454202.0	6812115.0	1801.0
454201.0	6812106.0	1806.0
454200.0	6812098.0	1811.0
454200.0	6812089.0	1816.0
454199.0	6812080.0	1821.0
454198.0	6812072.0	1826.0
454197.0	6812063.0	1831.0
454196.0	6812055.0	1836.0
454195.0	6812046.0	1841.0
454195.0	6812037.0	1846.0
454194.0	6812029.0	1851.0
454193.0	6812020.0	1856.0
454192.0	6812012.0	1861.0
454192.0	6812003.0	1866.0
454192.0	6811995.0	1872.0
454191.0	6811986.0	1877.0
454191.0	6811978.0	1883.0
454191.0	6811970.0	1888.0
454191.0	6811961.0	1894.0
454190.0	6811953.0	1899.0
454190.0	6811945.0	1905.0
454190.0	6811936.0	1910.0
454191.0	6811928.0	1916.0
454191.0	6811920.0	1922.0

454191.0	6811912.0	1928.0
454192.0	6811904.0	1933.0
454192.0	6811896.0	1940.0
454193.0	6811888.0	1946.0
454194.0	6811880.0	1952.0
454194.0	6811872.0	1958.0
454195.0	6811865.0	1964.0
454196.0	6811857.0	1971.0
454197.0	6811849.0	1977.0
454199.0	6811842.0	1983.0
454200.0	6811834.0	1990.0
454201.0	6811826.0	1996.0
454203.0	6811819.0	2002.0
454205.0	6811812.0	2009.0
454207.0	6811804.0	2016.0
454209.0	6811797.0	2022.0
454211.0	6811790.0	2029.0
454213.0	6811783.0	2036.0
454215.0	6811776.0	2042.0
454217.0	6811769.0	2049.0
454219.0	6811762.0	2056.0
454222.0	6811755.0	2063.0
454224.0	6811748.0	2069.0
454227.0	6811741.0	2076.0
454229.0	6811734.0	2083.0
454232.0	6811727.0	2090.0
454235.0	6811721.0	2097.0
454238.0	6811714.0	2103.0
454241.0	6811707.0	2110.0
454244.0	6811701.0	2117.0
454248.0	6811694.0	2124.0
454251.0	6811688.0	2131.0
454254.0	6811682.0	2138.0
454258.0	6811675.0	2145.0
454262.0	6811669.0	2152.0
454266.0	6811663.0	2159.0
454269.0	6811657.0	2166.0
454273.0	6811651.0	2173.0
454277.0	6811646.0	2180.0
454282.0	6811640.0	2187.0
454286.0	6811634.0	2194.0
454290.0	6811629.0	2201.0
454294.0	6811623.0	2209.0
454299.0	6811618.0	2216.0
454303.0	6811613.0	2223.0
454308.0	6811608.0	2230.0
454313.0	6811602.0	2237.0
454318.0	6811597.0	2244.0
454322.0	6811592.0	2252.0
454327.0	6811588.0	2259.0
454332.0	6811583.0	2266.0

454337.0	6811578.0	2273.0
454342.0	6811574.0	2281.0
454348.0	6811569.0	2288.0
454353.0	6811564.0	2295.0
454358.0	6811560.0	2302.0
454363.0	6811556.0	2310.0
454369.0	6811551.0	2317.0
454374.0	6811547.0	2324.0
454380.0	6811543.0	2331.0
454385.0	6811538.0	2338.0
454390.0	6811534.0	2346.0
454396.0	6811529.0	2353.0
454401.0	6811525.0	2360.0
454407.0	6811520.0	2367.0
454412.0	6811516.0	2374.0
454417.0	6811511.0	2381.0
454423.0	6811507.0	2388.0
454428.0	6811503.0	2396.0
454434.0	6811498.0	2403.0
454439.0	6811494.0	2410.0
454444.0	6811489.0	2417.0
454450.0	6811485.0	2424.0
454455.0	6811480.0	2431.0
454460.0	6811476.0	2438.0
454466.0	6811471.0	2446.0
454471.0	6811467.0	2453.0
454477.0	6811462.0	2460.0
454482.0	6811458.0	2467.0
454487.0	6811453.0	2474.0
454493.0	6811448.0	2481.0
454498.0	6811444.0	2488.0
454504.0	6811439.0	2495.0
454509.0	6811435.0	2502.0
454514.0	6811430.0	2509.0
454520.0	6811426.0	2516.0
454525.0	6811421.0	2524.0
454530.0	6811416.0	2531.0
454536.0	6811412.0	2538.0
454541.0	6811407.0	2545.0
454546.0	6811403.0	2552.0
454552.0	6811398.0	2559.0
454557.0	6811394.0	2566.0
454562.0	6811389.0	2574.0
454567.0	6811385.0	2581.0
454573.0	6811380.0	2588.0
454578.0	6811376.0	2595.0
454583.0	6811371.0	2603.0
454588.0	6811367.0	2610.0
454594.0	6811362.0	2617.0
454599.0	6811358.0	2624.0
454604.0	6811353.0	2631.0

454610.0	6811349.0	2638.0
454615.0	6811344.0	2646.0
454620.0	6811340.0	2653.0
454626.0	6811335.0	2660.0
454631.0	6811331.0	2667.0
454636.0	6811326.0	2674.0
454642.0	6811322.0	2681.0
454647.0	6811317.0	2689.0
454652.0	6811313.0	2696.0
454658.0	6811309.0	2703.0
454663.0	6811304.0	2710.0
454668.0	6811300.0	2718.0
454674.0	6811296.0	2725.0
454679.0	6811291.0	2732.0
454684.0	6811287.0	2739.0
454690.0	6811283.0	2747.0
454695.0	6811278.0	2754.0
454700.0	6811274.0	2761.0
454706.0	6811269.0	2769.0
454711.0	6811265.0	2776.0
454716.0	6811261.0	2783.0
454721.0	6811256.0	2790.0
454727.0	6811252.0	2798.0
454735.0	6811246.0	2809.0
454740.0	6811241.0	2816.0
454745.0	6811237.0	2823.0
454751.0	6811233.0	2831.0
454756.0	6811229.0	2838.0
454761.0	6811224.0	2845.0
454767.0	6811220.0	2853.0
454772.0	6811216.0	2860.0

Time, Depth and Interval Velocity for NIVSP and Rig Source

TC	Z	INT.VEL
0	0	1478
0,2091	-309	1478
0,2091	-309	2062
0,7408	-1405,5	2062
0,743	-1410,2	2162
0,7457	-1415,1	1817
0,7484	-1420,1	1830
0,7511	-1425,1	1837
0,7537	-1430	1907
0,7563	-1434,9	1903
0,759	-1439,9	1815
0,7617	-1444,8	1822
0,7639	-1449,7	2181
0,7662	-1454,6	2176
0,7685	-1459,5	2144
0,7706	-1464,5	2327
0,7732	-1469,4	1881
0,7756	-1474,3	2008
0,7783	-1479,2	1856
0,7809	-1484,1	1856
0,7832	-1489	2186
0,7857	-1494	1941
0,7881	-1498,9	2045
0,7907	-1503,8	1892
0,7933	-1508,8	1952
0,7958	-1513,8	1964
0,7986	-1518,8	1805
0,8014	-1523,8	1826
0,8043	-1528,9	1718
0,8073	-1534	1731
0,8101	-1539,1	1814
0,8128	-1544,2	1817
0,816	-1549,2	1600
0,8192	-1554,3	1592
0,8224	-1559,4	1597
0,8251	-1564,5	1906
0,828	-1569,6	1743
0,8309	-1574,7	1774
0,8335	-1579,8	1950
0,8363	-1585	1816
0,8392	-1590,1	1801
0,8419	-1595,3	1897
0,8446	-1600,4	1900
0,8478	-1605,6	1626
0,8509	-1610,7	1632
0,8534	-1615,9	2101
0,8559	-1621,1	2105
0,8585	-1626,2	1947
0,8612	-1631,4	1962
0,864	-1636,6	1850
0,8668	-1641,8	1850
0,8687	-1647,1	2767
0,8713	-1652,3	2027
0,8735	-1657,6	2342
0,8758	-1662,9	2346

0,8783	-1668,1	2071
0,8808	-1673,1	2008
0,8834	-1678	1903
0,886	-1682,9	1888
0,8884	-1687,8	2020
0,8902	-1692,7	2668
0,8929	-1697,7	1842
0,8949	-1702,6	2454
0,8974	-1707,5	1952
0,8994	-1712,4	2455
0,9018	-1717,3	2062
0,9042	-1722,2	2071
0,9065	-1727,2	2143
0,9088	-1732,1	2148
0,911	-1737	2210
0,9132	-1742	2225
0,9149	-1746,9	2940
0,9173	-1751,8	2020
0,9197	-1756,8	2110
0,9223	-1761,8	1915
0,925	-1766,8	1858
0,9269	-1771,8	2550
0,9291	-1776,8	2304
0,9313	-1781,8	2304
0,9335	-1786,8	2256
0,9353	-1791,8	2842
0,9378	-1797	1992
0,9397	-1802,2	2752

0,942	-1807,5	2364
0,9446	-1812,9	2041
0,9467	-1818,3	2643
0,9487	-1823,8	2671
0,9508	-1829,2	2663
0,9528	-1834,7	2668
0,955	-1840,2	2516
0,9577	-1845,8	2070
0,9602	-1851,4	2230
0,9628	-1857,1	2249
0,965	-1862,8	2553
0,9672	-1868,6	2589
0,9697	-1874,5	2366
0,9722	-1880,6	2420
0,9751	-1886,7	2174
0,9779	-1892,9	2192
0,9802	-1899,1	2665
0,983	-1905,3	2219
0,9854	-1911,6	2660
0,9884	-1917,9	2093
0,9908	-1924,3	2577
0,9937	-1930,6	2235
0,9963	-1937	2499
0,9989	-1943,5	2436
1,0018	-1950,1	2245
1,0049	-1956,7	2156
1,0074	-1963,4	2696
1,0105	-1970,1	2165

1,0131	-1976,8	2558
1,0161	-1983,5	2238
1,0191	-1990,3	2306
1,022	-1997,1	2310
1,0251	-2003,8	2160
1,0272	-2010,6	3154
1,0304	-2017,3	2106
1,0328	-2024,1	2880
1,0359	-2030,9	2172
1,039	-2037,7	2236
1,042	-2044,5	2239
1,0446	-2051,4	2693
1,0478	-2058,2	2110
1,0509	-2065,1	2277
1,0536	-2072,1	2516
1,0565	-2079	2393
1,0592	-2086	2549
1,062	-2092,9	2516
1,0653	-2099,9	2131
1,0681	-2106,9	2463
1,0712	-2114	2277
1,0734	-2121,1	3358
1,0762	-2128,3	2470
1,0783	-2135,4	3552
1,0814	-2142,5	2256
1,0836	-2149,7	3216
1,0871	-2156,8	2090
1,0891	-2164	3430

1,0917	-2171,2	2815
1,0941	-2178,4	3004
1,0966	-2185,5	2899
1,0991	-2192,8	2849
1,1015	-2200	2971
1,1042	-2207,2	2732
1,1069	-2214,5	2617
1,1094	-2221,7	2927
1,1119	-2229	2979
1,1141	-2236,3	3274
1,1171	-2243,5	2388
1,1195	-2250,8	3054
1,1223	-2258	2585
1,1247	-2265,2	2971
1,128	-2272,4	2219
1,1303	-2279,5	3090
1,1323	-2286,7	3534
1,1353	-2293,8	2348
1,1375	-2301	3216
1,1406	-2308,1	2307
1,1428	-2315,2	3270
1,1455	-2322,3	2611
1,1477	-2329,5	3281
1,1505	-2336,6	2522
1,1525	-2343,8	3666
1,1555	-2350,9	2347
1,1574	-2358,1	3768
1,1604	-2365,2	2386

1,1624	-2372,4	3580
1,1653	-2379,5	2505
1,168	-2386,6	2652
1,1709	-2393,7	2388
1,1738	-2400,8	2446
1,1766	-2407,9	2556
1,1791	-2415	2806
1,1817	-2422,1	2751
1,184	-2429,1	3069
1,1866	-2436,2	2688
1,1892	-2443,3	2792
1,1918	-2450,4	2721
1,1943	-2457,6	2852
1,1967	-2464,7	2954
1,1989	-2471,8	3221
1,2018	-2478,9	2489
1,204	-2486,1	3235
1,2065	-2493,2	2867
1,209	-2500,4	2818
1,2118	-2507,6	2605
1,215	-2514,8	2218
1,2173	-2522	3185
1,2201	-2529,2	2578
1,2222	-2536,4	3461
1,2247	-2543,6	2804
1,2267	-2550,8	3720
1,2293	-2558	2709
1,2315	-2565,2	3298

1,2338	-2572,3	3081
1,2364	-2579,5	2782
1,2382	-2586,7	3961
1,2406	-2593,9	3008
1,2426	-2601	3574
1,2446	-2608,2	3593
1,2466	-2615,3	3492
1,2487	-2622,5	3519
1,2505	-2629,7	3978
1,2523	-2636,9	4005
1,2544	-2644,1	3367
1,2564	-2651,4	3723
1,2586	-2658,7	3235
1,2607	-2666	3586
1,2631	-2673,2	2999
1,2652	-2680,5	3538
1,2679	-2687,8	2693
1,2701	-2695,1	3328
1,2724	-2702,4	3058
1,2748	-2709,7	3151
1,2768	-2717	3586
1,279	-2724,2	3323
1,2813	-2731,5	3106
1,2836	-2738,8	3161
1,2868	-2749,7	3414
1,2889	-2757	3422
1,2911	-2764,3	3413
1,2936	-2771,6	2955

1,2956	-2779	3628
1,2978	-2786,3	3375
1,3002	-2793,6	3024
1,3025	-2800,9	3206

TC	Z	INT.VEL
0	0	1477
0,2091	-309	1477
0,2091	-309	2072
0,7003	-1326,8	2072
0,7047	-1337	2268
0,7095	-1347	2110
0,7144	-1356,9	2019
0,7394	-1405,5	1942
0,7418	-1410,2	1946
0,7444	-1415,1	1872
0,7469	-1420,1	2015
0,7494	-1425,1	2024
0,7517	-1430	2081
0,7542	-1434,9	2006
0,7566	-1439,9	2085
0,7589	-1444,8	2075
0,7612	-1449,7	2209
0,7635	-1454,6	2070
0,7658	-1459,5	2163
0,7681	-1464,5	2111
0,7705	-1469,4	2087
0,7728	-1474,3	2083
0,7753	-1479,2	2006
0,7776	-1484,1	2123
0,78	-1489	2044
0,7824	-1494	2040
0,7849	-1498,9	2019
0,7873	-1503,8	2044
0,7897	-1508,8	2046
0,7922	-1513,8	1979
0,7947	-1518,8	1979
0,7974	-1523,8	1932
0,7999	-1528,9	1960
0,8026	-1534	1932
0,8051	-1539,1	1988
0,8077	-1544,2	1979
0,8104	-1549,2	1916
0,8131	-1554,3	1862
0,8159	-1559,4	1815
0,8187	-1564,5	1805
0,8214	-1569,6	1906
0,8241	-1574,7	1842
0,8268	-1579,8	1923
0,8298	-1585	1746
0,8326	-1590,1	1834
0,8356	-1595,3	1707
0,8383	-1600,4	1872
0,841	-1605,6	1906
0,8437	-1610,7	1929

0,8465	-1615,9	1866
0,8493	-1621,1	1861
0,8518	-1626,2	1999
0,8545	-1631,4	1942
0,8572	-1636,6	1968
0,8595	-1641,8	2244
0,8621	-1647,1	1963
0,8644	-1652,3	2306
0,8668	-1657,6	2211
0,8687	-1662,9	2722
0,8711	-1668,1	2175
0,8735	-1673,1	2160
0,8758	-1678	2074
0,878	-1682,9	2217
0,8804	-1687,8	2103
0,8826	-1692,7	2161
0,885	-1697,7	2120
0,8874	-1702,6	2032
0,8897	-1707,5	2123
0,8921	-1712,4	2047
0,8944	-1717,3	2110
0,8967	-1722,2	2209
0,8988	-1727,2	2345
0,901	-1732,1	2204
0,9033	-1737	2130
0,9056	-1742	2127
0,9078	-1746,9	2244
0,9101	-1751,8	2179
0,9124	-1756,8	2127
0,9149	-1761,8	2008
0,9171	-1766,8	2257
0,9194	-1771,8	2157
0,9215	-1776,8	2373
0,9238	-1781,8	2155
0,9258	-1786,8	2550
0,928	-1791,8	2308
0,93	-1797	2551
0,9323	-1802,2	2299
0,9343	-1807,5	2636
0,9365	-1812,9	2479
0,9386	-1818,3	2591
0,9407	-1823,8	2604
0,9427	-1829,2	2625
0,9449	-1834,7	2481
0,9471	-1840,2	2521
0,9495	-1845,8	2404
0,9517	-1851,4	2517
0,9541	-1857,1	2398
0,9564	-1862,8	2464
0,9586	-1868,6	2632

0,9608	-1874,5	2658
0,9631	-1880,6	2645
0,9656	-1886,7	2495
0,968	-1892,9	2487
0,9704	-1899,1	2604
0,9729	-1905,3	2508
0,9754	-1911,6	2502
0,978	-1917,9	2471
0,9804	-1924,3	2627
0,983	-1930,6	2427
0,9855	-1937	2519
0,9883	-1943,5	2344
0,9908	-1950,1	2589
0,9937	-1956,7	2299
0,9964	-1963,4	2476
0,9994	-1970,1	2277
1,002	-1976,8	2503
1,0049	-1983,5	2356
1,0077	-1990,3	2464
1,0106	-1997,1	2292
1,0133	-2003,8	2513
1,0161	-2010,6	2384
1,0187	-2017,3	2575
1,0216	-2024,1	2368
1,0242	-2030,9	2583
1,0271	-2037,7	2372
1,0297	-2044,5	2579
1,0325	-2051,4	2478
1,0352	-2058,2	2598
1,0379	-2065,1	2529
1,0406	-2072,1	2520
1,0432	-2079	2700
1,0459	-2086	2554
1,0486	-2092,9	2561
1,0515	-2099,9	2415
1,0545	-2106,9	2353
1,0574	-2114	2488
1,0602	-2121,1	2542
1,0628	-2128,3	2733
1,0654	-2135,4	2687
1,0681	-2142,5	2660
1,0708	-2149,7	2649
1,0735	-2156,8	2620
1,076	-2164	2871
1,0787	-2171,2	2692
1,0811	-2178,4	2936
1,0839	-2185,5	2577
1,0863	-2192,8	3084
1,089	-2200	2654
1,0914	-2207,2	3051

1,0942	-2214,5	2542
1,0967	-2221,7	2888
1,0996	-2229	2510
1,1021	-2236,3	2908
1,105	-2243,5	2518
1,1075	-2250,8	2922
1,1104	-2258	2520
1,1128	-2265,2	2927
1,1157	-2272,4	2492
1,1183	-2279,5	2758
1,121	-2286,7	2658
1,1235	-2293,8	2850
1,126	-2301	2818
1,1288	-2308,1	2575
1,1313	-2315,2	2873
1,1338	-2322,3	2787
1,1361	-2329,5	3127
1,1387	-2336,6	2714
1,1413	-2343,8	2800
1,144	-2350,9	2656
1,1465	-2358,1	2840
1,1492	-2365,2	2691
1,1518	-2372,4	2725
1,1546	-2379,5	2532
1,1573	-2386,6	2624
1,1601	-2393,7	2558
1,1627	-2400,8	2727
1,1653	-2407,9	2695
1,1679	-2415	2712
1,1704	-2422,1	2829
1,1728	-2429,1	2910
1,1752	-2436,2	3050
1,1776	-2443,3	2962
1,1799	-2450,4	2998
1,1822	-2457,6	3173
1,1844	-2464,7	3167
1,1867	-2471,8	3115
1,1891	-2478,9	2933
1,1915	-2486,1	3030
1,1939	-2493,2	3029
1,1962	-2500,4	3043
1,1987	-2507,6	2927
1,2011	-2514,8	2938
1,2035	-2522	2983
1,2058	-2529,2	3265
1,2079	-2536,4	3324
1,2099	-2543,6	3553
1,2121	-2550,8	3292
1,2142	-2558	3527
1,2164	-2565,2	3193

1,2186	-2572,3	3346
1,2208	-2579,5	3147
1,2229	-2586,7	3441
1,2249	-2593,9	3583
1,2269	-2601	3701
1,2288	-2608,2	3665
1,2308	-2615,3	3507
1,2328	-2622,5	3743
1,2347	-2629,7	3681
1,2365	-2636,9	3972
1,2386	-2644,1	3559
1,2406	-2651,4	3542
1,2428	-2658,7	3396
1,2448	-2666	3514
1,2469	-2673,2	3551
1,249	-2680,5	3382
1,2513	-2687,8	3239
1,2536	-2695,1	3139
1,2558	-2702,4	3260
1,258	-2709,7	3437
1,26	-2717	3517
1,2622	-2724,2	3441
1,2645	-2731,5	3129
1,2667	-2738,8	3208
1,2702	-2749,7	3190
1,2723	-2757	3429
1,2746	-2764,3	3218
1,2768	-2771,6	3324
1,279	-2779	3313
1,2811	-2786,3	3452
1,2834	-2793,6	3247
1,2858	-2800,9	3030